

Dissertation

Submitted to the

Faculty for Natural Sciences
and Mathematics of the
Christian-Albrechts University of Kiel, Germany

for the degree of

Doctor of Natural Sciences
(Dr. rer. nat.)

Presented by

Diplom-Biochemist Jan-Wilhelm Kornfeld

The role of Signal Transducer and Activator
of Transcription 5 (Stat5) and the
Glucocorticoid Receptor (GR) in hepatocyte
function

Conducted at the
Ludwig-Boltzmann-Institute for Cancer Research
(LBI-CR)

under supervision of Dr. Richard Moriggl

Referees:

Prof. Dr. Holger Kalthoff

Prof. Dr. Dr. h.c. Thomas C. G. Bosch

Table of contents

1.	Summary	8
	Zusammenfassung	10
2.	Introduction	12
2.1.	Metabolic homeostasis and the liver	12
2.1.1.	Uptake and systemic distribution of lipids.....	12
2.1.2.	Glycolysis and hepatic beta-oxidation.....	14
2.1.3.	Hepatic <i>de novo</i> lipogenesis.....	15
2.2.	Transcription factors and hepatic lipid metabolism	15
2.2.1.	Transcriptional regulation of hepatic beta-oxidation	16
2.2.2.	Transcriptional regulation of hepatic <i>de novo</i> lipogenesis	17
2.3.	Insulin signaling and insulin resistance	18
2.4.	Insulin resistance and liver steatosis.....	20
2.4.1.	Mouse models of NAFLD	21
2.5.	Fibrosis of the liver.....	22
2.5.1.	Molecular mechanisms underlying liver fibrogenesis.....	23
2.6.	Signal transducer and activator of transcription 5 (Stat5)	25
2.6.1.	Stat5 in health and disease	27
2.6.1.1.	Stat5 and postnatal body growth.....	28
2.6.1.2.	Stat5 and hepatic lipid metabolism.....	28
2.7.	The glucocorticoid receptor (GR).....	29
2.8.	Linear Stat5-GR signal transduction: Two transcription factor pathways converge	30
2.8.1.	Growth hormone, glucocorticoids and body composition	30

2.9.	Conditional gene deletion using the Cre/LoxP system.....	31
2.10.	Aim of the thesis	33
3.	Results.....	34
3.1.	A linear Stat5-GR axis controls postnatal body growth	34
3.1.1.	Loss of hepatic Stat5 and/or the GR signaling leads postnatal growth deficiency	34
3.1.2.	Loss of hepatic Stat5 and/or the GR signaling leads to similar changes in gene expression profiles	35
3.1.3.	The N-terminus of Stat5 constitutes the docking platform for the GR	38
3.1.4.	Socs2 as example for Stat5-GR co-dependent gene transcription.....	43
3.1.4.1.	The Socs2 promoter harbours putative Stat5-GR responsive elements	43
3.1.4.2.	Putative Stat5-GR DNA binding sites in the proximal Socs2 promoter are Stat5 responsive.....	45
3.1.4.3.	The proximal Socs2 promoter is synergistically transactivated by Stat5-GR interplay	47
3.1.4.4.	Full transactivation of the Socs2 promoter depends on Stat5 and GR.....	48
3.1.4.5.	Synergistic Stat5 and GR signaling is required for full Socs2 promoter transactivation.....	49
3.1.4.6.	A linear Stat5-GR pathway controls hepatic Socs2 transcription	51
3.2.	Compound loss of hepatic Stat5 and GR signaling leads to steatosis ...	52
3.2.1.	Loss of hepatic Stat5 signaling leads to increased lipogenesis	56
3.2.2.	Loss of hepatic Stat5 signaling induces hepatic insulin resistance.....	60
3.2.3.	Compound loss of hepatic Stat5 and GR signaling leads to peripheral lipodystrophy.	63
3.2.4.	Compound loss of hepatic Stat5 and Glucocorticoid Receptor signaling does not affect lipoprotein particle-mediated lipid distribution	66
3.2.5.	Loss of Stat5 is not compensatory counteracted by Stat1 and Stat3 activation	66
3.2.6.	Development of steatosis is independent of Jak2 upstream kinase	67
3.3.	Loss of hepatic Stat5 leads to severe liver fibrosis in MDR2 ⁻ mice	68

3.3.1.	Deletion of MDR2 proteins causes hepatic Stat5b activation	72
3.3.2.	MDR2/Stat5 ^{AlfpCre} mice display autocrine growth factor loops	73
3.3.3.	Fibrogenesis in MDR2/Stat5 ^{AlfpCre} mice is accompanied by ECM remodelling	74
3.3.4.	Loss of hepatic Stat5 in MDR2 ⁻ mice leads to impaired bile acid circulation....	76
4.	Discussion	79
4.1.	A linear Stat5-GR axis controls postnatal body growth	79
4.2.	Compound loss of hepatic Stat5 and GR signaling causes steatosis	82
4.3.	Loss of hepatic Stat5 signaling leads to severe liver fibrosis in the MDR2 ⁻ ^{l/-} mouse model of inflammatory liver cancer	85
5.	Materials and Methods.....	86
5.1.	Materials	86
5.1.1.	Chemicals and enzymes:	86
5.1.2.	Standard solutions.....	87
5.1.3.	Media for bacterial cultivation	87
5.1.4.	Plasmid constructs	88
5.2.	Molecular biology.....	88
5.2.1.	Standard techniques.....	88
5.2.1.1.	DNA electrophoresis.....	88
5.2.1.2.	Extraction of DNA fragments from agarose gels	88
5.2.1.3.	Transformation of bacteria	89
5.2.2.	Vector cloning	89
5.2.2.1.	Cloning strategy for Socs2 reporter constructs	89
5.2.3.	DNA isolation and analysis.....	90
5.2.3.1.	Isolation of plasmid DNA from bacteria.....	90
5.2.3.2.	Isolation of tail DNA for genotyping	90
5.2.3.3.	Genotyping PCR	90
5.2.4.	RNA isolation and analysis.....	92
5.2.4.1.	Isolation of messenger RNA from murine livers	92

5.2.4.2.	Reverse transcription.....	93
5.2.4.3.	Quantitative RT-PCR (qPCR)	93
5.2.4.4.	Whole genome expression profiling (Affymetrix) and bioinformatics	95
5.2.4.5.	Molecular signature analysis of Affymetrix expression data	95
5.3.	Protein chemistry	96
5.3.1.	Protein isolation	96
5.3.1.1.	Preparation of liver homogenates	96
5.3.1.2.	Preparation of cell line extracts.....	97
5.3.1.3.	Protein quantification with the Bradford method.....	97
5.3.2.	Immunoprecipitation	97
5.3.3.	Western Blot.....	98
5.3.3.1.	Sodium Dodecylsulfate Polyacrylamide Gel Electrophoresis.....	98
5.3.3.2.	Protein transfer onto Nylon membranes.....	99
5.3.3.3.	Immunoblot analysis (antibody staining)	99
5.3.4.	EMSA	100
5.3.5.	Tissue analysis and paraffin embedding	102
5.3.5.1.	Histopathology	102
5.3.5.2.	Immunohistochemistry	102
5.3.6.	Electron microscopy	103
5.4.	Cell biology	103
5.4.1.	Cell lines	103
5.4.2.	Handling of cell lines and transient transfection	103
5.4.3.	Luciferase reporter assay.....	105
5.5.	Colony breeding and management.....	106
5.5.1.	Transgenic mouse lines	106
5.5.2.	Metabolic function tests	106
5.5.2.1.	Glucose tolerance test	106
5.5.2.2.	Insulin tolerance test.....	107
5.5.3.	Blood sampling and serum parameter quantification	107
5.5.3.1.	Lipoprotein profile.....	107
5.5.4.	Immuno assays.....	107

5.5.4.1.	Radio Immunoassay (RIA)	108
5.5.4.2.	Enzyme Linked Immuno Sorbent Assay (ELISA).....	108
5.5.5.	Colorimetric assays	108
5.5.5.1.	Quantification of free fatty acids (FFA).....	108
5.5.5.2.	Isolation and quantification of hepatic triglycerides	109
6.	Literature:	110
7.	Abbreviations	123
8.	Bibliography	126
9.	Acknowledgements	128
10.	Acknowledgements	1289

1. Summary

Signal transducer and activator of transcription 5 (Stat5) represents a cytokine- and growth factor-dependent transcription factor regulating important biological processes such as postnatal body growth, erythropoiesis and the expression of milk protein genes. The glucocorticoid receptor (GR) binds Stat5 in a cofactor fashion and was reported to modulate Stat5 target gene specificity. In this study we aimed to elucidate the role of Stat5 in pivotal hepatocyte processes such as the regulation of postnatal body growth, fatty acid metabolism and liver fibrogenesis, taking into account its propensity to interact with the GR. The major findings of this study are summarized in the following:

(i) Hepatic loss of Stat5, the GR or both resulted in comparable defects in postnatal body growth. This was accompanied by quantitatively similar changes in transcription profiles, affecting predominantly growth-related Stat5 target genes (e.g. IGF-1 and Socs2). These observations suggested the existence of a linear Stat5-GR signal transduction pathway essential for regulating postnatal body growth. Using protein interaction studies the Stat5 aminoterminal was identified as docking platform for the GR. Luciferase reporter assays confirmed the Stat5-GR-dependent synergism *in vitro* exemplarily for transactivation of the Socs2 promoter.

(ii) Hepatic loss of Stat5 in mice leads to the pathological accumulation of lipids in hepatocytes (steatosis). This coincides with perturbations of hepatic lipid metabolism such as hepatic insulin resistance and induction of *de novo* lipogenesis mediated by lipogenic master regulators PPARgamma and SREBP-1c. Compound loss of Stat5 and GR in hepatocytes severely aggravates this phenotype, leading to late-stage hepatopathologies such as severe steatosis and liver fibrosis already in young animals. At older ages, these mutants additionally exhibit depletions of peripheral fat stores (lipodystrophy) leading to an increased lipid flux into hepatic tissues and thus exacerbating disease. The two-step pathogenesis observed in double knockout animals closely mimics the onset and progression of human non-alcoholic fatty liver disease (NAFLD).

(iii) Hepatic loss of Stat5 in a murine model for proinflammatory liver carcinogenesis (MDR2⁻ model) leads to extrahepatic cholestasis (bile duct obstruction) causing secondary liver fibrosis at young ages. The pathogenesis in these animals comprises major hallmarks observed in fibrotic states such as the activation of hepatic stellate cells and remodelling of the extracellular matrix. Ablation of Stat5 in hepatocytes leads to a direct loss of Stat5-dependent basolateral bile acid transporter transcription in hepatocytes and thus coincides with perturbations in hepatic bile acid circulation and recycling. This may eventually cause hepatocyte damage and, finally, liver fibrosis and cirrhosis.

Taken together, two published first-author manuscripts and one first-author manuscript in preparation resulted from this (see section 8).

Zusammenfassung

Signal transducer and activator of transcription 5 (Stat5) stellt einen wichtigen, Zytokin- und Wachstumsfaktor-abhängigen Transkriptionsfaktor dar mit essentiellen Funktionen z.B. bei der Regulation des postnatalen Größenwachstums, der Erythropoese sowie der Expression von Milchproteinen während der Laktation. Der Glukocorticoid Rezeptor (GR) bindet als akzessorischer Transkriptionskofaktor an Stat5 und kann dessen Zielgen Spezifität unter bestimmten Umständen modifizieren. In der vorliegenden Arbeit sollte der Einfluss von Stat5 auf Hepatozyten-vermittelte Prozesse wie postnatales Größenwachstum, Lipidstoffwechsel sowie Leberfibrogenese untersucht werden, unter Berücksichtigung der Proteinwechselwirkung mit dem GR. Die wichtigsten Resultate der vorliegenden Studie sind im Folgenden zusammengefasst:

(i) Die hepatische Deletion von entweder Stat5, dem GR oder beiden führt zu vergleichbaren Störungen des postnatalen Größenwachstums. Gleichzeitig wurden quantitativ ähnliche Änderungen des Transkriptionsprofils beobachtet, welche besonders solche Stat5-abhängige Gene betraf welche für das postnatal Größenwachstum essentiell sind (z.B. IGF-1 oder Socs2). Diese Beobachtungen ließen auf die Existenz eines linearen Stat5-GR Signaltransduktionsweges schließen, welcher wichtig für die Regulation des Größenwachstums nach der Geburt ist. Der Aminoterminus von Stat5 wurde als Stat5-GR Interaktionsdomäne identifiziert. Luciferase Reporter assays bestätigten eine synergistische Transaktivierung des Socs2 Promoters durch Stat5 und den GR *in vitro*.

(ii) Die hepatische Deletion von Stat5 führt zur milden Akkumulation von Fetten in Hepatozyten (Steatose). Dieses wird begleitet von Störungen des hepatischen Lipidstoffwechsels wie z.B. dem Auftreten von hepatischer Insulinresistenz sowie der Induktion der *de novo* Lipogenese, vermittelt durch die essentiellen prolipogenen Transkriptionsfaktoren PPARgamma und SREBP-1c. Die simultane Deletion von Stat5 und dem GR führt zu einer dramatischen Verschärfung der Steatose sowie zum frühen Auftreten von Leberfibrosen welche normalerweise erst im Endstadium von Steatosen beobachtet werden können. Mit zunehmendem Alter kommt es zu einer Abnahme peripherer Fettspeicher (Lipodystrophie). Dies

resultiert in einem verstärkten Zustrom von Fetten in die Leber und somit einer Verschlimmerung der bestehenden Steatose. Stat5/GR Doppelmutanten zeigen somit eine zweistufige Pathogenese, welche an den humanen NAFLD Krankheitsverlauf erinnert.

(iii) Die hepatische Deletion von Stat5 in einem murinen Modell für inflammatorische Leberkarzinogenese (MDR2⁻ Modell) führt zu extrahepatischer Cholestase (Verschluss der Gallengänge). Diese führt schon in jungen Mäusen zu einer schweren Leberfibrose und Zirrhose. Die Pathogenese in diesen Tieren wird begleitet durch das Auftreten Fibrose-assoziiierter Parameter wie z.B. der Aktivierung von hepatischen Sternzellen sowie der Akkumulation von extrazellulären Matrixproteinen. Mechanistisch führt die hepatische Deletion von Stat5 zu einem direkten, transkriptionellen Verlust wichtiger basolateraler Gallentransporter. Dies wiederum resultiert in indirekten Störungen der hepatischen Gallenzirkulation, welche eine konstante Schädigung von Hepatozyten und schließlich Leberfibrose und Leberzirrhose nach sich zieht.

2. Introduction

2.1. Metabolic homeostasis and the liver

Obesity and its underlying causes are major concerns in the industrialized world affecting both adults and children ¹. Little physical activity and calory excess are associated with the onset of obesity and constitute the second-most preventable source of death in the US ². Nutrition in the industrialized world is based predominantly on saturated fatty acids which leads to increasing body fat content, especially in concert with carbohydrate enriched, high-calory diets ³. Obesity is highly correlated to the Metabolic Syndrome, a cluster of nutrition-derived pathologies such as coronary hypertension, insulin resistance and Type 2 Diabetes (T2D) ⁴. Another epidemiologic feature associated with obesity and T2D is a condition called non-alcoholic fatty liver disease (NAFLD), usually coined to circumscribe a pathology reminiscent of liver damage caused by alcohol abuse. The liver as central metabolic organ possesses essential functions in synthesis and catabolism of nutrients. Postprandially, carbohydrates, lipids, vitamins and mineral salts are resorbed by the intestinal tract, funnelled into the liver and metabolised therein. During fasting periods, the liver releases stored nutrients in order to ensure proper functioning of metabolite-sensitive extrahepatic tissues like the brain. The liver also controls the body's protein, glucose and lipid metabolism ⁵ and synthesises essential lipid carrier proteins such as lipoproteins and albumins which are abundantly secreted into the circulation ⁶. Another hepatic function is the synthesis and secretion of bile, which aids in emulsifying and thus resorbing dietary lipids. In addition, the liver possesses important detoxification properties as it clears xenobiotics and metabolic waste such as bilirubin, an abundantly heme degradation product. Finally, it removes peptide hormones from the circulation and exhibits immunomodulatory as well as vitamin storage functions ⁷.

2.1.1. Uptake and systemic distribution of lipids

The liver is crucial for metabolizing dietary lipids. These lipids are composed primarily of free fatty acids (FFA) and triglycerides (TG), a tricarboxylic acid esterified with

saturated and unsaturated fatty acids (FA). A three step process is necessary for proper absorption of FFA and TG in the intestinal lumen and subsequent transport into the liver:

(i) Nutritional triglycerides are emulsified by endogenous detergents such as bile acids (BA) and enzymatically cleaved by the pancreatic lipase (PL) in the intestinal tract yielding free fatty acids and monocarboxylic acid esters. Other dietary sources of fatty acids are hydrolysed phospholipids and cholesterol esters.

(ii) Triglyceride cleavage products are subsequently absorbed by the intestinal epithelium in the distal jejunum and ileum via facilitated transport across the epithelial cell layer⁸.

(iii) Finally, triglycerides are resynthesised and loaded onto lipoprotein particles (chylomicrons) which enter the bloodstream and efficiently deliver dietary triglycerides into hepatic, adipose and other target tissues. In the liver, hepatic lipase (HL) cleaves triglycerides off the lipoproteinparticle surface and translocates fatty acids into the cytoplasm⁹. Subsequently, fatty acids are catabolically degraded by the mitochondrial and peroxisomal beta-oxidation machinery leading eventually to synthesis of ATP energy equivalents. Alternatively, lipids are incorporated into newly synthesised triglycerides for long-term storage. Of note, the hepatic fat-storage capabilities are limited; the most abundant lipid store is represented by the peripheral white adipose tissue (WAT). Moreover, fatty acids are utilized for synthesis of hepatic inflammation mediators such as prostaglandins and leukotrienes. Finally, via enzymatic remodelling of the fatty acid carbon backbone, fatty acids cleavage products indirectly serve as substrates for synthesis of glucose (gluconeogenesis).

The liver possesses potent lipogenic properties: Triglycerides are synthesized in hepatocytes by esterification of glycerol and fatty acids hailing from two sources: Non-esterified fatty acids (NEFA) derived from lipolysis of peripheral fat stores (adipose tissues) and dietary fatty acids.

Newly synthesised triglycerides and excess dietary TG are packaged onto very-low density lipoparticles (VLDL) and shuttled into the periphery. Subsequently, the lipoprotein lipase (LPL), which is abundantly expressed on adipocytes in the periphery efficiently cleaves triglycerides from VLDL particles and releases glycerol and fatty acids into the adipocyte cytoplasm¹⁰. Thus, in the periphery, consecutive triglyceride hydrolysis of lipoproteinparticles leads to an increase in their protein/lipid ratio. So called 'remnants' of hydrolysed lipoproteinparticles are recycled in the liver

via clathrin-mediated endocytosis. Alternatively, excess lipoparticles are conveyed to the hepatic proteasome machinery for protein degradation ¹¹.

2.1.2. Glycolysis and hepatic beta-oxidation

The liver constitutes the key regulator of energy homeostasis in the body. Two major substrates can be metabolised by hepatic tissue to yield energy equivalents such as ATP and pyruvate eventually utilised to catalyze energy-consuming processes in the body:

(i) Glucose, (a six-carbon (6-C) carbohydrate) is enzymatically processed in an oxygen-independent process called glycolysis yielding two pyruvate molecules (3-C). Pyruvate is decarboxylated into a two-carbon residue (2-C, Acetyl residue) esterified to Coenzyme A (Acetyl-CoA). The Acetyl-CoA pool is constantly replenished by oxidative catabolism of proteins, lipids and carbohydrates. Subsequently, Acetyl-CoA is funnelled into the cytoplasmic citrate cycle, where two consecutive decarboxylations of the acetyl residue yield eight reduced reduction equivalents (NADH/H and FADH₂). These reduction equivalents are used to replenish cellular ATP stores via oxidative phosphorylation of ADP, a reaction catalyzed by respiratory complexes localized in the outer mitochondrial membranes.

(ii) Fatty acids, long-chain carbohydrates hailing either from hydrolysed triglycerides or hepatic *de novo* lipogenesis are catabolised by beta-oxidation in mitochondria and peroxisomes. Mitochondria are specialised in beta-oxidation of saturated short, medium and long-chain fatty acids. In contrast, peroxisomes accommodate enzymes specialised in metabolising more exotic and branched fatty acids. Prior to beta-oxidation, fatty acids are activated by esterification to Coenzyme A yielding high energy Acyl-(n)-CoA thioesters. Subsequently, repetitive cleavage of two-carbon residues from the Acyl carbon backbone leads to Acetyl-CoA and truncated Acyl-(n⁻²)-CoA molecules. Acetyl-CoA is processed via translocation across the mitochondrial membranes and funnelled into the citrate cycle (see above). Alternatively, Acetyl-CoA is utilised for biosynthesis of cholesterol. Under conditions of energy deprivation, Acetyl-CoA may serve as substrate for the biosynthesis of ketone bodies. These compounds serve as energy carriers nourishing glucose-dependent tissues (e.g. the brain) under conditions of glucose deprivation.

2.1.3. Hepatic *de novo* lipogenesis

The biosynthesis of fatty acids takes place in the cytoplasm of most somatic cells. Enzymatic carboxylation of Acetyl-CoA residues yields activated three-carbon-CoA compounds (Malonyl-CoA); a reaction catalyzed by the Acetyl-CoA Carboxylase (ACC), the rate limiting enzyme of hepatic *de novo* lipogenesis. The biosynthesis of fatty acids is orchestrated by a multi-enzyme complex called fatty acid synthase (FAS). FAS catalyses the condensation of long-chain, saturated fatty acids under consumption of Malonyl-CoA substrates. During fatty acids synthesis, precursor thioesters (Acyl-CoA) get elongated by two carbon residues (2-C) in each step, leading to saturated 16-C (palmityl-CoA) or 18-C (stearyl-CoA) fatty acids. Branched and unsaturated fatty acids are essential for high membrane fluidity and are generated by enzymatic oxidation of saturated fatty acids. So-called 'essential fatty acids' have to be provided by the nutrition as they cannot be synthesised in the body. Hepatic *de novo* lipogenesis of fatty acids is tightly controlled by allosteric inhibition of rate limiting enzymes (e.g. ACC). Independently, metabolic master regulators like insulin lead to increased transcription of lipogenic enzymes (see below); whereas others repress lipogenesis indirectly by inhibiting FAS through elevated intracellular cAMP concentrations (e.g. elicited by glucagon or catecholamines). Long-chain, poly-unsaturated fatty acids also inhibit FAS activity, constituting an efficient negative feedback loop essential for times of abundant fatty acid levels ¹².

2.2. Transcription factors and hepatic lipid metabolism

Eukaryotic chromatin consists of long stretches of DNA intertwined to spatially compact structures called nucleosomes. Each nucleosome consists of octamer nucleoprotein (histones) complexes bound to chromosomal DNA ¹³. Efficient transcription of exonic DNA sequences into complementary messenger RNA (mRNA) strands thus depends on conformational rearrangement of nucleosomes facilitating binding to basal transcription machinery components such as RNA polymerase II.

Transcription factors are DNA-binding proteins characterized by strong binding affinities towards defined DNA sequences (responsive elements; RE). Transcription factors are essential for the recruitment of additional transcription cofactors like p300/CBP which possess potent histone acetylases (HAT) activity crucial for

removing acetyl residues from nucleosome lysine moieties. These modifications lead to electrostatic repulsion of nucleoproteins resulting in accessible, 'open chromatin' structures^{14, 15}. Histone Deacetylases (HDAT) reverse this process leading to 'closed chromatin' and abrogated gene expression¹⁶. Classical transcription factors are activated by 'upstream kinases', which itself are triggered by extracellular stimuli such as cytokines or growth factors binding to cognate receptors. Alternatively, nuclear hormone transcription factors are activated directly via binding of membrane-permeable ligands. Generally, activated transcription factors integrate extracellular signals, leading to specific gene expression changes. This flexibility enables the cell to react to everchanging extracellular nutrient supplies. Aberrant transcription factor activity and concomitant dysregulation of target gene expression was demonstrated to account for a rising number of metabolic disorders¹⁷.

2.2.1. Transcriptional regulation of hepatic beta-oxidation

Beta-oxidation of fatty acids takes place in subcellular organelles such as mitochondria and peroxisomes. In addition, the endoplasmatic reticulum harbours high levels of cytochrome p450 family members (e.g. CYP4a) which catalyze the so-called omega-oxidation, the hydroxylation and subsequent catabolic breakdown of saturated and unsaturated fatty acids yielding Acetyl-CoA and dicarboxylic acids in times of nutrient excess. Dicarboxylic acids in turn constitute potent ligands for PPARalpha, a member of the PPAR class of transcription factors. This class of nuclear hormone receptors was initially discovered for binding compounds known to induce proliferation of peroxisomes¹⁸. The PPAR class of transcription factors consists of four isoforms, which exhibited distinct functions in hepatic lipid metabolism^{19, 20}. Whereas PPARgamma constitutes the key regulator for lipid biosynthesis in liver and adipose tissue (section 2.2.2 and²¹), PPARalpha regulates the beta-oxidation of lipids in hepatocytes in concert with PPARbeta and PPARdelta²². PPARalpha was identified as key transcriptional regulator for beta-oxidation of fatty acids in hepatocytes²³. PPARalpha senses extracellular serum levels of dietary lipids and, under satiety conditions, stimulates transcription of lipid-degrading enzymes²⁴. Upon prolonged fasting, fatty acids get shuttled from peripheral fat depots into hepatocytes, leading to activation of PPARalpha and induction of beta-oxidation in order to fulfil the body's energy demands²⁵. PPAR isoforms require

heterodimerization with the retinoic acid receptor (RXR) in order to initiate transcription of PPAR target genes²³. PPAR-RXR complexes specifically recognize and bind DNA elements containing AGGTCAAnAGGTCA sequences termed PPAR responsive elements (PPRE) in the 5'-promoter region of target genes²³. Most rodent and human genes, which possess crucial functions in transport or catabolism of fatty acids contain at least one PPRE in their promoter sequence (reviewed in²⁶). Experimentally validated PPAR target genes encode apolipoproteins, fatty acid translocases, lipases, cytochrome p450 family members and Acyl-CoA oxidases, yet many putative PPAR target genes still lack experimental proof²⁶. Very-long chain fatty acids represent the most established *in vivo* ligand of PPARalpha²⁷. The importance of PPARalpha in regulating fatty acid catabolism is underpinned by the phenotypes observed in PPARalpha knockout mice. These animals are unable to translocate fatty acids into the hepatocyte cytoplasm²⁸ and exhibit defects in clearance of fatty acids accumulated in hepatocytes upon prolonged fasting²⁹. The same phenotype is observed upon feeding of special diets known to channel the flux of lipids into the liver³⁰. The same hold true for mice harbouring a genetic abrogation of PPARalpha downstream targets (e.g. ACOX1)²⁷.

2.2.2. Transcriptional regulation of hepatic *de novo* lipogenesis

Three nuclear hormone transcription factors, which are independently regulated by glucose and insulin orchestrate the hepatic biosynthesis of fatty acids (*de novo* lipogenesis)^{31, 32}:

(i) Insulin induces the *de novo* lipogenesis of fatty acids by activating the sterol regulatory element binding protein 1-c (SREBP-1c), a membrane-tethered member of the basic helix-loop-helix leucine zipper family of transcription factors (bHLH-Leu-Zip)³³. Upon triggering by insulin, SREBP-1c translocates into the nucleus and initiates the transcription of lipogenic target genes^{34, 35}. Hepatic insulin resistance, the insensitivity of the liver to respond to insulin action leads to unbalanced increases in serum insulin levels (hyperinsulinaemia) and concomitant rises in lipogenic SREBP-1c activity^{35, 36}. Thus, insulin resistance is characterized by a high biosynthesis of fatty acids contributing to the development of steatosis³⁷. The significance of SREBP-1c-dependent lipogenesis has been demonstrated *in vivo* by generating SREBP-1c transgenic mice. These mutants exhibit a severe accumulation of

intrahepatic fat ³⁸. On the contrary, loss of SREBP-1c in hepatocytes leads to significant reductions of the hepatic lipid load ³⁹.

(ii) The carbohydrate response element binding factor/protein (ChREBP), another bHLH-Leu-Zip transcription factor mediates hepatic responses to varying plasma glucose levels ⁴⁰. Briefly, glucose induces binding of ChREBP to the promoter region of rate-limiting glycolytic enzymes such as pyruvate kinase (PK), in turn leading to an increased catabolism of glucose, the cleavage products of which are metabolized in the tricarboxylic acid cycle. Studies utilizing ChREBP knockout mice pinpointed towards additional lipogenic properties of ChREBP under hyperglycaemic conditions ⁴¹. High serum glucose levels (hyperglycaemia, closely associated with insulin resistant states) thus lead to ChREBP-1c-mediated induction of hepatic lipid biosynthesis and a concomitant accumulation of intrahepatic lipids.

(iii) PPAR γ , a member of the PPAR nuclear hormone receptor class of transcription factors exhibits key functions in the biosynthesis of fatty acids in liver. Abundantly expressed in adipocytes, PPAR γ was initially thought to be solely implicated in the differentiation of peripheral adipose tissues ^{42, 43}. Later, it was recognized that PPAR γ is expressed at low levels in hepatocytes. Interestingly, loss of hepatic PPAR γ expression interferes with the development of steatosis in respective mouse models ⁴⁴, whereas PPAR γ overexpression leads to development of fatty liver disease ^{45, 46}. Strikingly, a rising number of steatotic mouse models display increased hepatic PPAR γ transcript and protein levels ⁴⁷. Finally, an indirect crossactivation of PPAR γ -dependent transcription by SREBP-1c-mediated biosynthesis of PPAR γ ligands was demonstrated, thereby exacerbating fatty liver disease ⁴⁸.

2.3. Insulin signaling and insulin resistance

Binding of insulin to the heterotetrameric insulin receptor (IR) triggers insulin-dependent signal transduction. Two intracellular beta-chains and two extracellular alpha-chains (alpha₂beta₂) form the functional IR. Upon ligand binding, insulin induces conformational changes in the IR leading to autophosphorylation of specific tyrosine (Tyr⁹⁶⁰) residues in the IR beta-subunit (IRb) and subsequent exposure of docking sites for the Insulin Receptor Substrate 1 (IRS-1) adaptor protein ⁴⁹. IRS proteins (in humans comprising the IRS-1, IRS-2, and IRS4 isoform) are activated by IR-

mediated tyrosine phosphorylation leading to simultaneous recruitment of specific effector proteins such as Grb2 and Shc, which are responsible for triggering non-canonical IR-dependent signal transduction^{50, 51}, e.g. the Mitogen Activated Protein Kinase (MAPK) and Stat5 pathways upon insulin challenge⁵²⁻⁵⁴. MAPK eventually phosphorylates IRS-1 at specific serine residues leading to abrogation of IR-dependent signal transduction⁵⁵. In contrast, the canonical insulin-dependent signaling are conveyed via activation of phosphatidyl-inositol-3-kinase (PI3K) effector proteins, which in turn synthesise phosphatidyl-inositol (3,4,5) trisphosphate (PIP₃), a potent intracellular second messenger⁵⁶. PIP₃ triggers activation of the AKT family of serine and threonine kinases leading to the translocation glucose transporters to the plasma membrane (e.g. GLUT4).

Studies using IR knockout animals shed further light onto the role of individual IR signal transduction components: Hepatocyte-specific loss of IR proteins led to severely insulin resistant states and concomitant hyperinsulinaemia, decreased insulin clearance and adenoma formation⁵⁷. Deletion of either IRS-1 or IRS-2 in the liver surprisingly had little effects^{58, 59}, yet combined loss of IRS-1 and IRS-2 was embryonically lethal⁶⁰. Thus, redundant roles of IRS-1 and IRS-2 in hepatic metabolism were assumed⁶¹ although this concept recently came under scrutiny as refined genetic analyses rather claimed distinct functions for IRS-1 in the regulation of hepatic glucose metabolism and for IRS-2 in regulation of hepatic lipid metabolism⁵¹.

The term insulin resistance was coined to circumscribe a condition frequently observed in metabolic disorders such as obesity and NAFLD⁶². Insulin resistant states are generally characterized by blunted responses towards insulin action and harbour molecular impairments in IR-dependent signal transduction. Clinically relevant, insulin resistance often precedes severe metabolic conditions like T2D and NAFLD for decades and is associated with high risks for contracting cardiovascular diseases⁶³. Interestingly, an inverse correlation exists between hepatic insulin sensitivity and the accumulation of intrahepatic lipids (steatosis)⁶⁴, yet the causal relationship between steatosis and insulin resistance remains enigmatic^{65, 66}. It is undisputed that central and visceral obesity constitute a risk factor for developing insulin resistance. Surprisingly, serious insulin resistance is also observed among patients suffering from dystrophies of peripheral adipose tissues (lipodystrophy)⁶⁷.

2.4. Insulin resistance and liver steatosis

The development of fatty liver disease is closely associated with chronic alcohol abuse (alcoholic fatty liver disease; AFLD) ⁶⁸ as well as calory-excess; both leading to obesity and insulin resistance and NAFLD ^{22, 69}. NAFLD comprises a wide spectrum of diseases, ranging from the simple accumulation of intrahepatic lipids (steatosis) to inflammatory processes such as non-alcoholic steatohepatitis (NASH), fibrosis and degenerative processes such as liver cirrhosis and hepatocellular carcinoma (HCC) ⁷⁰. Steatosis as component of NAFLD was initially regarded as a benign condition, but was recently recognized to lead to more severe liver pathologies such as steatohepatitis and hepatic fibrosis. The incidence of NAFLD is considerable in the industrialized world, affecting up to 25 % of the population ⁷¹, more than 50 % of chronically obese and up to 90 % of morbidly obese patients ^{72, 73}. The significance of NAFLD is reflected in the observation that steatosis constitutes the leading cause of pathological liver tests in the US ⁷⁰. In addition, liver biopsies of one third of adult US citizens exhibit steatosis ⁷⁴. Microscopically, steatosis is diagnosed by the appearance of abundant cytoplasmic lipid droplets ⁷⁵. Macroscopically, steatosis is diagnosed whenever the amount of intrahepatic fat exceeds >5 % of total liver weight ⁷⁶.

The causal relationship between steatosis and insulin resistance remains uncertain (see section 2.2 and 2.3), although a significant correlation between insulin resistance and fatty liver disease exists ^{77, 78}. A similar correlation is observed in several mouse models for steatosis (section 2.4.1). Mechanistically, hepatic insulin resistance-derived hyperinsulinaemia was proposed to trigger SREBP-1c-mediated lipogenesis which subsequently induces steatosis ^{79, 80} (see section 2.2.2 and Figure 1). An alternative notion, the clinical manifestation of insulin resistance secondary to liver steatosis remains provocative, although recently researchers reported that transgenic overexpression of DGAT1, the rate-limiting enzymes of hepatic lipogenesis induces steatosis without accompanying insulin resistance ⁶⁵.

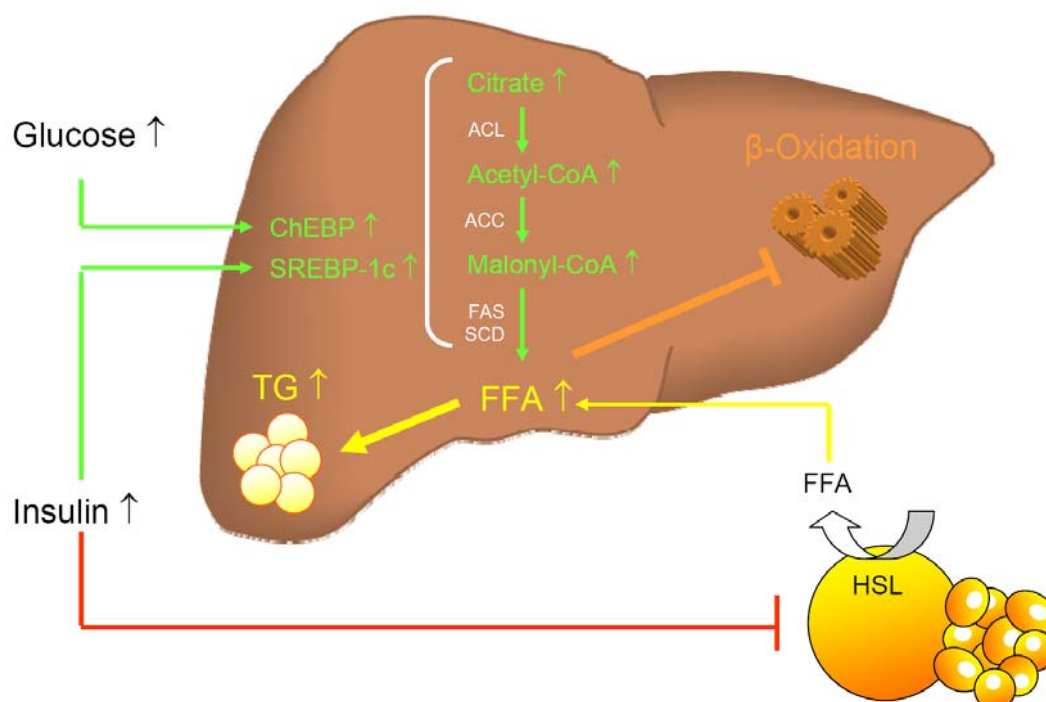


Figure 1. Interplay between insulin resistance and liver steatosis

Metabolic perturbations leading to the hepatic accumulation of triglycerides (steatosis) in insulin resistant states: One aspect of hepatic insulin resistance is the concomitant hyperinsulinaemia leading to increases in gluconeogenesis and induction of ChREBP-mediated lipogenesis. Insulin resistance in the adipose tissue triggers the activity of hormone-sensitive lipase (HSL), leading to hydrolysis of triglycerides in adipocytes and increased serum levels of free fatty acids which are eventually stored in the liver. High serum levels of insulin trigger SREBP-1c activation and results in increased hepatic lipogenesis. In concert with ChREBP, SREBP-1c activates enzymes essential for hepatic lipogenesis (ACL, ACC, FAS and SCD). Another aspect of insulin resistance is the impaired capability of hepatocytes to remove excess FFA by beta-oxidation.

2.4.1. Mouse models of NAFLD

NAFLD affects approximately one quarter of the healthy population in the western world ⁸¹, constituting a significant risk factor for contracting more severe liver diseases. Therefore it represents a logic disease stage applicable for therapeutic intervention. Apart from obvious modification of lifestyle habits this could also involve pharmacological manipulation. The need for animal models mimicking the complex onset and progression of NAFLD through genetic and environmental factor is apparent. The laboratory mouse, *Mus Musculus* shares many physiological, anatomical and metabolic features with humans and has been accepted as the species of choice in metabolic research. Transgenic mice harbouring specific genetic manipulations leading to defined metabolic phenotypes are well-suitable for therapeutic interventions in defined, homogenous populations. Generally, murine models for NAFLD are subdivided into two classes:

(i) Mouse models harbouring specific genetic modifications leading to deletion or overexpression of lipid metabolism-related genes. This strategy is exemplified in the ablation of anorexigenic genes (e.g. leptin) leading to hyperphagia and weight gain (*ob/ob* mouse⁸²; *db/db* mouse⁸³). An alternative approach is based on the systemic relocation of fatty acids from peripheral adipose tissues to the liver (*CD36*^{-/-} mouse⁸⁴) or on increased hepatic *de novo* lipogenesis by transgenic overexpression of lipogenic transcription factors (PPAR γ ^{tg}^{45, 46}, SREBP-1c^{tg}^{85, 86} and ChREBP^{tg}⁴¹). Finally, the hepatic combustion of fatty acids can be disrupted, leading to the defective clearance of lipids by beta-oxidation and the development of steatosis (*ACOX*^{-/-} mouse;²⁷).

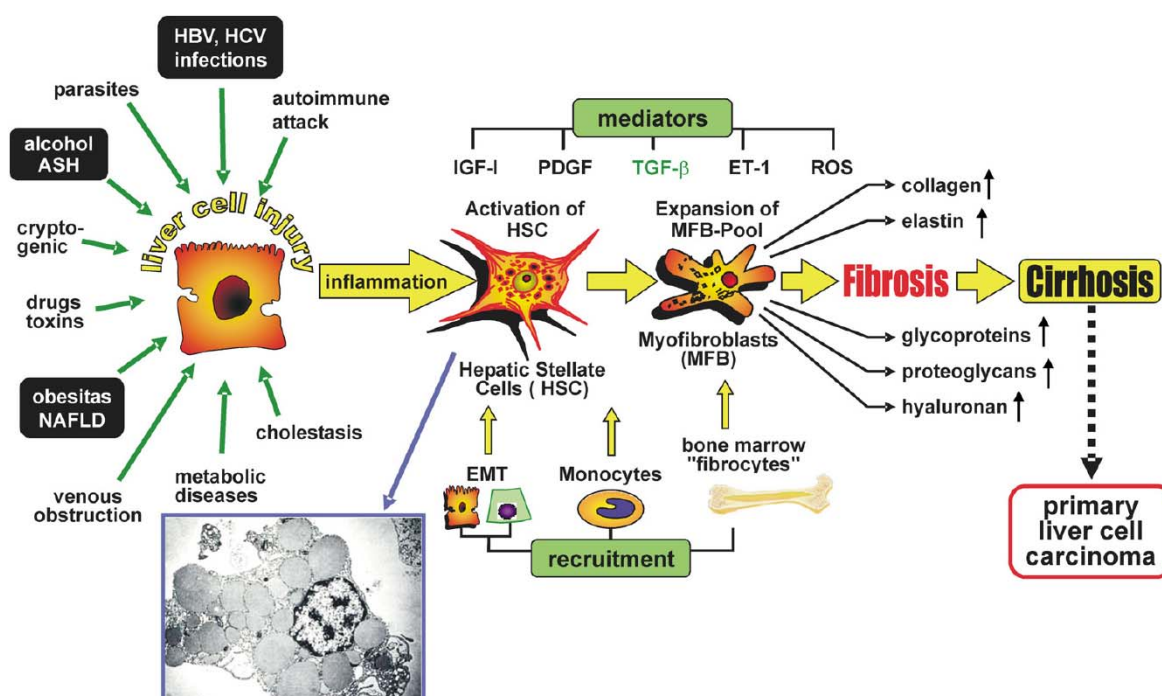
(ii) Mice develop NAFLD-like symptoms upon feeding high-calory, carbohydrate-rich diets⁸⁷. Moreover, specific diets, e.g. deficient for methionine and choline (MCD diet) interfere with the hepatic beta-oxidation machinery⁸⁸ leading to steatosis, late-stage steatohepatitis and hepatic fibrosis. The exact mechanism underlying pathogenesis remains elusive, yet an increase in reactive oxygen species (ROS) was noted⁸⁹.

Taken together, the rising morbidity of diseases like insulin resistance, obesity and NAFLD make animal models closely mimicking human disease imperative. Genetic and nutritional mouse models for NAFLD are well-suited for dissecting the complex metabolic processes underlying NAFLD pathogenesis.

2.5. Fibrosis of the liver

Liver fibrosis constitutes an abundantly diagnosed intermediate step in the progression of chronic liver diseases. It is widely believed to be secondary to multiple viral, bacterial and metabolic liver insults⁹⁰. One hallmark of liver fibrosis is the remodelling of extracellular matrix (ECM) constituents leading to abundant collagen deposition around hepatic lobes. High amounts of collagen eventually impede vital hepatic processes and lead to degenerative processes like fibrosis, cirrhosis and HCC⁹¹. These processes are accompanied by activation and transdifferentiation of non-epithelial, mesenchymal cells termed hepatic stellate cells (HSC)⁹². A multitude of stimuli such as high ROS level, immunological activation by parasites (*Schistosoma mansoni*) or intrahepatic accumulation of lipids was demonstrated to activate HSCs which in turn transdifferentiate into pro-fibrogenic cells called

myfibroblasts (MFB). This is accompanied by the appearance of mesenchymal differentiation markers such as alpha-smooth-muscle actin (SMA) and the subsequent deposition of collagens and proteoglycans⁹³ in the space of Dissé secondary to perturbations in ECM turnover such as an altered matrix metalloproteinase (MMPs) and tissue inhibitor of MMPs (TIMPs) secretion. Following transdifferentiation, MFB are rendered responsive to pro-fibrogenic signals such as platelet-derived growth factor (PDGF) and transforming growth factor beta (TGF β)⁹⁴. This in turn leads to activation of MAPK signaling⁹⁵, further proliferation of MFB and aggravation of disease. If left untreated, liver fibrosis cumulates in cirrhotic organ failure, liver carcinoma and death (Figure 2).



reproduction with author's consent from⁹⁶

Figure 2. Canonical pathogenesis of liver fibrosis (fibrogenesis)

According to the "canonical principle of fibrogenesis" primary hepatocyte damage leads to cell death and activation of HSC. The latter undergo epithelial-mesenchymal transition (EMT) into MFB. This process is accompanied by synthesis and secretion of ECM components such as collagen. Repetitive damage of fibrotic tissues leads to necrotic processes such as liver cirrhosis if left untreated. The MFB pool is replenished by bone marrow-derived fibrocytes, circulating monocytes or transdifferentiation hepatocytes and bile duct cells. Constantly refuelled, the MFB pool actively synthesizes ECM components, a process mediated by canonical fibrosis mediators such as platelet derived growth factor (PDGF), IGF-1, endothelin 1 (ET-1) or ROS. Abbreviations: ASH – alcoholic steatohepatitis; HBV/HCV, hepatitis B/C virus.

2.5.1. Molecular mechanisms underlying liver fibrogenesis

Specific cellular events accompany hepatic fibrogenesis: Firstly, HSC undergo transdifferentiation into MFB, upon which they actively secrete collagen into the intercellular space of Dissé. Secondly, activated MFB possess high proliferation capacities leading to elevated numbers of fibrogenic cells. These processes are mirrored in activation of two distinct PDGF-dependent mitogenic signaling pathways^{97, 98}.

(i) PDGF receptor (PDGFR) activation triggers activation of Raf, Mitogen Induced Extracellular Kinase (MEK) and Extracellular Signal Regulated Kinase (ERK) signaling^{99, 100}. Simultaneous activation of multiple MAPK pathways leads to accelerated MFB cell cycle progression¹⁰¹ and cellular proliferation¹⁰². The significance of PDGFR-driven cell proliferation is reflected in the observation that pharmacological targeting of MAPK family members delays MFB proliferation and decelerates progression of liver fibrosis¹⁰².

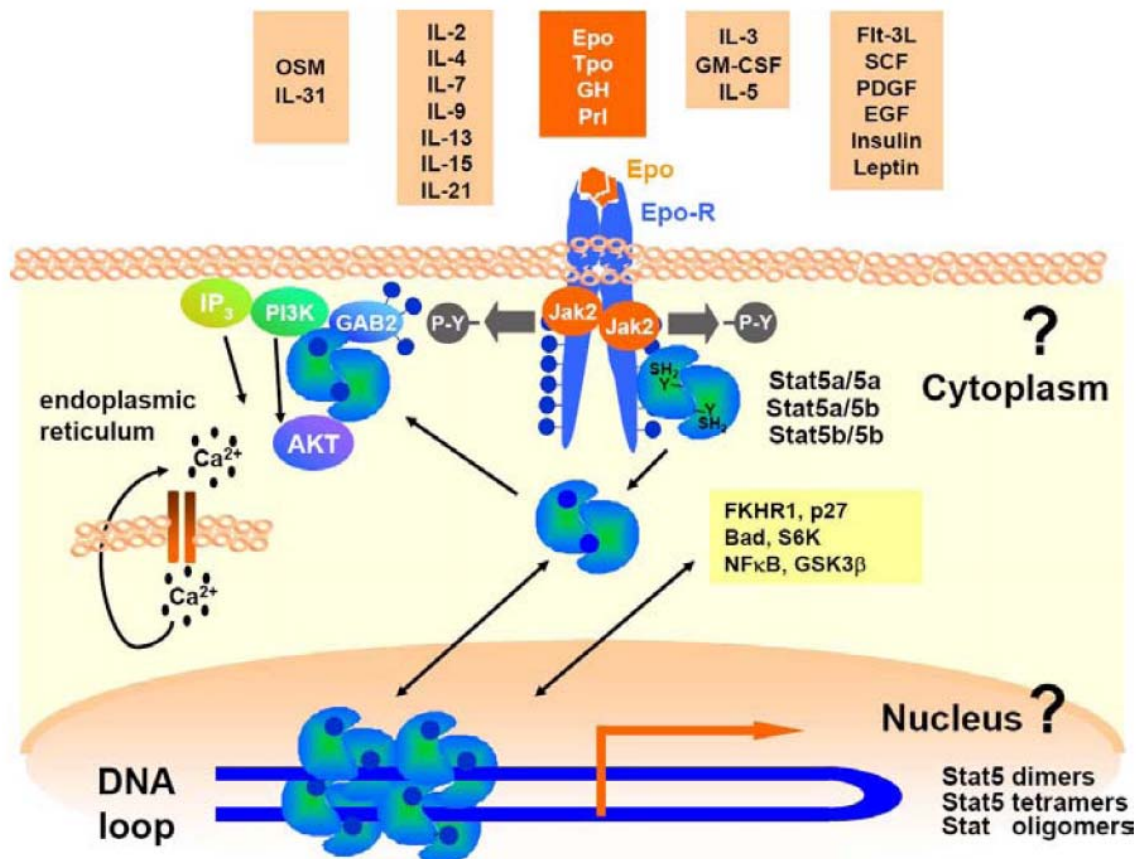
(ii) In addition, PDGFR phosphorylates Focal Adhesion Kinase (FAK) leading to active PI3K signaling¹⁰³. FAK and PI3K then synergistically drive MFB proliferation¹⁰⁴. Furthermore, phosphorylated PI3K activates AKT, an essential survival regulator stimulating cellular proliferation¹⁰⁵ leading to phosphorylation of p70 kinase: Taken together, these cellular events, result in sustained protein synthesis and the concomitant growth of fibrogenic cells¹⁰⁶. The paramount significance of PDGFR-FAK-PI3K-AKT pathway activation for fibrogenesis was confirmed by studies demonstrating that pharmacological inhibition of pathway constituents severely impairs MFB proliferation and ameliorates liver disease^{104, 107}.

Transforming growth factor beta (TGF β) constitutes another crucial profibrogenic cytokine. Upon ligand binding to the TGF β receptor (TGF β R), TGF β -derived signals are relayed to the nucleus by activation of cytoplasmic SMAD2 and SMAD3 transcription factors. SMAD2 and SMAD3 are closely associated with the TGF β R, constituting activated core complexes. Secondary association with SMAD4 yields trimeric transcription-competent complexes initiating RNA transcription of profibrogenic genes like type I and III collagens (COL1 and COL3)¹⁰⁸.

Taken together it is widely recognized that activation of PDGF signaling leads to potent HSC proliferation which triggers multiple cellular signaling cascades simultaneously (e.g. the MAPK and FAK-PI3K-AKT-p70 axes). MFB which have undergone the process of transdifferentiation from quiescent HSC require autocrine TGF β stimuli to sustain their fibrogenic properties.

2.6. Signal transducer and activator of transcription 5 (Stat5)

Signal transducer and activator of transcription 5 (Stat5) constitutes a critical transcription factor involved in controlling developmental and differentiation processes throughout the body. A component of linear Jak (Janus Kinase)/Stat signal transduction pathway, Stat5 is essential for the signal transduction of external stimuli triggered by upstream cytokine and growth factor receptor binding (Figure 3). Mechanistically, ligand binding induces conformation changes in receptors which in turn activate Jak kinases (Jak2 in the case of Stat5). This leads to phosphorylation and nuclear translocation of latent cytosolic Stat transcription factors. Activated Stat5 proteins recognize and bind specific DNA sequence motifs (so-called Stat5 responsive elements or Stat5 RE) located in the 5' promoter region of Stat5 target genes. Additional cofactors essential for transcriptional initiation are recruited, leading to the formation of transcription-competent protein complexes and transcription of genes implicated in cell proliferation, development, differentiation and survival (reviewed in ¹⁰⁹). A schematic illustration of growth factors and cytokines known to activate Stat5 is given in (Figure 3). Latent Stat5 monomers form homodimers upon phosphorylation, yet heterodimeric Stat3/Stat5 complexes have been reported, putatively in order to modulate Stat5 target gene specificity ¹¹⁰. Stat5 comprises two distinct isoforms, Stat5a and Stat5b, encoded by two different genes, precursors of which are already found in *Drosophila* ¹¹¹. The Stat5a/b isoforms readily form heterodimers and thus complicate the understanding of Stat5 biology. Stat5a is predominantly expressed in the hematopoietic system and mammary epithelia, whereas Stat5b constitutes the most frequent isoform expressed in hepatocytes. Because of this tissue-specific pattern, we focussed predominantly on the role of Stat5b in the current work.



(Kornfeld et al., *Front. Biosci.*, 2008)

Figure 3. Mechanisms of Stat5 activation by growth factors and cytokines

Stat5 is activated by ligands binding to cytokine and growth factor receptors. In this representation, cytokines and growth factor were clustered according to structural and functional homologies. After ligand binding, receptors undergo conformational changes leading to recruitment of Jak2 molecules in turn phosphorylating monomeric Stat5 molecules in the cytosol. Following nuclear translocation phosphorylated Stat5 dimers bind to Stat5 RE found in Stat5 target gene promoters. Among others, Stat5 target genes regulate postnatal body growth, cytochrome p450-dependent detoxification and hepatic lipid metabolism. Stat5 hyperactivation, e.g. by transformed tyrosine kinases such as Bcr-Abl, can induce leukaemic transformation. Hypoactivated Stat5 results in defective erythropoiesis and anaemia. Finally, Stat5 molecules possess a propensity to form oligomeric structures inducing conformational chromatin changes (DNA loop formation).

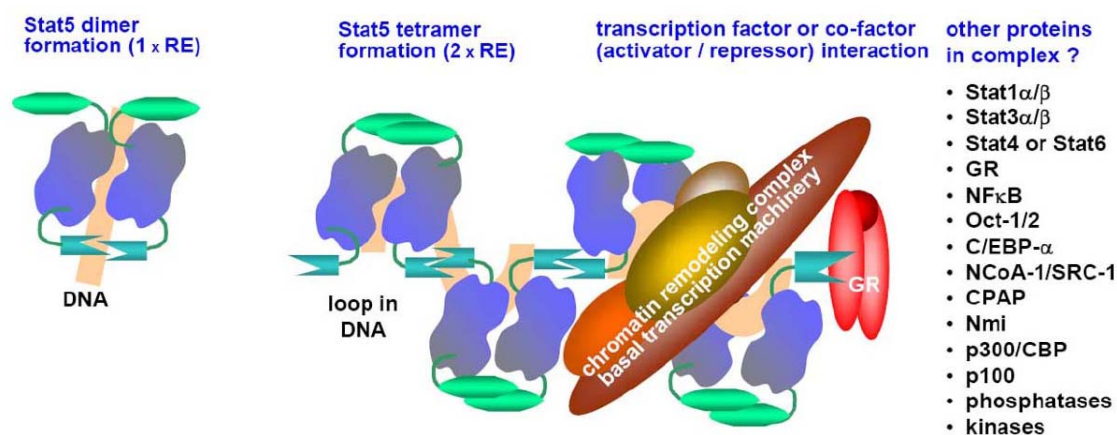
Like most Stat molecules, Stat5 consists of a flexible aminoterminal domain (N-terminus) followed by a alpha-helical coiled-coil (CCD) and a src homology 2 (SH2) domain; the latter is located in vicinity to the tyrosine residue critical for activation by Jak kinases such as Jak1-3. The carboxyterminal transactivation domain (TAD) constitutes the most divergent part of Stat5. A schematic illustration of the protein structure of Stat5a is given in Figure 4.



Figure 4. Protein structure of Stat5a

Stat5a proteins are encoded by seventeen exons leading to translation of five functionally discriminable domains: The N-terminal domain (NTD), responsible for cofactor interaction, (e.g. with the glucocorticoid receptor (GR, see below)), the coiled-coil domain (CCD), essential for lateral diffusion of Stat5 molecules on the DNA. Efficient DNA binding is also warranted by the DBD. The SH2 domain is indispensable for Stat5 protein interaction with its upstream kinase Jak2. The C-terminal transactivation domain (TAD) harbours critical tyrosine and serine residues, which are phosphorylated by Jak2 and lead to efficient dimerization and nuclear translocation of Stat5 molecules. Transcriptional coactivators like CBP/p300 also interact with this domain.

Unphosphorylated Stat5 forms rigid, antiparallel dimers with the N-terminal domain retaining its flexibility leading to protrusion from the dimeric Stat5 core complex. Formation of higher order complexes of Stat5 (particular Stat5 tetramers) depends on the Stat5 N-terminus. In addition, the Stat5 N-terminus constitutes the docking platform for essential transcription cofactors like TUDOR domain coactivators ¹¹², CBP/p300 ¹¹³ and (as revealed in this work), the glucocorticoid receptor (GR) ¹¹⁴. A schematic representation of established Stat5 protein interactors is given in Figure 5.



(Kornfeld et al., *Front. Biosci.*, 2008)

Figure 5. Stat5 oligomerization and cofactor interaction

Oligomeric Stat5 molecules (Stat5 tetramers) potentially rearrange the chromatic architecture and induce DNA loop formation. In addition, Stat5 tetramers recruit transcriptional cofactors/corepressors which in turn modulate Stat5 target gene specificity. Several components of the basal transcription machinery are reported to interact with Stat5 and are illustrated to the right.

2.6.1. Stat5 in health and disease

Among others, Stat5 possesses critical functions in regulating hematopoiesis and hepatic lipid metabolism. Hyperactivation of Stat5 is associated with severe conditions such as myeloproliferative diseases ^{115, 116}, inflammation ¹¹⁷, autoimmunity ¹¹⁸ and cancer ¹¹⁹. However, Stat5 hypoactivation can cause diseases such as myeloid hyperplasia and anaemia ^{120, 121}, dwarfism ^{122, 123}, immunodeficiency and metabolic problems ¹²⁴. One important aspect of this work was unravelling the significance of hepatic Stat5 signaling in regulating the postnatal body growth and

hepatic lipid metabolism. Hitherto known functions of Stat5 in controlling body growth and lipid metabolism are summarized in the following (section 2.6.1.1 and 2.6.1.2).

2.6.1.1. Stat5 and postnatal body growth

Serum Growth hormone (GH) potently activates hepatic Stat5 which in turn mediates the effects of GH on longitudinal body growth by transcription of bioactive Insulin-Like growth factor (IGF-1) ¹²⁵. Using transgenic mouse models, which express dysfunctional GH receptors (GHR) ¹²⁶ or harbours deletions of hepatic Stat5 ^{123, 127}, it was confirmed that GH signal transduction is largely mediated via Stat5 activation ^{122, 124}. Impaired secretion of GH or mutations of the GHR leads to dwarfism secondary to reduced levels of IGF-1, a condition termed Laron's syndrome ¹²⁸. In line with this, human patients harbouring Stat5 missense mutations are severely growth retarded ¹²⁹. Interestingly, a role for the glucocorticoid receptor (GR) in synergistic transcription of Stat5 target genes ^{114, 122} was demonstrated.

2.6.1.2. Stat5 and hepatic lipid metabolism

Stat5 signal transduction in the liver differs from other tissues in the regard that hepatocytes express predominantly the Stat5b isoform transcribing Stat5 target genes. An essential role of hepatic Stat5b, among others, is transcription of growth-promoting genes (e.g. IGF-1 and ALS) upon rhythmic GH pulses ^{129, 130}. Strikingly, hepatic loss of Stat5b leads to impairments of postnatal body growth and elevated levels of serum GH ¹²³. Studies involving GHR knockout mice elegantly demonstrated that elevated levels of lipolytic GH lead to substantial reductions of peripheral adipose tissues (lipodystrophy), an effect mediated by Stat5 in adipocytes ¹³¹. Further proof for the role of hepatic Stat5 in indirectly influencing adipose tissues came from mice expressing aminotermally truncated Stat5 proteins (termed Stat5^{ΔN} mice) ¹²⁷. These animals harboured reduced lipid reservoirs (lipodystrophy) ^{122, 127, 132} and in this regard resembled GHR knockout mice. The lipodystrophy was attributed to impaired negative feedback signaling via IGF-1. In both strains (GHR^{-/-} and Stat5^{ΔN}) ^{126, 133}, the main feedback inhibitor of GH secretion in the anterior pituitary gland.

Recently, the ablation of hepatic Stat5 was reported utilising Albumin-Cre-mediated recombination of floxed Stat5 alleles (Stat5^{AlbCre})¹²⁴, a targeting approach leading to an approximate 80% reduction in protein levels. Missing defects in postnatal body growth were attributed to incomplete losses of Stat5 in hepatocytes. Interestingly, mild perturbations of hepatic fat metabolism leading to mild liver steatosis were reported. Compensatory activation of Stat1 and Stat3 signaling was another consequence of incomplete hepatic Stat5 loss.

2.7. The glucocorticoid receptor (GR)

The GR transcription factor is expressed in most somatic cell types and is activated by compounds called glucocorticoids (GC), which are secreted under stress conditions by the adrenal gland. The GR constitutes an important executor of the neuroendocrine hypothalamus-pituitary-adrenal (HPA) axis. After GC binding, cytoplasmic GR dissociates from bound heat shock proteins (e.g. Hsp90), translocates into the nucleus and induces the transcription of GR-target genes^{134, 135}. Loss of hepatic GR signaling leads to well-studied defects in glucose metabolism such as impaired gluconeogenesis leading to hypoglycaemia under fasting conditions¹³⁶. This was attributed to blunted transcription of key gluconeogenic enzymes like phosphoenol pyruvate carboxykinase (PEPCK)¹³⁷ and glucose-6-phosphatase (G6P)¹³⁸. Adrenal release of GC is negatively regulated by serum GC itself. Impaired negative feedback leads to hypercortisolic conditions which are characterized by pathological lipid accumulation in peripheral adipose tissue or dermis¹³⁹. Structurally, murine GR is composed of several unique domains forming structural units: An aminoterminal TAD domain (termed AF-1) was shown to be responsible for cooperation with Stat5¹⁴⁰. The AF-1 function is followed by a DBD, which comprises two zinc finger domains, warranting specific GR binding to hormone response elements. The carboxyterminal ligand binding domain (LBD) guarantees ligand specificity and contains amino acid sequences important to homogenous dimerization, nuclear localisation signals and possesses another TAD termed AF-2 (Figure 6).



Figure 6. Gene and protein structure of the glucocorticoid receptor

GR proteins are encoded by nine exons encoding the aminoterminal TAD (also termed AF-1) responsible for binding to GRE in the promoter region of GR target genes. The DBD encompasses two zinc finger moieties and is indispensable for GR homodimerization. Finally, the LBD harbours nuclear localisation sequences, a second dimerization domain and the carboxyterminal AF-2 TAD.

2.8. Linear Stat5-GR signal transduction: Two transcription factor pathways converge

Activated GR not only potently binds onto GRE sequences leading to activation or repression of GR target genes. Strikingly, the GR was demonstrated to bind as cofactor to other transcription factors, thus modulating their transcriptome. This process does not require DNA binding of the GR¹⁴¹. The existence of a linear Stat5-GR signal transduction pathway was initially found in mammary epithelia, in which efficient Stat5-GR protein interaction was demonstrated to be a prerequisite for transcription of milk proteins during lactation (e.g. beta-Casein)¹⁴². Interestingly, loss of hepatic GR leads to stunted postnatal body growth reminiscent of mice deficient for hepatic Stat5¹¹⁴. Thus, it has been postulated that Stat5-GR protein interaction is mandatory for transcription of hepatic target genes essential for postnatal growth.

2.8.1. Growth hormone, glucocorticoids and body composition

Growth hormone and GCs, two major effectors of the neuroendocrine HPA axis potently activate Stat5 and GR in various organs. Both compounds have profound effects on body composition^{143, 144}. In adipose tissues, GCs possess anti-lipolytic properties and stimulate fat accumulation via LPL-mediated triglyceride hydrolysis¹⁴⁵, whereas GH exerts lipolytic effects by accelerating basal lipolysis in adipocytes¹⁴³. In addition, GH blunts fatty acid synthesis in adipose tissues¹⁴⁶ and impairs sensitivity towards insulin action, thereby leading to a reduction of transcript and protein levels of crucial lipogenic genes¹⁴⁷.

Thus, single administration of GH and GC leads to opposite effects on peripheral lipolysis¹⁴⁸. Intriguingly, combined stimulation with GH and GC *in vivo* leads to the dramatic mobilisation of peripheral adipose tissues exceeding GH-mediated lipolysis

alone¹⁴⁹. This concept was confirmed by *in vitro* reports demonstrating dramatic lipolytic drive in rat adipocytes elicited by co-administration of GH and Dexamethasone (DEX, a synthetic GR agonist extensively used in clinics)¹⁵⁰.

2.9. Conditional gene deletion using the Cre/LoxP system

The Cre/LoxP recombination system allows tissue-specific gene deletion in defined species such as the laboratory mouse¹⁵¹. First described in bacteriophages, the Cre/LoxP system consists of two components¹⁵²:

(i) DNA sequences essential for the function/structure of targeted proteins are flanked by palindromic loxP sequences (yielding a 'floxed allele').

(ii) The tissue-specific expression of the Cre proteins induces DNA recombination of floxed alleles resulting in the excision or inversion of respective DNA sequences, depending on either parallel or anti-parallel orientation of the loxP sites¹⁵³. The tissue-specificity of Cre expression is warranted by respective tissue-specific suituated upstream of the Cre expression cassette. This restricts Cre activity solely to promoter-responsive tissues. Usually, gene-sequences are floxed which do not interfere with overall expression of the protein; rather small domains essential for protein function are flanked by loxP sites. For example, for conditional inactivation of the GR, only the first zinc finger in the DNA binding domain is targeted, leading to transactivation-defective GR molecules. Another strategy is flanking whole genes loci with loxP sites. This is exemplified by conditional deletion of Stat5 by flanking the whole chromosomal locus of 110 kb containing Stat5a and Stat5b. Upon Cre activity, both Stat5 isoforms are excised. This representative example is illustrated in Figure 7.

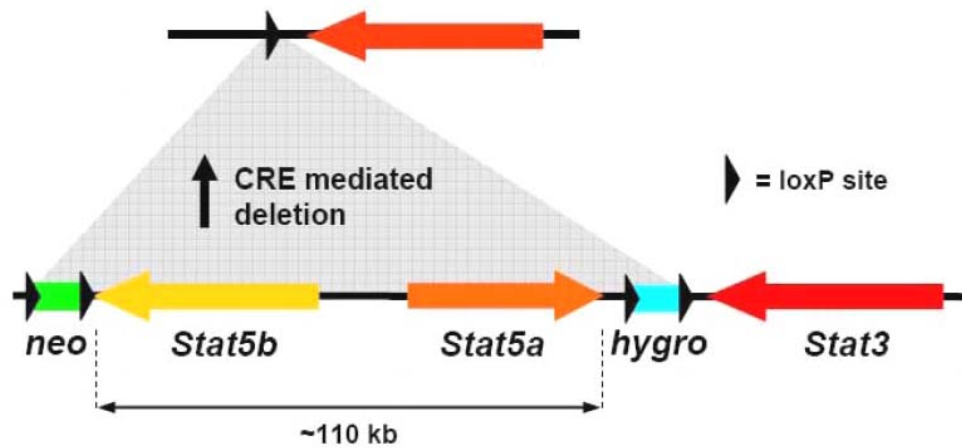


Figure 7. Tissue-specific loss of Stat5 using Cre/LoxP technology

The complete murine *Stat5a/b* locus, spanning 110kb of genomic DNA on chromosome 17, is flanked by loxP sites ('floxed' locus, *Stat5^{fl/fl}*). The crossing of *Stat5^{fl/fl}* mice with animals expressing Cre recombinase in a tissue-specific manner results in the excision of floxed DNA sequences.

2.10. Aim of the thesis

Stat5 possesses well-established functions critical for mediating cytokine and growth factors responses in the hematopoietic system. In contrast, the role of Stat5 in solid organs such as the liver remains poorly understood. It is widely recognized, that Stat5 in hepatocytes regulates postnatal body growth by transactivation of growth-mediating target genes such as IGF-1. Apart from classical functions as cytokine and growth factor responsive transcription factor, Stat5 interacts with the glucocorticoid receptor (GR), together constituting a linear Stat5-GR signal transduction axis leading to modulation of the Stat5 transcriptome.

Deletion of hepatic Stat5 alone leads to

- (i) severe perturbations of postnatal body growth
- (ii) (ii) an increased biosynthesis of lipids leading to fat accumulation in hepatocytes and
- (iii) (iii) defects in bile uptake leading to cholestasis, jaundice and secondary liver fibrosis.

In this study we aimed to investigate the underlying molecular processes leading to aforementioned phenotypes observed upon hepatic ablation of Stat5. Using knockout mice in concert with molecular biological techniques such as expression profiling, quantitative mRNA analysis, protein biochemistry and immunohistochemistry we aimed to shed further light on the role of hepatic Stat5 in health and disease. In addition, we put special emphasis on addressing the question whether above phenotypes were solely the effect of loss of hepatic Stat5 signaling or necessitated additional ablation of the GR.

3. Results

3.1. A linear Stat5-GR axis controls postnatal body growth

Hepatic Stat5 influences postnatal body growth via transcription of growth-related genes like IGF-1 and ALS upon GH action¹⁵⁴. Bioactive IGF-1 consists of IGF-1•ALS complexes, necessary for longitudinal growth of extremities such as bones and internal organs¹⁵⁵. Interestingly, hepatic deletion of the GR (GR^{AlfpCre}) leads to similar growth retardations as observed for Stat5 knockout mice (Stat5^{AlfpCre})¹⁵⁶. In addition, classical GH-triggered Stat5 target genes like IGF-1 and ALS were significantly reduced in GR^{AlfpCre} animals. Furthermore, Stat5 and the GR were reported to physically interact in the liver and the GR binds to Stat5 REs located in the promoter sequences of IGF-1 and ALS¹¹⁴. Collectively, this indicates that Stat5 and the GR are constituents of a linear signal transduction pathway in hepatocytes necessary for full transcription of growth hormone regulated Stat5 target genes like IGF-1 and ALS. This however stands in stark contrast to the hypothesis that postnatal growth is mediated by local production of IGF-1 in bone, cartilage and muscles upon GH action and that GH action in liver is dispensable¹⁵⁷. However, the possibility remains that the dwarfism observed in GR^{AlfpCre} mice is due to indirect consequences independent of Stat5, e.g. metabolic disturbances. To address the question whether (i) GH action in the liver is necessary for postnatal growth and (ii) whether and how this phenomenon involves physical Stat5-GR interaction, we generated mice harbouring deletions of Stat5 (Stat5^{AlfpCre}), the GR (GR^{AlfpCre}) or both (Stat5/GR^{AlfpCre}) in hepatocytes.

3.1.1. Loss of hepatic Stat5 and/or the GR signaling leads postnatal growth deficiency

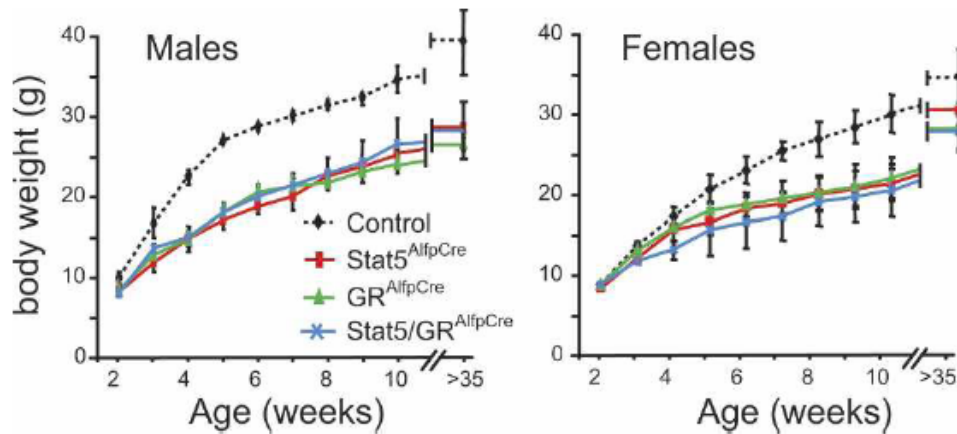


Figure 8. Growth deficiency in $Stat5^{AlfpCre}$, $GR^{AlfpCre}$ and $Stat5/GR^{AlfpCre}$ mice

Growth curves from control mice (control, **black dashed line**), mice lacking Stat5 in the hepatocytes ($Stat5^{AlfpCre}$, **red line**), mice lacking GR in hepatocytes ($GR^{AlfpCre}$, **green line**), and mice lacking both Stat5 and GR in hepatocytes ($Stat5/GR^{AlfpCre}$, **blue line**). All mutants show a very similar growth defect starting around 3 wk. Error bars indicate mean \pm SEM.

We wanted to confirm the growth-promoting role of Stat5¹²³ in mice harbouring conditional deletions of Stat5 selectively in hepatocytes using Cre/loxP technology. We crossed mice carrying the Cre recombinase under control of the albumin promoter and alpha-fetoprotein enhancer elements (AlfpCre)¹⁵⁸ with mice harbouring Stat5a and Stat5b genes flanked by loxP sites¹¹⁹. The resulting mutants ($Stat5^{AlfpCre}$) displayed normal postnatal body growth up to 2-3 weeks of age. After weaning at 3-4 weeks animals started exhibiting a severe growth retardation of ~30 % in males and ~20 % in females (Figure 8). Notably, the postnatal growth pattern of these mice was identical to those observed in mice lacking the GR in hepatocytes ($GR^{AlfpCre}$)¹¹⁴. To investigate whether the dwarfism resulting from ablation of either Stat5 or GR in hepatocytes was causally linked, we generated mice with a combined loss of hepatic Stat5 and GR signaling ($Stat5/GR^{AlfpCre}$). These animals showed overlapping growth curves compared to those of observed in $Stat5^{AlfpCre}$ and $GR^{AlfpCre}$ animals. This indicates that the dwarfism displayed by $GR^{AlfpCre}$, $Stat5^{AlfpCre}$ and $Stat5/GR^{AlfpCre}$ mice is linked, likely by a linear signal transduction pathway involving transcription-competent complexes consisting of Stat5 and GR.

3.1.2. Loss of hepatic Stat5 and/or the GR signaling leads to similar changes in gene expression profiles

We aimed to further underpin our hypothesis of a linear signal transduction axis comprising Stat5 and GR controlling growth-related genes upon GH action. In

addition, we questioned the fraction of the transcriptome co-dependently regulated by Stat5 and GR. We analysed livers from control, Stat5^{AlfpCre} and GR^{AlfpCre} animals and undertook Affymetrix whole genome expression analysis. Interestingly, the gene signatures significantly downregulated by ablation of either Stat5 or the GR overlap to a high extent (Figure 9A, left). The significance criterion was defined as either (i) $p < 0.001$ or (ii) $p < 0.05$ and fold change $> 2 / < 2^{-1}$. According to these criteria, 42 % of genes downregulated in GR^{AlfpCre} mice were concomitantly downregulated in Stat5^{AlfpCre} animals. Correspondingly, 26 % of genes downregulated in Stat5^{AlfpCre} mice were also downregulated in GR^{AlfpCre} mutants. The genes significantly upregulated in both mutants were far less abundant (Figure 9A, right). The high extent of overlapping genes was in the same range if less stringent criteria were applied (e.g. $p < 0.005$ or $p < 0.01$, not shown). To further corroborate the coordinate change of Stat5-GR co-dependent genes, we determined their expression changes in Stat5/GR^{AlfpCre} double knockout animals. As expected, we observed that genes significantly changed in a given direction in the single mutants were changed in the same direction with the same magnitude in Stat5/GR^{AlfpCre} mutants (Table 1A).

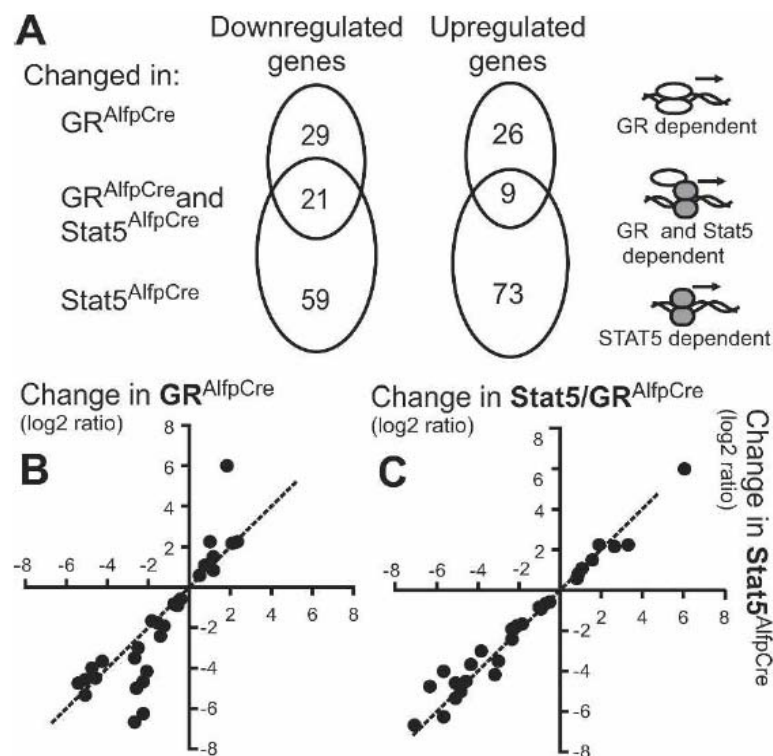


Figure 9. Substantial similarities in expression profiles from Stat5^{AlfpCre}, GR^{AlfpCre} and Stat5/GR^{AlfpCre} mice

(A) Venn diagrams showing the overlap of genes significantly changed in livers from mice with hepatocyte-specific deletion of Stat5 or GR. As criterion for calling a gene significantly changed we

used $p < 0.001$, or the combined criterion of $p < 0.0025$ and a log ratio >1 or less than -1 (fold change >2 or <0.5). Note the substantial overlap of genes downregulated by the two mutations. (B) Comparison between $Stat5^{AlfpCre}$ and $GR^{AlfpCre}$ mutants of the expression changes for genes significantly changed in both mutants. All of these genes are changed in the same direction in the two mutants and the magnitude of change correlates tightly. (C) Comparison of expression changes in $Stat5^{AlfpCre}$ and $Stat5/GR^{AlfpCre}$ livers for the same genes as in B. There is no additional effect of deleting GR in the absence of Stat5 for the expression levels of these genes.

The genes found to be significantly dependent on both, GR and Stat5, are listed in (Table 1), the complete list of genes significantly changed in a single knockout is accessible online at: <http://www.genesdev.org/cgi/content/full/21/10/1157/DC1> (Supplementary Table 1).

(A) Individual genes						
Down in $GR^{AlfpCre}$ and $Stat5^{AlfpCre}$		$Stat5^{AlfpCre}$	$GR^{AlfpCre}$	$Stat5^{AlfpCre}/GR^{AlfpCre}$	$Stat5^{\Delta N}$	Functional set
Gene name		Changes (log2 ratios)				
IGF-binding protein, acid labile subunit	Igfals	-6.7	-2.6	-7.1	-1.9	s, g
Insulin-like growth factor 1	Igfl	-6.3	-2.2	-5.7	-1.1	s, g
Epidermal growth factor receptor	Egfr	-5.3	-5.1	-5.1	-5.4	g, m
Cysteine sulfinic acid decarboxylase	Csad	-5.0	-2.6	-4.8	-3.3	g
Hydroxysteroid dehydrogenase-5	Hsd3b5	-4.8	-5.5	-6.3	-4.0	g, m, d
Suppressor of cytokine signaling 2	Socs2	-4.6	-5.1	-5.1	-2.8	g
Peroxiredoxin 4	Prdx4	-4.5	-4.6	-4.6	-3.6	
DNA segment, human D4S114	D0H4S114	-4.2	-2.1	-3.2	-2.5	
Serine proteinase inhibitor A3K (SPI2)	Serpina3k	-3.5	-2.7	-3.0	-2.5	g
Flavin-containing monooxygenase 3	Fmo3	-3.0	-2.5	-3.8	-3.6	
Hydroxysteroid 17 β dehydrogenase 2	Hsd17b2	-2.4	-1.4	-2.3	-0.9	d
Hydroxysteroid dehydrogenase-2	Hsd3b2	-1.8	-1.6	-2.1	-0.9	d
ζ -chain-associated protein kinase	Zap70	-1.7	-1.8	-1.8	-0.6	
Acidic ribosomal phosphoprotein P0	Arbp	-0.9	-0.6	-0.9	-0.4	
Leukemia inhibitory factor receptor	Lifr	-0.8	-0.8	-1.0	-1.0	
Cytochrome P450, 4f13	Cyp4f13	-0.7	-0.5	-0.7	-0.1	
Ribosomal protein L27a	Rp127a	-0.6	-0.4	-0.5	-0.3	r

(B) Groups of genes			
Down in $GR^{AlfpCre}$ and $Stat5^{AlfpCre}$		Up in $GR^{AlfpCre}$ and $Stat5^{AlfpCre}$	
	<i>p</i> -value		<i>p</i> -value
Somatomedin (IGF-1/ALS)	0	Genes repressed by GH	0
GH-responsive genes	0	Fatty acid metabolism	0.02
Ribosomal proteins (Rpl/Rps)	0		
Male predominant genes	0.003	Down in $Stat5^{AlfpCre}$	<i>p</i> -value
Steroid dehydrogenase	0.015		
		IFN- γ dependent genes	0
		Immune response	0
		Acute-phase response	0

Table 1. Genes and functional groups of genes that are regulated by Stat5-GR interaction
 (A) Genes significantly downregulated in $Stat5^{AlfpCre}$, $GR^{AlfpCre}$, $Stat5/GR^{AlfpCre}$ and $Stat5^{\Delta N}$ mice. Expression changes are given as log2 ratios of fold changes. If they belong to any of the significantly changes gene sets (see below, B) it is indicated in the far right bar. Abbreviations indicate (s) Somatomedin mediators; (g) GH responsive genes; (m) male predominant genes; (d) steroid dehydrogenase; (r) genes encoding ribosomal proteins. (B) Functional gene sets in which changed genes are enriched, determined using MAPPfinder software (see Methods).

The extensive overlap between expression changes observed in either single-deletion knockout mouse could be explained by (i) a direct functional interaction of the two transcription factors acting in a linear signal transduction fashion or (ii) may

be due to independent regulation of the same set of genes. To distinguish between those two putative mechanisms, we argued the following way: If there is a direct physical interaction between Stat5 and the GR, the magnitude of change of a given gene should correlate in Stat5^{AlfpCre} and GR^{AlfpCre} mice. If, in contrast, this is not the case, the actions are probably independent. To address this issue, we plotted the fold change as log₂ ratio of significantly changed genes in Stat5^{AlfpCre} and GR^{AlfpCre} against each other (Figure 9B). The positive correlation of fold changes between the two single mutants indicated the presence of a 'positive' interaction. In contrast to the general tendency, a small subset of genes was less affected in the GR^{AlfpCre} mutants, indicating that Stat5 action on these Stat5-dependent promoters is not totally dependent on the GR. To further expand the interpretation of our data, we similarly plotted the expression changes of coregulated genes in Stat5/GR^{AlfpCre} versus Stat5^{AlfpCre} (Figure 9C). The similar positive correlation indicated that the GR is not able to significantly alter the expression changes under conditions in which Stat5 is lacking. We concluded that the activating effect of the GR is completely dependent on protein-protein interaction with Stat5. Collectively, these findings strongly support a model of Stat5 and GR regulated expression of specific gene subsets via direct interaction with each other.

Next, we aimed to elucidate which functional groups of genes are predominantly affected by Stat5-GR interaction in the liver. We utilized the MAPPfinder software to find gene groups with coordinate changes¹⁵⁹. This approach can detect low-amplitude changes common to many genes attributed to a functional group. This is superior to detecting high-amplitude changes given for a single gene as compensatory mechanisms exerted by functionally related genes are not taken into account. We found that Stat5-GR interaction is important for many gene sets (Table 1B). Noteworthy was the strong dependency of the gene sets designated to "fatty acid metabolism" and "genes repressed by GH". The coordinate expression changes elicited by Stat5 and the GR correlate closely with those found for various truncations of the GH receptor (GHR)¹⁶⁰. The observed changes for male-predominant genes were in line with earlier reports from the Waxman group¹⁶¹ which reported sex-specific gene expression to be dependent on GH action and hepatic Stat5.

3.1.3. The N-terminus of Stat5 constitutes the docking platform for the GR

To shed further light on the nature of Stat5-GR protein interaction in hepatocytes, we utilized livers from mice harbouring N-terminally truncated versions of Stat5a and Stat5b proteins (Stat5^{ΔN} mice). The N-terminus of Stat5 was reported to be of importance for oligomerization of Stat5 proteins¹⁶². Initially designed as complete Stat5 knockout mouse, Stat5^{ΔN} mice still express considerable amounts of N-terminally truncated Stat5 proteins, approximately 30-40% of control protein levels¹¹⁵. We further utilized Stat5^{ΔN} mice because they displayed growth retardations comparable to Stat5^{AlfpCre}, GR^{AlfpCre} and Stat5/GR^{AlfpCre} mutants¹¹⁴, putatively due to similar molecular perturbations in the liver. Collectively, these mice are regarded as an *in vivo* model for studying the physiological consequences which are secondary to the loss of the Stat5b N-terminus. As Stat5b is the predominant Stat5 isoform expressed in the liver, no considerable amounts of Stat5a were detected (not shown). We thus detected only the low-molecular weight Stat5b^{ΔN} isoform in livers of Stat5^{ΔN} mutants, which were fully tyrosine phosphorylated upon GH stimulation (Figure 11A). Also, GR^{AlfpCre} mice exhibited normal tyrosine phosphorylation properties upon GH challenge. To further investigate whether GH-induced tyrosine phosphorylation led to normal DNA binding of Stat5b^{ΔN} proteins we performed electrophoretic mobility shift assays (EMSA) on classical Stat5 responsive promoter elements (beta-Casein elements). Stat5b^{ΔN} proteins fully bound beta-Casein elements upon GH activation compared with full-length Stat5b (Figure 10).

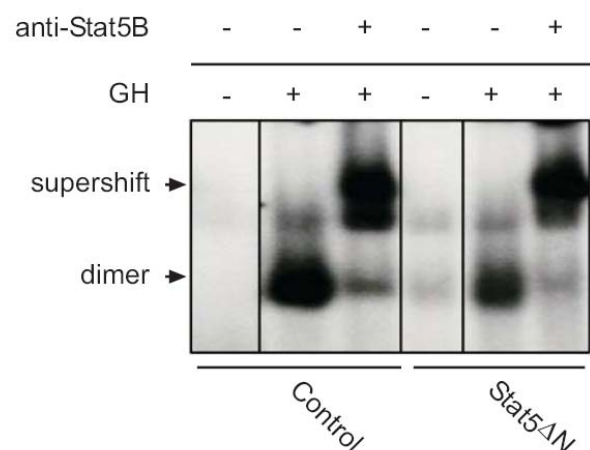


Figure 10. Stat5^{ΔN} proteins fully bind to Stat5 responsive elements upon GH challenge *in vivo*
 Liver extracts from control and Stat5^{ΔN} mice were subjected to EMSA analysis in order to assess the DNA-binding properties of Stat5 isoforms *in vivo* upon GH stimulation. Tyrosine phosphorylation of Stat5b^{ΔN} proteins resulted in a comparable DNA binding activity on classical Stat5 RE from the beta-Casein promoter compared with full-length Stat5b.

Next, we performed chromatin-immunoprecipitation (ChIP) assays to investigate the chromatin-binding properties of Stat5b^{ΔN} proteins on classical GH-triggered Stat5 targets. GH stimulation led to significant binding of Stat5b as well as Stat5b^{ΔN} proteins to specific Stat5 responsive elements in the promoter regions of IGF, ALS and Socs2. N-terminally truncated Stat5b^{ΔN} proteins retained an approximately 70-80% binding capacity to these chromatin regions compared with full-length Stat5b proteins (Figure 10B). To further investigate whether the N-terminus of Stat5b is essential for protein interaction with GR, we performed immunoprecipitation (IP) assays (Figure 10C). Reciprocal co-immunoprecipitation with anti-GR or anti-Stat5 specific antibodies revealed Stat5-GR protein interaction in both directions. However, the specific Stat5-GR interplay was lost in Stat5b^{ΔN} mice.

Thus, we concluded that the N-terminus of Stat5b constitutes the docking platform for the GR in hepatocytes.

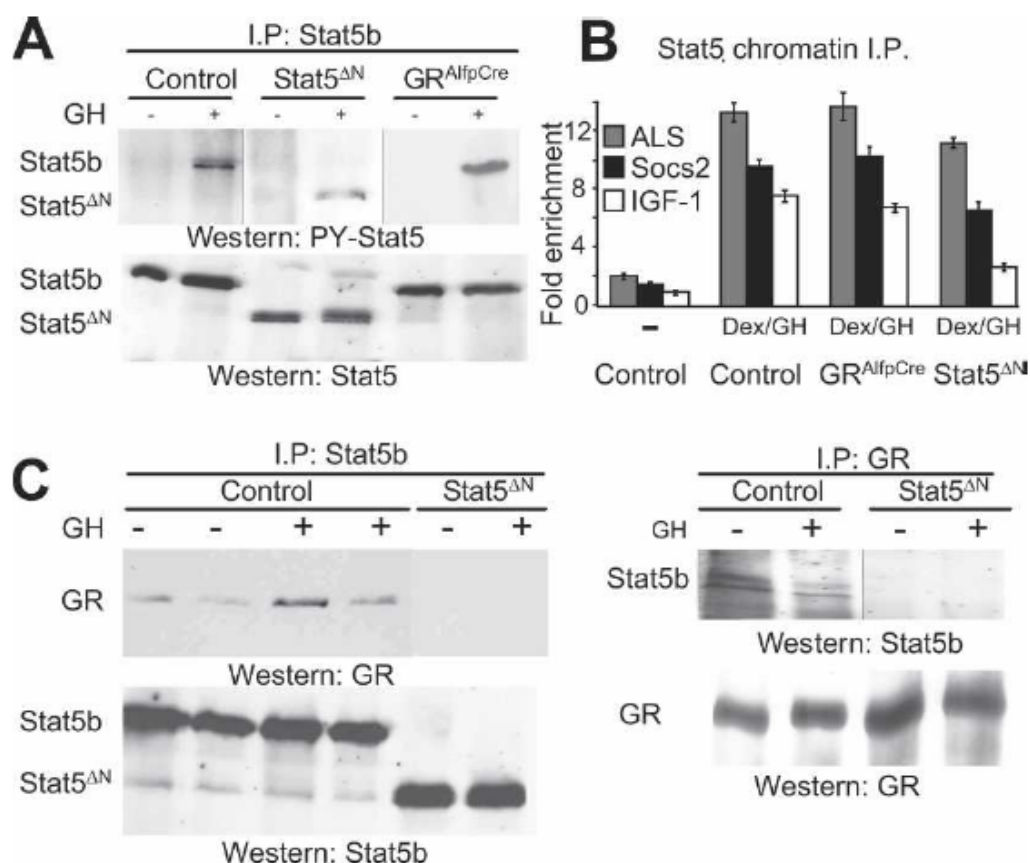


Figure 11. Stat5-GR interaction is dependent on the Stat5b N-terminus

(A, top) Liver extracts were prepared from untreated or GH injected mice, followed by quantitative anti-Stat5b immunoprecipitation (IP) and subsequent immunoblotting with an anti-pY-Stat5 antiserum. (A, bottom) Blots were stripped and reprobed with an anti-Stat5b-specific antiserum. Stat5b and Stat5b^{ΔN} proteins are fully tyrosine-phosphorylated upon GH stimulation. The amounts of total Stat5b were reduced to ~40% in Stat5^{ΔN} mice. (B) *In vivo* binding of Stat5 to proximal enhancers of ALS, Socs2 and IGF-1. The fold enrichment for each DNA fragment upon immunoprecipitation by anti-Stat5 followed by quantitative PCR is illustrated as bar graphs (mean ± SEM). Upon GH stimulation, wild-type Stat5b is highly bound to chromatin. Stat5b^{ΔN} displays ~50–70 % of the

DNA binding capacity of full-length Stat5b. (C) The N-terminus of Stat5b is essential for Stat5b-GR interplay. Reciprocal immunoprecipitation of liver extracts using anti-Stat5b (left) or anti-GR (right) antisera. (Left) Stat5b^{ΔN} as well as full-length Stat5b proteins are efficiently immunoprecipitated with anti-Stat5b antisera (bottom), but only wild-type Stat5b interacts with the GR (top). (Right) GR proteins are comparably pulled down (bottom), but only full-length Stat5b is co-immunoprecipitated (top). Four similar experiments were performed and one representative analysis is shown.

Expression profiling of Stat^{ΔN} livers revealed that some of those genes previously identified as Stat5 responsive genes were expressed at normal levels while some others were downregulated. Notably, most genes that were exclusively dependent on Stat5 but not on interaction between Stat5 and the GR were unchanged in Stat^{ΔN} mice. In contrast, most genes co-dependent on Stat5-GR interaction displayed compromised expression in Stat^{ΔN} animals (Figure 12A, B). In addition, Stat5 responsive genes that were only partially dependent on the interaction with GR were concomitantly only partially dependent on the N-terminus of Stat5b (Figure 12C). These results supported our hypothesis that the N-terminus of Stat5 is important for protein interaction between Stat5 and the GR. Moreover, the overlapping expression changes observed in Stat5^{-AlfpCre}, GR^{AlfpCre}, Stat5/GR^{AlfpCre} and Stat5^{ΔN} mutants are likely due to the disruption of Stat5-GR protein complexes.

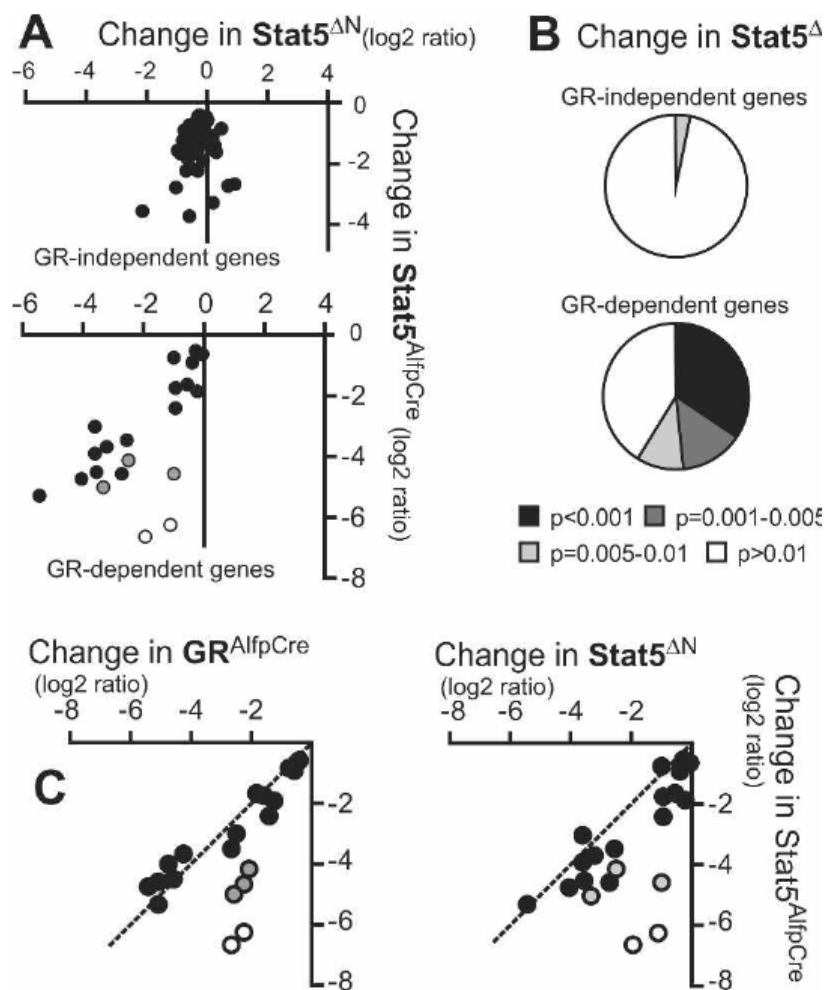


Figure 12. Deletion of the Stat5 N-terminus selectively reduces the expression of Stat5-GR co-dependent genes

(A, B) Magnitude (A) and significance (B) of expression changes of (i) GR independent (top panel) and (ii) GR dependent (bottom panel) Stat5 responsive genes in livers of mice lacking the N-terminus of Stat5 ($\text{Stat5}^{\Delta N}$). Those Stat5 responsive genes that are not dependent on the GR show very little dependence on the N-terminus while many of the Stat5 responsive genes that are dependent on the GR are severely affected by the loss of the Stat5 N-terminus. (C) Comparison within the group of GR dependent Stat5 target genes. Those genes that are only partially GR dependent (white and gray dots, left panel) are also only partially dependent on the N-terminus of Stat5 (right panel).

Collectively, we could show that physical protein interaction between Stat5 and the GR in hepatocytes is necessary for ensuring proper postnatal growth. Using conditional mouse models, whole genome expression profiling (Affymetrix analysis) and biochemical methods we could corroborate that physical Stat5-GR interaction is necessary for full transcription of specific gene subsets. Functional gene groups depending on Stat5-GR interplay include genes responsible for fatty acid metabolism (not shown herein) and postnatal body growth. The latter includes genes like IGF-1, ALS and Socs2, important genes implicated in regulation of longitudinal body growth. In addition, we could identify the N-terminus of Stat5b as docking platform for the GR

in hepatocytes. Growth defects observed in mice harbouring N-terminally truncated Stat5 proteins (Stat5^{ΔN} mice) are likely due to an impaired Stat5-GR protein interaction. GH-induced tyrosine phosphorylation and DNA binding of Stat5^{ΔN} proteins were unaltered and thus could not account for the dwarfism seen in Stat5^{ΔN} mice.

3.1.4. Socs2 as example for Stat5-GR co-dependent gene transcription

Suppressor of cytokine signaling 2 (Socs2) belongs to the Socs family of proteins which are transcribed upon cytokine action and serve as potent negative feedback regulators, e.g. for signals leading to activation of the Jak/Stat pathway¹⁶³. Although Socs proteins are rather promiscuous in their upstream specificity, the transcription of the Socs2 isoform is widely recognized to be driven by GH-induced Stat5 activation alone^{164, 165}. A growing body of evidence supports the notion of Socs2 serving as major negative regulator of the GH-Stat5 axis¹⁶⁶. Genetic studies underpinned the pivotal role of Socs2 in growth and development: Socs2 knockout mice exhibit gigantism, a severe increase in longitudinal growth due to sustained Stat5 activation and elevated IGF-1 levels. Recent reports revealed roles for activated glucocorticoid receptor (GR) in supporting Stat5-mediated transcription of Socs2 mRNA¹¹⁴. In addition, a substantial decrease of Socs2 mRNA transcription in knockout mice lacking either Stat5 (Stat5^{AlfpCre}; log2ratio (L2R) -4.6 vs. controls), the GR (GR^{AlfpCre}; L2R -5.1 vs. controls) or both (Stat5/GR^{AlfpCre}; L2R -5.1 vs. controls) in hepatocytes was observed using our whole genome expression analysis (Table 1). Moreover, Socs2 mRNA levels were severely decreased in mice which lack the aminoterminal Stat5 domain, which is critical for interaction with the GR (Stat5^{ΔN}; L2R -2.8 vs. controls). Thus, we presumed that the decrease in Socs2 transcription was due to disrupted Stat5-GR protein interaction serving as example for genes regulated by linear Stat5-GR signal transduction. Interfering with either Stat5 or GR signaling thus results in decreased levels of Socs2 mRNA.

3.1.4.1. The Socs2 promoter harbours putative Stat5-GR responsive elements

It is widely recognized that ample transcription of Stat5 target genes requires oligomerization/tetramerization of Stat family members, exemplified for Stat5a/b proteins^{167, 168}. Interestingly, those genes demonstrated to depend on functional Stat5-GR protein interaction often harbour tandem Stat5 responsive elements (Stat5 tetramer sites, Stat5 2xRE) in their 5' promoter regions. Promoters with several Stat5 2xRE were especially found in growth-related genes such as IGF-1, ALS and Socs2¹¹⁴. To investigate this phenomenon in more detail we utilized bioinformatics screening of the Socs2 promoter region and identified three Stat5 2xRE therein (Accession No. NT_039500, Figure 13). All tandem sites were spaced in close vicinity (<30 bp), which could allow for DNA loop formation as a prerequisite for Stat5 tetramerization.

```

* = 3443bp 5' of translation start [ATG]

*ttaagtttacagaaaacgtagggacctaagaaggaagcatcctgtaagttactccctggcttacacaggcttctaaaactgagt
aagaggcatcctcccacaaagatccaggaaaacagcctccccctccgaggccacacatacgaatctatcgctgacaagcccct
gtaagctggctatgtctcccctcgcttaccattctgtaagtgcataagaattttaagaggaaaaaattactgtggataaaaattggt
cggggcttggaattggccgctgctgtgttctccaggccggcaggcggggaccaggcaaggcttgaagccgctctct
caacctctcctggccaccctgcccactcccatagacacagcttcaactaaaagtgccattgaccttcaagctttgagcagtg
gcaacagaacagtattcaagaaaaatggtatcgaaattcgaatccggttcccatgaggtttttttgttttctgttaaaaaa
aaaaaagtaggtcattcaagtggtcacgtttcaggagccggctgcctggatgcggcgaggaggtaggtggcctcttacaga
gtgggaggtgagggtccaataggaagaagtagctgggatcaatacgaactccgggtccctggcttgaaggattcacagagaaa
acgcaccaggcctgtgacccccacccccgggcacaggaagggcacctcctctgtaggtggcagggtgggtctcccgaag
ggcaagcaggagttgagctgaggaggaaggagaagctgggcaaggctgatcaggggactaccagttggagctccagggggg
agggattgagggcagctctgcagctttaaggaggcgctcagctctcttctcctggcctctaggatgctggcggaggggacagctct
ggtcgtctcccagggtcccgaggtagtgtagctgagctggcagctgctgtagctctgctgtgtgtcttagagaggaggga
cggacatctgagccccccccctcccgacgctgctcctccacatggaggagaggaggtcgctctggcaggcgacagc
gggtggatggctggcctaaaggtccctcctacgtggagggtggggagaagagggtgctattcggggaccgaggtgctcagct
gttcagacacaggggcaGGTACgtgtgcttaataggcattggctgggacttctctTGTTCCcgagcaccgaggtgag
ggtcagaggagggcgagctgcaggctccacccccgagccaccagcaccagcaccgacccgctctctccaccggctcccctg
aagcctgcgattagcggccgggctcttaagcgctggcggggctcgggtcacgtgaggggctctggaaactctctggaa
gcgccctccgcgggccggggcgaggggggggaggggaggggagggcgctgggaggtcgcg
cacactcggtccggggaca**

** = 1832bp 5' of translation start [ATG]

```

Figure 13. The Socs2 promoter (-3443 to +1 bp) harbours three tandem Stat5 RE (Stat5 2xRE)

Tandem Stat5 REs (Stat5 2xRE) were identified in the 5' promoter region of Socs2 by bioinformatics screening for two tandem linked Stat5 RE (TTC(T/C)N(G/A)GAA) in close vicinity ($n < 30$ bp; gray). Underlined sequences were used for EMSA analysis (see Figure 15). Black arrows indicate Stat5 2xRE#1 (-3351/-3329 bp upstream of ATG; top), Stat5 2xRE #2 (-2976/-2931bp; middle) and Stat5 2xRE #3 (-1964/-1944bp; bottom). Additional GR responsive elements found in the Socs2 promoter are capitalized.

To test whether transactivation of the Socs2 promoter requires synergistic Stat5 and GR signaling, we designed three Luciferase (LUC) reporter constructs harbouring truncated versions of the proximal Socs2 promoter. Each of these constructs (termed I-III) harboured:

- (i) A core region of the Socs2 promoter containing the three Stat5 2xRE (-3443 bp/-1832 bp)
- (ii) Additional 5'- and 3' regions flanking the three Stat5 2xRE-containing core region to assess the requirement for putative enhancer sequences.

Promoter constructs I-III were amplified by polymerase chain reaction (PCR) as described in Methods (section 5.2.2.1) using 5' overhang primers containing restriction sites for enzymes MluI, BglII and HindIII. Subsequently, PCR products were cloned by appropriate restriction enzyme digestion and T4 ligation into the multiple cloning site (MCS) of a LUC reporter vector under the control of a 5'-minimal TA promoter (Figure 14 and Methods).

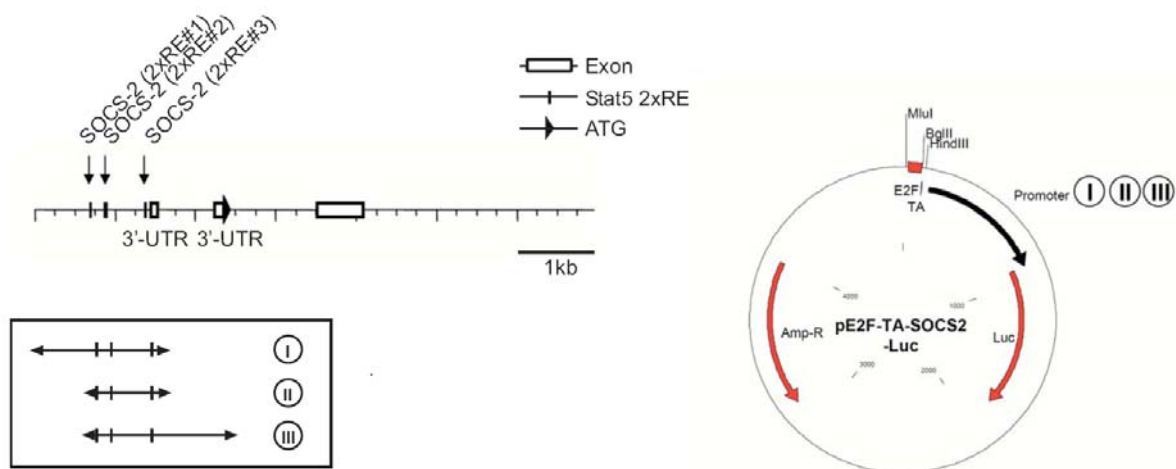


Figure 14. Socs2 promoter regions cloned for LUC reporter assays

Socs2 reporter constructs No. I-III containing the three Stat5 2xREs (Stat5 2xRE#1-3; left) were cloned into the MCS of a LUC reporter vector under the control of a minimal TA promoter (right). Additional 5'- and 3'- regions of the Socs2 promoter were included in Construct I+III to assess for putative enhancer elements. Correct assembly of vector constructs was confirmed by restriction analysis and DNA sequencing.

3.1.4.2. Putative Stat5-GR DNA binding sites in the proximal Socs2 promoter are Stat5 responsive

First, we investigated whether the three Stat5 2xREs located in murine Socs2 promoters are recognized activated Stat5 molecules. Figure 15 shows an EMSA analysis illustrating the Stat5 binding properties *in vitro* and *in vivo* on all three Stat5 2xRE located in the Socs2 promoter. First, human HEK 293 cells were transfected with Stat5b and the erythropoietin (Epo) receptor (EpoR), a cytokine receptor structurally related to the GHR triggering potent activation of Stat5 upon Epo ligand binding. Subsequent stimulation with 25 U/ml Epo for 30 min led to significant binding of Stat5 protein onto all three Stat5 2xRE#1-3 *in vitro*, albeit to a less extent onto Stat5 2xRE #2. No DNA binding of Stat5 molecules was observed under basal, non-stimulated conditions. Stat5 specificity was confirmed via supershift analysis using high affinity Stat5b-specific antisera. This led to the specific retention of ³²P-labeled oligomer-Stat5-antibody complexes (Figure 15; upper panel). Similar as observed upon Epo stimulation of HEK293 cells *in vitro*, GH potently activated hepatic Stat5 *in vivo* leading to high affinity binding of Stat5 onto Stat5 2xRE#1-3 elements in the murine Socs2 promoter. Interestingly, Stat5 2xRE #2 recruited significantly less phosphorylated Stat5 molecules, corroborating observations for *in vitro* stimulated Stat5. All complexes bound to ³²P-labeled oligomers contained Stat5 molecules as confirmed by supershift analysis (Figure 15; lower panel). Evidence for Stat5b tetramerisation on the Socs2 binding sites was not predominant; rather Stat5b dimers were detected.

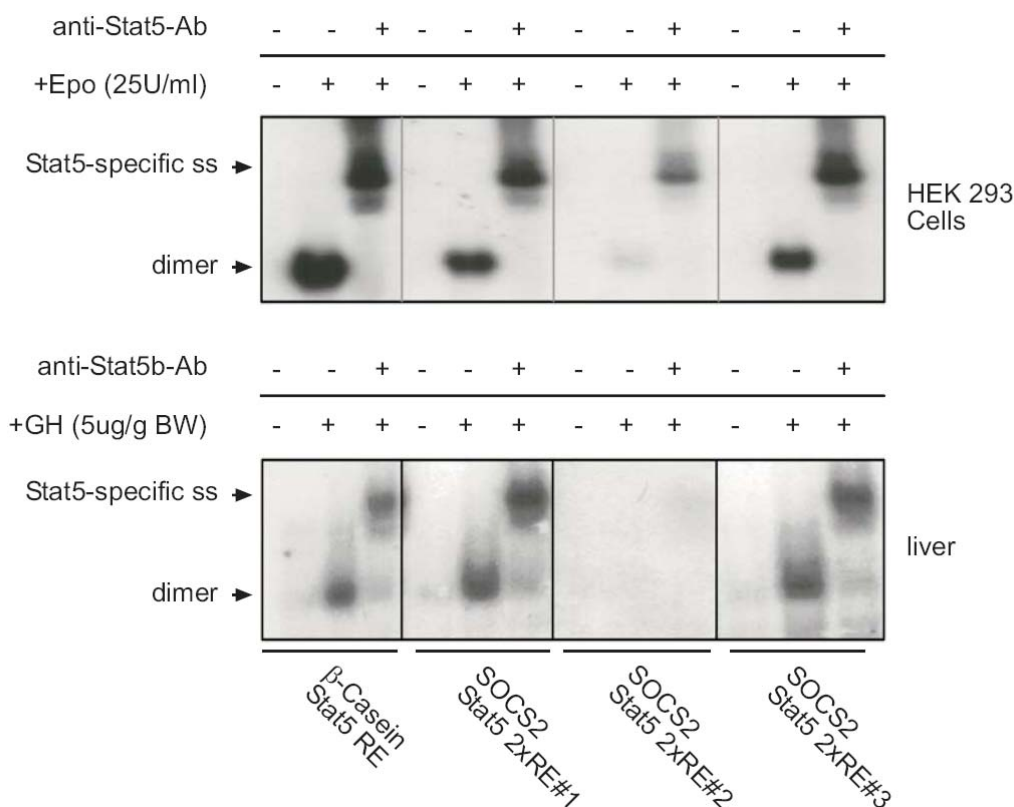


Figure 15. Activated Stat5 binds to Stat5 2xRE in the Socs2 promoter *in vitro* and *in vivo*

Electromobility shift assay (EMSA) analysis of Stat5 2xRE#1-3 (as introduced in Figure 13). (Top) HEK 293 cell extracts were transfected with the EpoR and Stat5 and Epo-stimulated for 30 min. Extracts were analysed for binding of activated Stat5 onto Stat5 2xRE#1-3 located in the murine Socs2 promoter. (Bottom) Mice were stimulated with GH for 30 min and liver homogenates analysed for DNA binding properties of activated Stat5 on Stat5 2xRE#1-3. Fast-migrating complexes represent Stat5 dimers bound to ³²P-labeled oligomers. Stat5-specific binding was confirmed via Stat5 antibodies yielding high molecular weight complexes migrating slower on respective oligomers (ss, supershift). Beta-Casein was used as positive control for a Stat5 responsive promoter sequence.

Thus, Epo treatment stimulated high affinity binding of Stat5 onto all three Stat5 2xRE located in the murine Socs2 promoter *in vitro*. *In vivo* analysis of GH activated Stat5 confirmed these results.

3.1.4.3. The proximal Socs2 promoter is synergistically transactivated by Stat5-GR interplay

We demonstrated that the Stat5 2xRE#1-3 located in the proximal Socs2 promoter are recognized and bound by phosphorylated Stat5 dimers. Subsequently, we studied the transactivation properties of promoter fragments containing all three Stat5 2xRE when placed in front of a LUC reporter construct (Reporter constructs I-III, see Figure 14). For this, pMSCV plasmids expressing murine Stat5, GR and EpoR were transiently transfected into COS7 cells and after 48 h stimulated for 30 min with 25

U/ml Epo and/or the glucocorticoid agonist Dexamethasone (Dex) at a final concentration of 10 nM. As shown in Figure 16 (bars 1-8), no LUC activity was observed upon Stat5-GR transactivation of the two distal Socs2 promoter fragments No. I+II. Contrarily, the 3'-most proximal Socs2 promoter fragment No. III exhibited LUC activity already under non-stimulated conditions (bar 9). Stimulation with Epo led to ~2fold increases in LUC activity (bar 10). No effect of Dex treatment alone was observed (bar 12). Strikingly, co-activation of Stat5 and GR signaling by simultaneous Epo and Dex treatment led to significant increases in LUC activity (~5fold, bar 11).

Thus, Stat5 and GR signaling synergistically transactivated the Socs2 promoter. This effect was demonstrated for the proximal Socs2 promoter, whereas distal promoter fragments did not show these synergies. This pinpointed towards additional 3'- enhancer elements, either located in the proximal Socs2 promoter itself or in Socs2 intron sequences.

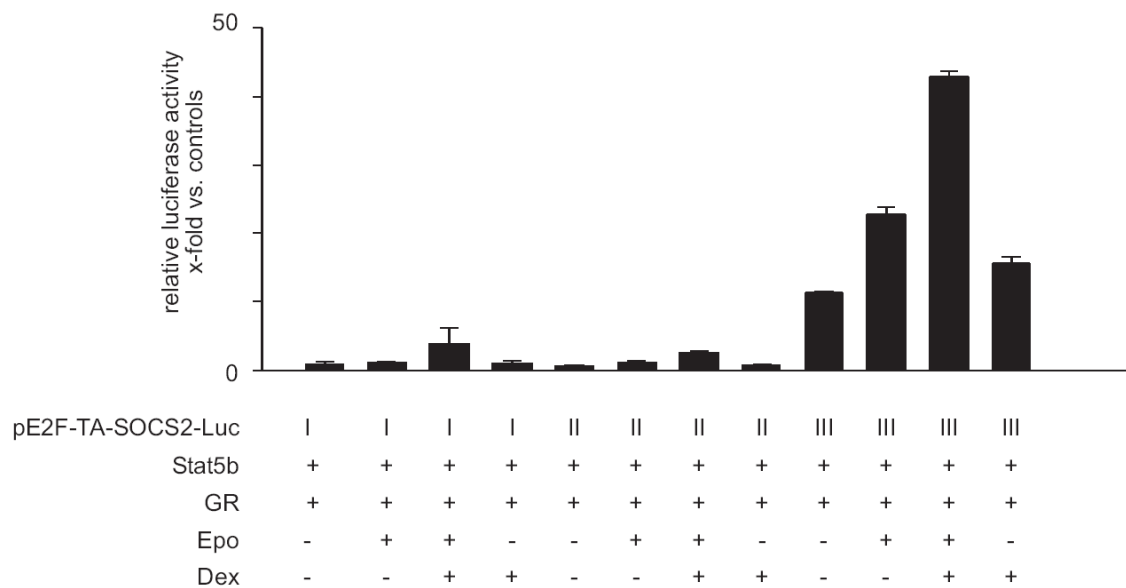


Figure 16. The proximal Socs2 promoter is synergistically activated by Stat5-GR signaling

Synergistic Stat5-GR transactivation properties of three Socs2 LUC constructs (No. I-III, as schematically shown in Figure 14) were determined. Briefly, COS7 cells were transfected with pMSCV plasmids expressing murine Stat5b, GR and EpoR. After 48 h, cells were stimulated with 25 U/ml Epo and/or 10 nM Dex. Cellular extracts were prepared and the LUC activity measured as described in Methods. Equal transfection efficiency was determined by co-transfection of a beta-Galactosidase (beta-Gal) expression plasmid and normalization of LUC activity to beta-Gal activity. Assays were performed in triplicate.

3.1.4.4. Full transactivation of the Socs2 promoter depends on Stat5 and GR

We identified the proximal Socs2 promoter to be strongly responsive to synergistic Stat5-GR transactivation. Next, we addressed the question whether this effect

required Stat5 and GR proteins. Thus, we compared conditions of Stat5 and GR overexpression and subsequent cytokine stimulation by Epo and/or Dex with mock-transfected COS7 cells. COS7 cells were chosen since they lack endogenous Stat5 expression. Untransfected COS7 cells exhibited a mere ~1.5fold induction in LUC activity upon Epo/Dex co-stimulation (Figure 17, bar 3). Epo treatment alone had no effect (Figure 17, bars 1-2). Dex treatment led to ~2fold increases in LUC activity compared with untreated cells. In strong contrast, overexpression of Stat5 and GR proteins led to potent increases in LUC activity (Figure 17, bars 5-8). A modest ~2fold increase of LUC activity was observed upon Epo stimulation alone. Combinatorial stimulation of Stat5 and GR proteins led to approximately 5fold increases in LUC activity, thereby significantly bypassing the effects of Epo treatment alone.

Thus, we confirmed that the observed synergism of Stat5 and GR signaling in transactivating the proximal Socs2 promoter depends on Stat5-GR interaction.

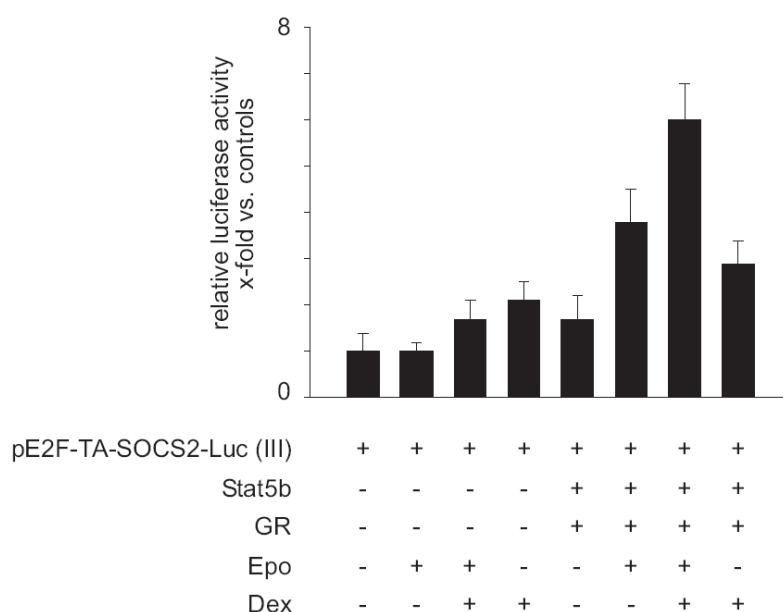


Figure 17. Synergistic Epo/Dex-dependent transactivation of the Socs2 promoter depends on Stat5 and GR proteins

The Stat5-GR co-dependent transactivation of Socs2 LUC construct No. III (as schematically shown in Figure 14) was determined. Briefly, COS7 cells were transfected with pMSCV plasmids expressing murine Stat5b, GR and EpoR. After 48 h, cells were stimulated with 25 U/ml Epo and/or 10 nM Dex. Cellular extracts were prepared and the LUC activity measured as described in Methods. Equal transfection efficiency was determined by co-transfection of a beta-Galactosidase (beta-Gal) expression plasmid and normalization of LUC activity to beta-Gal activity. Assays were performed in triplicate.

3.1.4.5. Synergistic Stat5 and GR signaling is required for full Socs2 promoter transactivation.

Synergistic activation of Stat5 and GR signaling led to a pronounced transactivation of the proximal Socs2 promoter. This effect was dependent on Stat5 and GR proteins. We next followed the question whether two distinct Stat5 and GR or rather one linear Stat5-GR signal transduction pathway was responsible for the observed synergism. We previously identified the Stat5b N-terminus as the GR-docking domain disrupting the Stat5-GR protein interaction upon N-terminal truncation of Stat5b¹²². We took advantage of these findings and transiently transfected cells with pMSCV plasmids encoding murine GR, EpoR and full-length Stat5b as well as aminoterminally (Stat5b^{ΔN}) or carboxyterminally (Stat5b^{Δ754}) truncated Stat5b isoforms. The latter isoform lacks the carboxyterminal transactivation domain essential for cofactor recruitment of the basal transcription machinery. Transfection of full length Stat5b together with GR led to potent, synergistic Socs2 transactivation following Epo/Dex treatment (Figure 18, bar 3). Interestingly, this effect was severely impaired upon transfection with plasmid encoding Stat5b^{ΔN} instead of full-length Stat5b (Figure 18, bar 7). Transfection of the Stat5b^{Δ754} isoform almost completely abrogated Socs2 transcription upon Epo or Epo/Dex treatment (Figure 18, bar 11).

Thus, synergistic Stat5-GR co-dependent transactivation of the proximal Socs2 promoter required Stat5-GR protein interaction, the disruption of which led to severe decreases in Socs2 transcription. Abrogation of Stat5 transactivation properties resulted in the complete shutdown of Socs2 transcription.

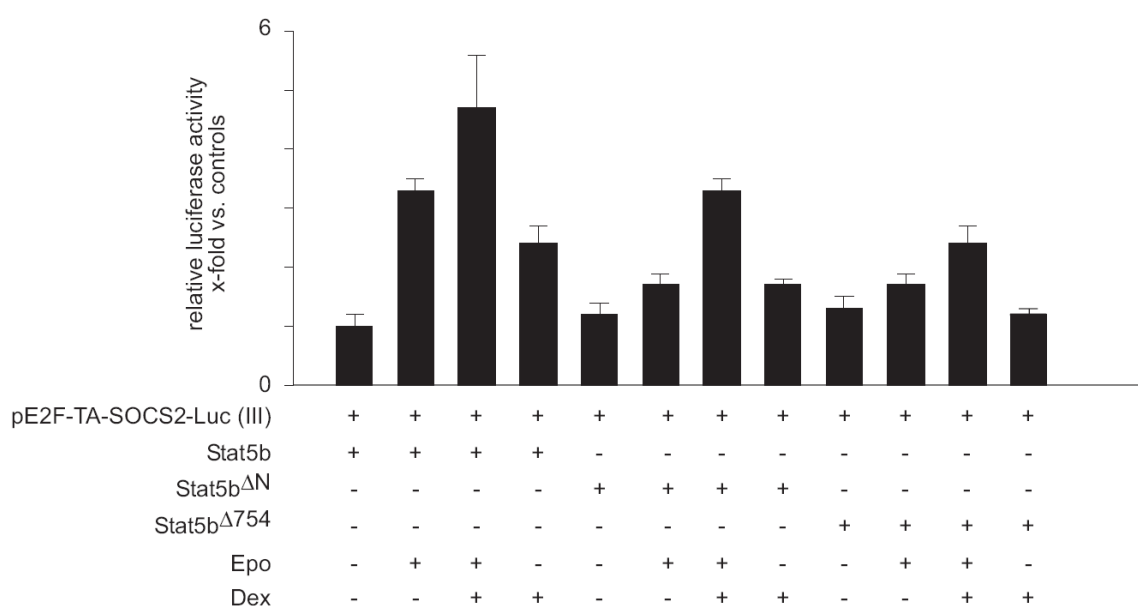


Figure 18. Socs2 transactivation depends on physical Stat5-GR protein interaction

The Stat5-GR co-dependent transactivation of Socs2 LUC construct No. III (as schematically shown in Figure 14) was determined. Briefly, COS7 cells were transfected with pMSCV plasmids expressing murine Stat5, Stat5^{ΔN}, Stat5^{Δ754}, GR and EpoR. After 48 h, cells were stimulated with 25 U/ml Epo and/or 10 nM Dex. Cellular extracts were prepared and the LUC activity measured as described in Methods. Equal transfection efficiency was determined by co-transfection of a beta-Galactosidase (beta-Gal) expression plasmid and normalization of LUC activity to beta-Gal activity. Assays were performed in triplicate.

3.1.4.6. A linear Stat5-GR pathway controls hepatic Socs2 transcription

We demonstrated the existence of a linear Stat5-GR signaling pathway essential for full transactivation of murine Socs2 in a standard epithelial cell line (COS7 cells). As Stat5 functions depend largely on the cellular context we wanted to further investigate the extent of Stat5-GR synergism in transactivating the Socs2 promoter in other, more physiologically relevant cells such as hepatocytes. For this, we utilized primary hepatocytes isolated from p16/19^{ARF} deficient mice (MIMp16/19ARF^{-/-}). Growth factor supplementation with a defined panel of growth factors (IGF-II, TGFb and insulin) rendered these cells immortal *in vitro*, yet an epithelial polarity and expression of hepatocyte markers was kept¹⁶⁹. A variant of this cell line was generated via genomic integration of the Ras proto-oncogene (MIMp16/19ARF^{-/-}-Ras), rendering these cells independent of growth factors stimuli and facilitating handling of cells¹⁷⁰. Transfection of pMSCV plasmids encoding murine Stat5b, the GR, the EpoR and subsequent cytokine stimulation with 25 U/ml Epo and 10 nM Dex for 30 min induced significant increases in LUC activity in both cell lines: The increase in LUC activity was more pronounced MIMp16/19ARF^{-/-}-Ras cells (~6.5fold; Figure 19 bar 7) compared with MIMp16/19ARF^{-/-} cells (~4.5fold; Figure 19, bar 3). Stimulation with 25 U/ml Epo alone led to limited inductions of LUC activity in both cell lines (~2.5fold; Figure 19, bar 2 and 6). Treatment with 10 nM Dexamethasone led to increases in LUC activity of borderline significance.

Thus, we demonstrated, that full Socs2 transactivation is regulated by linear Stat5-GR signaling also in hepatocytes. As the liver represents the primary site of action for GH-mediated Stat5 activation, potent GR signaling as observed under stress conditions might modulate the magnitude of Stat5-derived Socs2 transcription *in vivo* and thus affecting liver function, metabolism and body growth.

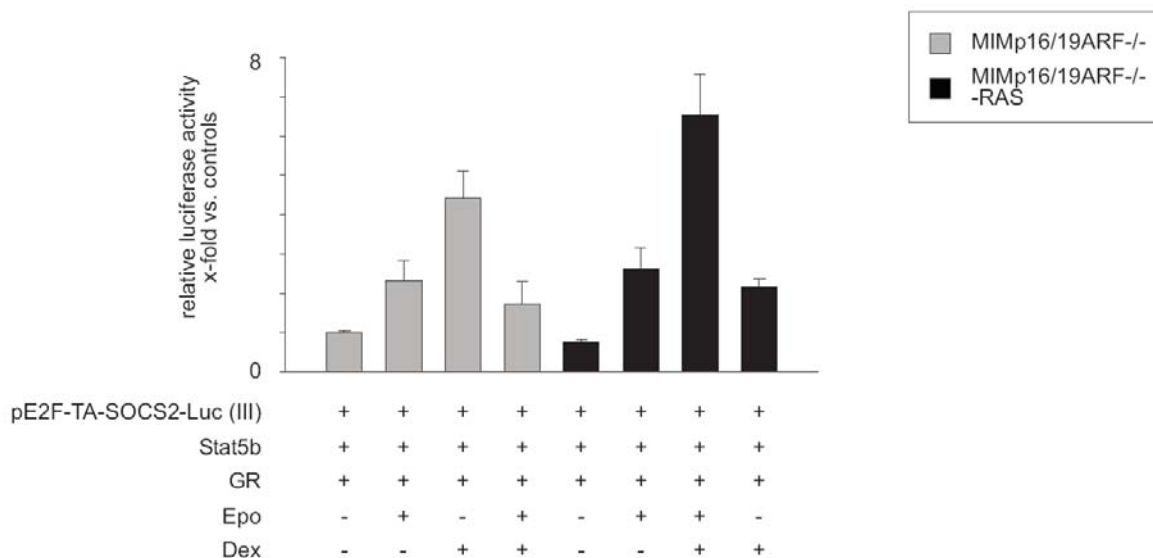


Figure 19. Full Socs2 promoter transactivation in primary hepatocytes is dependent on the Stat5-GR interaction

The Stat5-GR co-dependent transactivation of Socs2 LUC construct No. III (as schematically shown in Figure 14) was determined. Briefly, MIMp16/19ARF^{-/-} and MIMp16/19ARF^{-/-}-Ras cells were transfected with pMSCV plasmids encoding for murine Stat5b, GR and EpoR. After 48 h, cells were stimulated with 25 U/ml Epo and/or 10 nM Dex. Cellular extracts were prepared and LUC activity measured as described in Methods. Equal transfection efficiency was determined by co-transfection of a beta-Gal expression plasmid and normalization of LUC activity to beta-Gal activity. Assays were performed in triplicate.

3.2. Compound loss of hepatic Stat5 and GR signaling leads to steatosis

Fat accumulation in the liver (steatosis) is either the result of excessive fatty acid biosynthesis relative to oxidative clearance¹⁷¹ or alternatively impaired hepatic release of lipids and thus net deposition of fat in hepatocytes¹⁰. Fatty acid synthesis, clearance and release are regulated by multiple endocrine factors including hypothalamic and adrenal effectors like GH and glucocorticoids. Stat5 mediates the body's response to numerous cytokines and growth factors including GH¹²⁵. Both, gain- and loss-of-function studies have shown a critical role of hepatic Stat5 in regulation of postnatal body growth, sexual dimorphism and detoxification control¹²². These GH-derived effects are largely attributed to activated Stat5 efficiently transcribing IGF-1. We could demonstrated *in vivo* that the GR binds as essential cofactor to the aminotermisus of Stat5b in order to fully drive IGF-1 synthesis upon GH action¹²². IGF-1 in turn inhibits GH secretion in the anterior pituitary^{123, 127}, constituting an auto-inhibitory feedback loop preserving appropriate pathway activation¹³⁰. In addition to the existence of a Stat5b knockout line, mice harbouring N-terminal truncations in both Stat5 isoforms were reported (Stat5^{ΔN} mice). Both Stat5 knockout strains exhibit reduced peripheral lipid reservoirs^{123, 127} resembling in

many ways the lipodystrophic phenotype of growth hormone receptor deficient (GHR^{-/-}) mice. This and once again supports the notion of GH-Stat5 negative feedback inhibition¹³³.

In contrast to GH and Stat5, adrenally derived glucocorticoids such as corticosterone signal through the glucocorticoid receptor (GR) and trigger multiple downstream effects including inhibition of peripheral lipolysis. Glucocorticoids constitute a critical arm of the HPA axis, a neuroendocrine system which integrates stress signals to modulate multiple processes including digestion, immune activation, and energy supply. Like GH, glucocorticoids tightly regulate their own secretion through an autocrine negative feedback loop, the impairment of which leads to one of several hypercortisolic conditions characterized in part by pathological accumulation of lipids in peripheral adipose tissues¹³⁹. Deletion of the GR in hepatocytes leads to well-studied defects in hepatic glucose metabolism such as impaired gluconeogenesis leading to fasting-induced hypoglycaemia¹³⁶. In this study, we addressed the question whether Stat5 and GR proteins act separately in regulating hepatic lipid homeostasis or rather require a functional Stat5-GR signaling axis. *In vitro* studies claimed an inhibitory role of Stat5 during adipogenesis¹⁷². Thus, we generated mice lacking Stat5 and/or the GR in hepatocytes.

By macroscopic examination we discovered a remarkable dependence on Stat5 and GR proteins in regulating hepatic lipid homeostasis: Preliminary macroscopic analyses at sacrifice revealed graded hepatic pathologies between genotypes. Whereas both control and GR^{AlfpCre} mice displayed normal liver morphology, hepatic steatosis and hepatomegaly were observed in both Stat5^{AlfpCre} and Stat5/GR^{AlfpCre} mutants as early as 4 weeks postnatally. Strikingly, while the extent of steatosis in Stat5^{AlfpCre} single mutants remained mild and stable at all time points analysed, Stat5/GR^{AlfpCre} mutant mice displayed a marked and progressive pathology exhibiting 3-4 fold increases in liver mass by 12 months of age (Figure 20A, B) and ~8fold increases in the triglyceride content as early as 2 months of age (Figure 20C). Further, whereas control and GR^{AlfpCre} animals displayed only mild pathologies with time, detailed histopathological analysis revealed marked age-dependent micro- and macrovesicular steatosis in livers from both Stat5^{AlfpCre} (moderate) and Stat5/GR^{AlfpCre} (extreme) mice (Figure 21B) suggesting a critical role for Stat5 in the regulation of hepatic lipid homeostasis. As an additional testament to the severity of disease in

Stat5/GR^{AlfpCre} double mutants, maximal fatty degeneration of hepatocytes was detected as early as 8 weeks of age (Figure 21B) in these mutants.

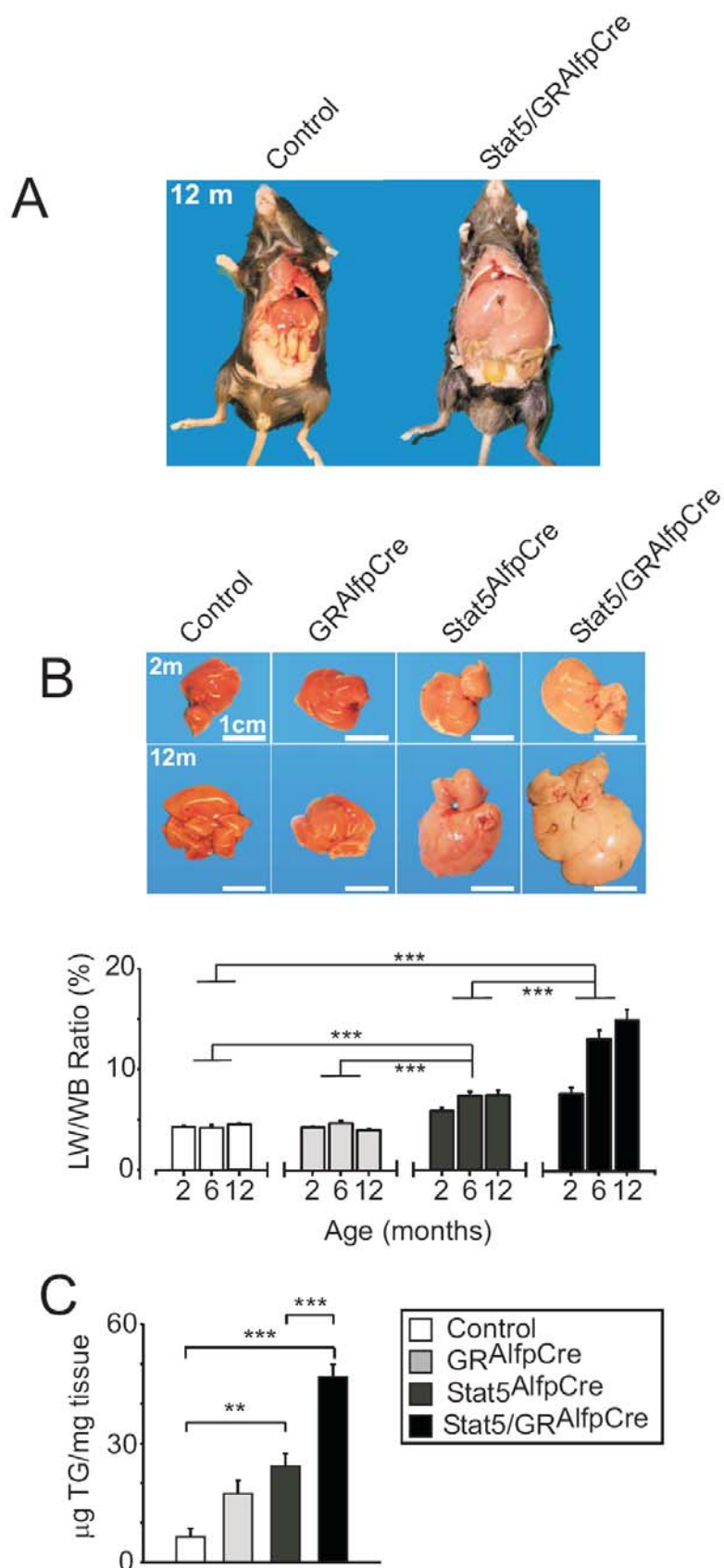


Figure 20. Liver steatosis in Stat5^{AlfpCre} and Stat5/GR^{AlfpCre} mice

(A) Macroscopic appearance of steatosis in 12-months-old mutant mice. (B) Livers from 8-weeks-old and 12-months old male mice of the indicated genotypes (top). Liver/Body Weight (LW/BW) ratio in male mice at indicated time points (bottom). Data represent mean \pm SEM (n=8/genotype/timepoint). (C) Hepatic triglyceride content as measured by colorimetric assays in 8-weeks-old male mice. Data represent mean \pm SEM (n=5/genotype).

Also observed with a consistent graded severity between genotypes were elevated serum ALT levels (Table 3) and extensive lobular and portal fibrosis histopathologies (Figure 21A). Thus, hepatic Stat5 deficiency caused mild, stable steatosis that, when coupled to a GR loss, initiated overt progressive hepatosteatosis reminiscent of human NAFLD.

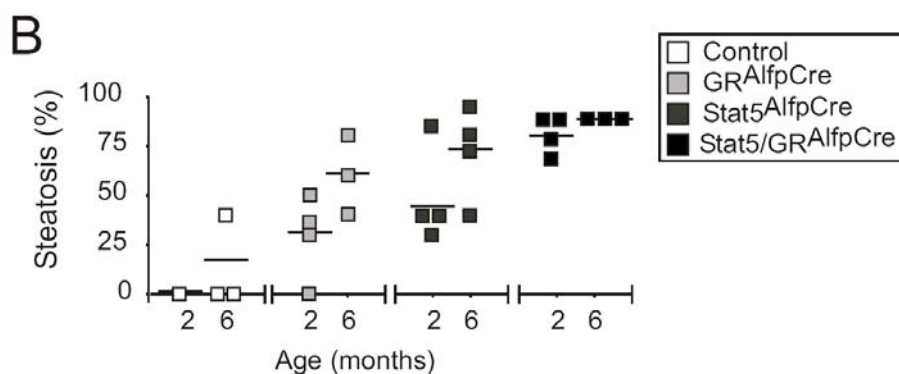
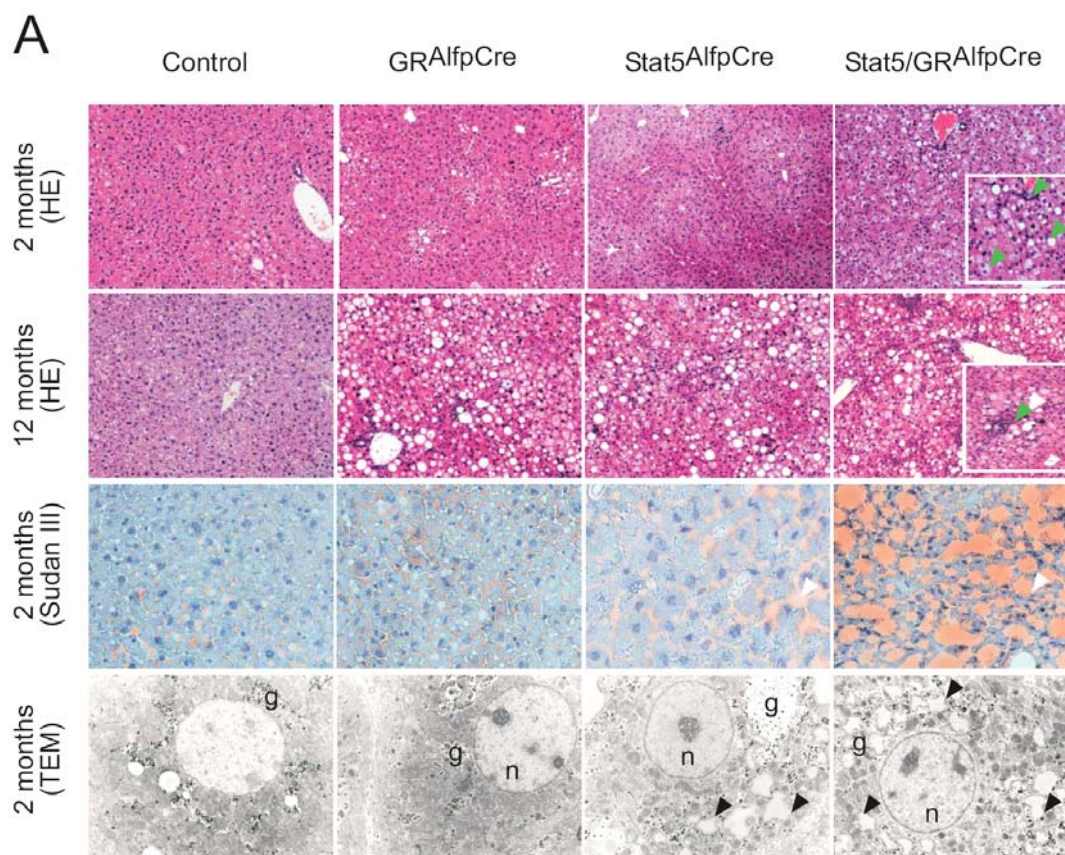


Figure 21. Histological steatosis in Stat5^{AlfpCre} and Stat5/GR^{AlfpCre} mice

(A) Histological analyses of liver sections from 8-weeks and 12-months-old mutant mice. Tissue sections were fixed and stained with HE (row 1 and 2). Lipid accumulation was visualized by Sudan III on cryosections (row 3). Electron microscopy analysis of subcellular fat distribution in liver samples (row 4). (B) Histological degree of steatosis in HE-stained livers was scored semi-quantitatively by two certified pathologists [in collaboration].

3.2.1. Loss of hepatic Stat5 signaling leads to increased lipogenesis

Since hepatic steatosis can either result from an imbalance in fatty acid synthesis and oxidation or from an imbalance in build-up versus shuttling of lipids out of hepatocytes we examined these processes in more detail. As no apparent changes in lipoprotein particle-mediated shuttling of TG were observed (Figure 27, see below), we postulated that Stat5^{AlfpCre} and Stat5/GR^{AlfpCre} mutant phenotypes were caused either by an induction of hepatic *de novo* lipid synthesis or by inhibition of hepatic fatty acid catabolism. Affymetrix whole-genome expression and subsequent molecular signature analysis identified a marked induction of genes controlled by the lipogenic master regulators SREBP-1c and PPARgamma in Stat5^{AlfpCre} and Stat5/GR^{AlfpCre} mice (Table 2).

Symbol	Name	TF pathway	Stat5/GR ^{AlfpCre}		Stat5 ^{AlfpCre}		GR ^{AlfpCre}	
			fold change	P	fold change	P	fold change	P
Lipid metabolism, lipogenic								
PPARG	PPARgamma		1,77	0,004	1,68	0,006	1,38	0,071
SCD1	stearoyl-Coenzyme A desaturase 1	PPARgamma SREBP-1c	1,53	0,009	1,31	0,076	1,40	0,028
SCD2	stearoyl-Coenzyme A desaturase 2	SREBP-1c	9,13	0,000	4,76	0,000	4,53	0,000
LIPE	lipase, hormone sensitive	PPARgamma	1,46	0,000	1,19	0,032	1,14	0,100
MOD1	malic enzyme, supernatant	PPARgamma	2,75	0,002	1,72	0,061	2,13	0,012
ADFP	adipose differentiation related protein	PPARalpha	1,78	0,011	1,44	0,087	1,01	0,963
FASN	fatty acid synthase	PPARgamma SREBP-1c	1,56	0,032	1,18	0,400	1,65	0,018
CD36	CD36 antigen (fatty acid translocase)	PPARgamma	1,37	0,049	1,53	0,010	1,29	0,098
FABP4	fatty acid binding protein 4, adipocyte	PPARgamma	1,07	0,2906	0,98	0,81	0,98	0,81
DGAT1	diacylglycerol O-acyltransferase 1	PPARgamma	1,04	0,466	1,09	0,250	1,01	0,924
Lipid metabolism, catabolic								
PPARA	PPAR alpha		2,45	0,1686	2,14	0,8936	2,14	0,1618
ACOX1	acyl-Coenzyme A oxidase 1, palmitoyl	PPARalpha	2,03	0,0000	1,60	0,0001	1,32	0,0077
ACACA	acetyl-Coenzyme A acyltransferase 1	PPARalpha	2,95	0,0000	1,64	0,0063	2,62	0,0000
ACACB	3-ketoacyl-CoA thiolase B	PPARalpha	1,93	0,0000	1,65	0,0005	1,89	0,0000
ACADM	acetyl-CoA dehydrogenase, medium chain	PPARalpha	1,65	0,0012	1,65	0,0012	1,31	0,0477
HADHSC	L-3-hydroxyacyl-CoA dehydr. short chain	PPARalpha	1,82	0,0000	1,56	0,0000	1,36	0,0007
ABCD2	ATP-binding cassette D2	PPARalpha	2,33	0,0024	1,71	0,0360	1,38	0,1970
CRAT	carnitine acetyltransferase		2,60	0,0215	2,43	0,0311	2,08	0,0421
EHHADH	enoyl-CoA, hydratase/3-hydroxyacyl CoA dehydrogenase	PPARalpha/ PPARgamma	1,80	0,0147	1,38	0,1558	2,36	0,0010
ACADL	acetyl-Coenzyme A dehydrogenase, long-chain	PPARalpha	1,60	0,0728	1,57	0,0865	1,16	0,4780
ACAIDL	acetyl-Coenzyme A dehydrogenase, very long-chain	PPARalpha	1,01	0,8619	1,07	0,3800	0,96	0,58
CPT1a	carnitine palmitoyl-transferase 1a, liver	PPARalpha	1,14	0,3211	1,23	0,1444	0,91	0,50
Lipid metabolism, others								
LPIN1	lipin 1		0,08	0,000	0,39	0,033	0,27	0,005
FABP5	fatty acid binding protein 5, epidermal		0,20	0,000	0,08	0,000	0,37	0,015
APOA4	apolipoprotein A-IV		0,22	0,007	0,44	0,115	0,10	0,000
HDLBP	high density lipoprotein (HDL) binding protein		0,73	0,002	0,85	0,070	0,83	0,037
DBI	diazepam binding inhibitor		1,25	0,010	1,04	0,564	1,23	0,013
APOC2	apolipoprotein C-II		1,88	0,001	1,74	0,003	1,15	0,400
FTO	fatso		0,63	0,008	0,92	0,587	0,86	0,324
LIPC	lipase, hepatic		0,69	0,006	0,64	0,001	1,14	0,259
ES31	esterase 31		0,33	0,004	0,30	0,002	0,17	0,000
CEBPB	CCAAT/enhancer binding protein (C/EBP), beta		2,00	0,0446	1,51	0,1964	0,56	0,13

Table 2. Analysis of transcription factor signatures upregulated in Affymetrix profiling

Lipid metabolism-related genes significantly deregulated under either knockout condition (Stat5^{AlfpCre}, GR^{AlfpCre} or Stat5/GR^{AlfpCre}). Genes are clustered according to upstream transcription factor activation (PPARalpha/gamma) or gene function (lipogenic, catabolic or others). Other major liporegulatory master genes are included for interpretation of the metabolic phenotype.

Indeed, quantitative RT-PCR (qPCR), Western blot, and immunohistochemical analyses confirmed induction of both critical liporegulatory transcription factors at both the transcript and protein levels (Figure 22A, B and Figure 23A, B). Importantly, upregulation of gene expression of lipogenic SREBP-1c (FASN, SCD1 and SCD2) and PPARgamma targets (DGAT1, DGAT2, CD36, FABP4 and MOD1) were shown to be increased over 2-fold in both Stat5-deficient lines indicating a strong underlying role for SREBP-1c/PPARgamma-regulated *de novo* lipogenesis in the observed phenotype. Though somewhat counterintuitive in the context of steatosis, transcription of catabolic genes regulated by PPARalpha also appeared upregulated in Stat5^{AlfpCre} and Stat5/GR^{AlfpCre} animals. Expression profiling (Table 2) and qPCR (Figure 22C) analyses revealed significant increases in PPARalpha expression as well as the downstream targets ACOX1, EHHADH, ACADM, ACADL, ACADVL and CPT1, important mediators of peroxisomal and mitochondrial beta-oxidation. Also noteworthy, the typically adipose tissue specific transcription factors C/EBPalpha and C/EBPbeta which control adipogenesis and lipogenesis in concert with PPARgamma¹⁷³ showed similar elevations in both Stat5^{AlfpCre} and Stat/GR^{AlfpCre} further supporting the idea of an induced lipogenic/adipogenic program (Figure 22D). Interestingly, neither the PPARgamma coactivators PGC1alpha and RXRalpha, nor the hepatocyte transcriptional marker HNF1alpha showed evidence of altered expression (Figure 22D and Figure 23A).

Thus deletion of Stat5 in the liver causes a marked induction of lipogenic and adipogenic programs including *de novo* lipogenesis.

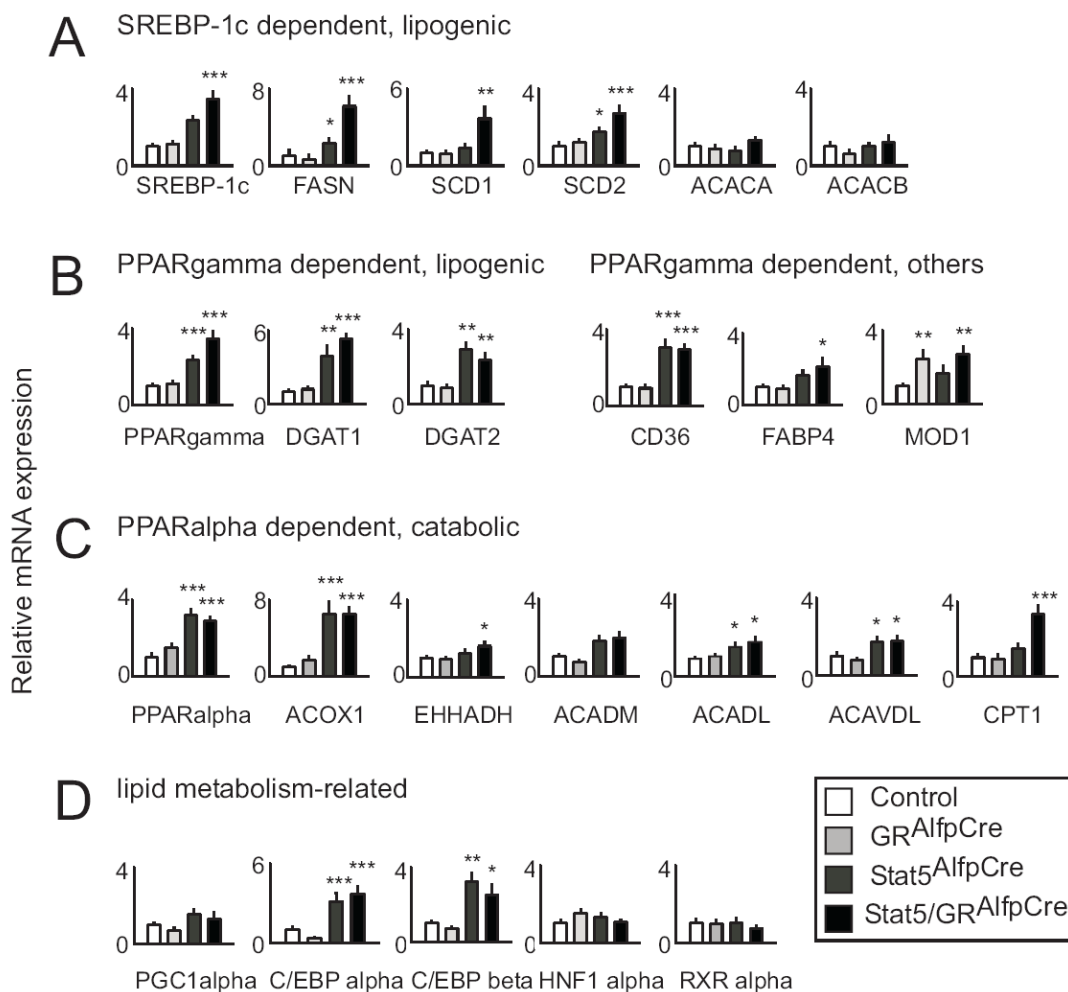


Figure 22. Induction of *de novo* lipogenesis in Stat5^{AlfpCre} and Stat5/GR^{AlfpCre} mice

Relative hepatic mRNA levels were quantified by qPCR in 8-week-old mice of indicated genotypes. Ct values were normalized to endogenous GAPDH levels (Δ Ct method). n=6/genotype; *, p<0.05; **, p<0.01, ***, p<0.001. Error bars represent mean \pm SEM. Genes with known functions in hepatic lipid metabolism were subdivided into the following four groups: (A) Lipogenic genes transcriptionally regulated by SREBP-1c. (B) Lipogenic (left) or other (right) genes transcriptionally regulated by PPARgamma. (C) Lipolytic genes transcriptionally regulated by PPARalpha. (D) Other lipid metabolism-related genes.

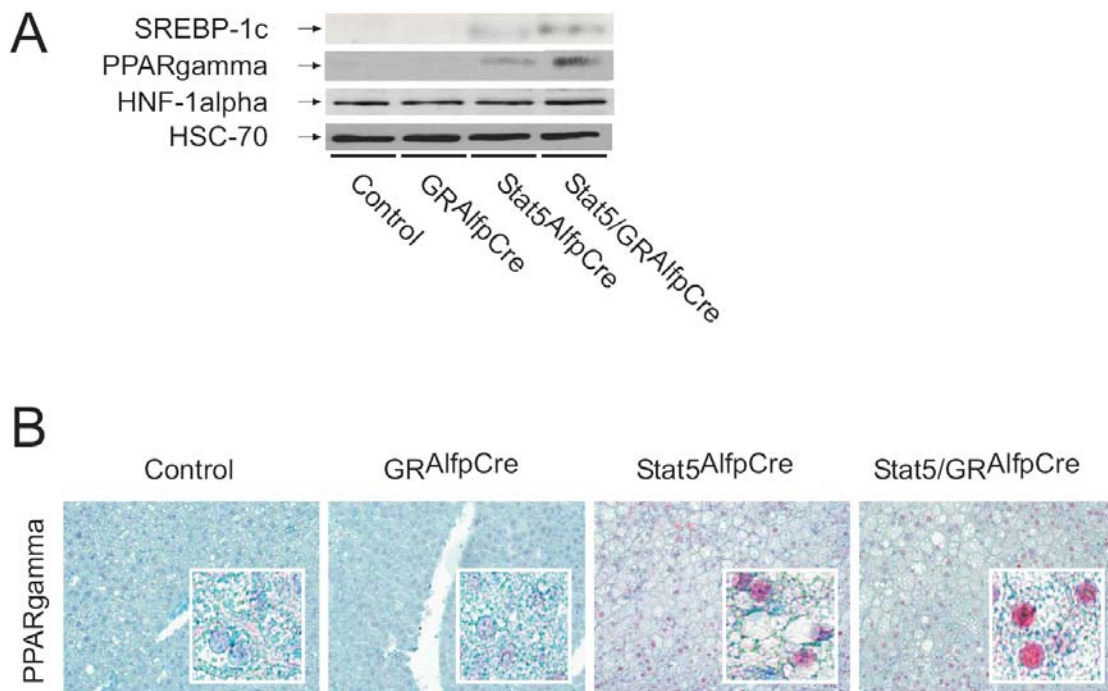


Figure 23. Increased SREBP-1c/PPARgamma protein expression upon Stat5 deletion in liver
 (A) Representative immunoblots showing expression of nuclear SREBP-1 and PPARgamma protein in liver. HNF1alpha served as hepatocyte-specific marker. HSC70 was used as loading control. (B) Immunohistochemical staining for PPARgamma protein expression in liver.

3.2.2. Loss of hepatic Stat5 signaling induces hepatic insulin resistance

One hallmark of most steatotic disorders is an impaired insulin responsiveness of the liver (hepatic insulin resistance). Preliminary measures of fasting and fed glucose in concert with significant hyperinsulinaemia and elevated levels of serum resistin pinpointed towards insulin resistance in $Stat5^{AlfpCre}$ and $Stat5/GR^{AlfpCre}$ mice (Table 3). Administration of 0.75 U/kg body weight insulin intraperitoneally revealed blunted hypoglycaemic responses in both $Stat5^{AlfpCre}$ and $Stat5/GR^{AlfpCre}$ mutants (Figure 24A), corroborating the notion of insulin resistance in Stat5-deficient animals. Next, glucose tolerance tests were performed to assess overall glucose homeostasis. They yielded similar findings: $GR^{AlfpCre}$ and $Stat5^{AlfpCre}$ mice displayed mild glucose intolerance in response to 1 g/kg body weight oral glucose, while double mutant mice exhibited overt diabetes. Of note, $Stat5^{AlfpCre}$ and $Stat5/GR^{AlfpCre}$ mice displayed marked fasting and glucose-challenged hyperinsulinaemia further suggestive of significant insulin resistance (Figure 24A). The significantly mitigated insulin sensitivity observed in $Stat5/GR^{AlfpCre}$ double knockouts in comparison to $Stat5^{AlfpCre}$ mutants may reflect the additive and independent effects of pronounced insulin resistance (due to deletion of Stat5) and established glucose intolerance (due to

deletion of GR). Finally, Western blot analysis of Stat5^{AlfpCre} and Stat5/GR^{AlfpCre} liver revealed severely impaired insulin receptor (IR) downstream signaling 15 min after intraperitoneal insulin administration. Tyrosine phosphorylation of the insulin receptor beta-subunit (IRbeta), insulin-response substrates -1 and -2 (IRS-1 and IRS-2) and the downstream effector kinase AKT were reduced in Stat5/GR^{AlfpCre} livers (Figure 24B). Once again, changes in the Stat5^{AlfpCre} mice were more modest with reductions in phosphorylation only observed in IRS-1 and Akt.

Thus, hepatocyte-specific deletion of Stat5 alone or in combination with GR leads to marked hepatic insulin resistance.

Table 3: Biochemical and metabolic serum parameters in male mutant mice

Parameter	n=	Control		GR ^{AlfpCre}		Stat5 ^{AlfpCre}		Stat5/GR ^{AlfpCre}	
		2 months	12 months	2 months	12 months	2 months	12 months	2 months	12 months
ALT (U/l)	7	57 ± 5	83 ± 15	63 ± 4	ND	94 ± 6 ^c	562 ± 151 ^c	191 ± 49 ^c	614 ± 126 ^c
ALP (U/l)	7	45 ± 11	37 ± 17	59 ± 3	ND	64 ^a ± 4	69 ± 4	64 ² ± 5	66 ± 2
TG (mg/dl)	8	174 ± 34	160 ± 26	84 ± 12 ^a	ND	165 ± 22	180 ± 32	179 ± 24	177 ± 12
Cholesterol (mg/dl)	5	158 ± 23	118 ± 10	98 ± 26	143 ± 30	132 ± 15	171 ± 34	203 ± 15	267 ± 12 ^a
FFA (mmol/l)	5	0.84 ± 0.2	0.71 ± 0.1	0.69 ± 0.1	0.54 ± 0.1	0.77 ± 0.1	0.95 ± 0.2	1.11 ± 0.2	0.67 ± 0.1
Glucose (mg/dl)									
fed	7	130 ± 21	149 ± 22	73 ± 5	ND	199 ± 23 ^a	190 ± 13 ^a	222 ± 24 ^a	220 ± 37 ^a
after 4h fast	8	182 ± 9	ND	187 ± 11	ND	179 ± 15	ND	219 ± 11 ^a	ND
after 16h fast	8	73 ± 4	ND	84 ± 7	ND	91 ± 8 ^a	ND	92 ± 14 ^a	ND
Insulin (pg/ml)	7	173 ± 25	ND	108 ± 27	ND	482 ± 63 ^c	ND	401 ± 25 ^c	ND
Leptin (ng/ml)	8	0.6 ± 0.1	9.4 ± 1.2	2.1 ± 0.5 ^a	10.8 ± 1.0	0.9 ± 0.1 ^a	4.8 ± 1.2 ^b	0.8 ± 0.1	6.6 ± 1.9 ^b
TNFa (pg/ml)	8	3.9 ± 0.8	5.1 ± 1.2	2.1 ± 0.7	5.6 ± 1.9	4.6 ± 1.0	5.4 ± 2.3	4.4 ± 1.6	10.0 ± 2.0 ^c
Resistin (ng/ml)	8	3.3 ± 0.4	2.6 ± 0.5	1.6 ± 0.2 ^b	1.9 ± 0.3	5.5 ± 0.7 ^a	3.3 ± 1.0	6.1 ± 0.4 ^c	4.2 ± 0.7 ^b

Eight weeks old male mice were fed with given chow and sacrificed by carbon dioxide asphyxiation. Results are expressed as mean ± SEM for indicated number of mice from each genotype. ALT, alanine transaminase; ALP, alkaline phosphatase; FFA, free fatty acids; TG, triglycerides; TNFa, tumour necrosis factor alpha; ND = not determined. All values represent mean ± SEM. ^a = p-Value <0.05 vs. Control, ^b = p-Value <0.01 vs. Control, ^c = p-Value <0.001 vs. Control

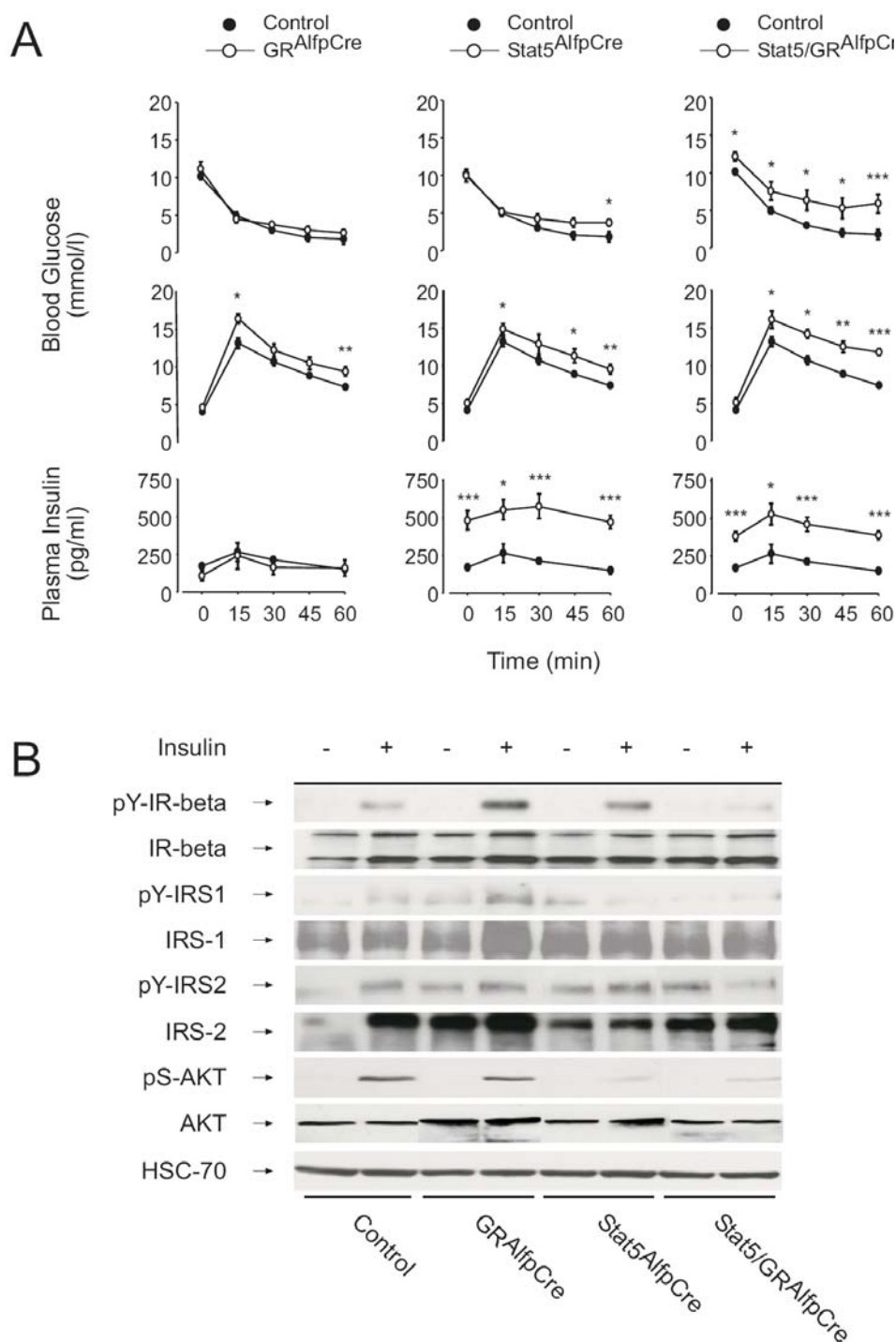


Figure 24. Impaired Glucose and Insulin Metabolism in Control, $GR^{AlfpCre}$, $Stat5^{AlfpCre}$ and $Stat5/GR^{AlfpCre}$ mice

Male mice were analysed at 8-weeks-of age for Insulin Tolerance Tests (ITT) and Oral Glucose Tolerance Tests (OGTT). (A) ITT: Insulin was injected intraperitoneally following a 4h fast. Blood glucose levels were determined at given time points (row 1). OGTT: Mice were fasted overnight and glucose orally administered. Blood glucose levels were determined at given time points (row 2). Plasma insulin levels following OGTT challenge. The insulin levels were determined by ELISA (row 3). For ITT/OGTT analyses: $n=6-8/genotype$; *, $p<0.05$; **, $p<0.01$, ***, $p<0.001$. Error bars in ITT/OGTT assays represent mean \pm SEM. (B) Phosphorylation of proteins downstream of the insulin receptor upon insulin challenge in 8-weeks-old mice. Levels of phosphorylated and total protein were determined 15 min after intraperitoneal insulin injection by immunoprecipitation and phospho-tyrosine-specific immunoblot analysis.

3.2.3. Compound loss of hepatic Stat5 and GR signaling leads to peripheral lipodystrophy.

Interestingly, despite the divergent steatotic phenotypes observed between Stat5^{Alfpcre} single and Stat5/GR^{Alfpcre} double knock-outs, SREBP-1c/PPARgamma-dependent *de novo* lipogenesis appeared equally induced in both sets of animals. These findings suggested an additional independent stimulus for lipid deposition in Stat5/GR^{Alfpcre} livers and prompted us to examine peripheral fat stores as a potential source of additional lipid fuels. Interestingly, while the independent single mutants exhibited either modest increases (+29 %; GR^{AlfpCre}) or decreases (-28 %; Stat5^{AlfpCre}) in white fat pad mass, double mutant animals displayed a clear depletion of both white and brown adipose tissue stores (-58 %, Stat5/GR^{AlfpCre}; Figure 25A, B). Histological analysis of Stat5/GR^{AlfpCre} white (WAT) and brown adipose tissues (BAT) confirmed peripheral lipodystrophy characterized by grossly reduced lipid droplet size (Figure 25C). Interestingly, measurement of multiple serum lipid regulators revealed elevated levels of GH and decreased levels of IGF-1 in Stat5^{AlfpCre} and Stat5/GR^{AlfpCre} mice (Figure 26A, B). Consistent with systemically elevated serum GH levels, Stat5 phosphorylation in WAT was significantly increased (Figure 26C). In addition, in GR^{AlfpCre} and Stat5/GR^{AlfpCre} mutants, serum corticosterone and ACTH were elevated (Figure 26D, E) consistent with increased nuclear translocation of the GR in WAT (Figure 26F) and the lipodystrophic phenotype in the double mutants. Thus, Stat5/GR^{AlfpCre} mice displayed peripheral lipodystrophy driven by the compound effects of hepatocyte non-responsiveness towards GH action. This eventually led to elevated lipolytic drive through additive effects of elevated GH and corticosterone levels mobilising lipids in the adipose tissue.

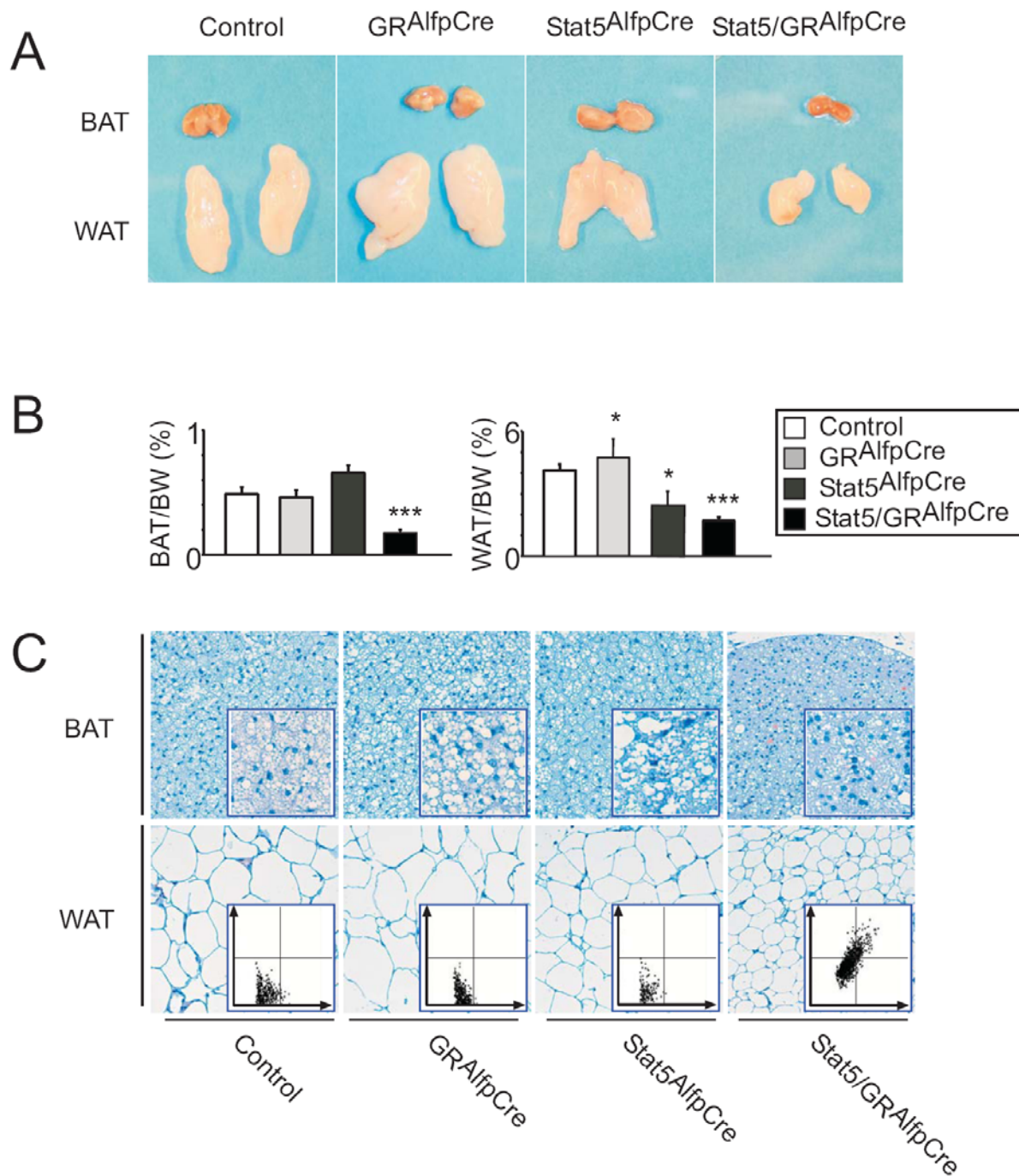


Figure 25. Atrophy of peripheral adipose tissues (lipodystrophy) in Stat5/GR^{AlfpCre} mice

For all subsequent panels, male mice at 12 months of age were analyzed. (A) Macroscopic appearance of intrascapular BAT and epididymal WAT. (B) WAT/Body Weight (WAT/BW) and BAT/Body Weight (BAT/BW) ratios. $n=8/\text{genotype}$; *, $p<0.05$; **, $p<0.01$, ***, $p<0.001$. Error bars represent mean \pm SEM. (C) Histology of BAT and WAT. Tissues were fixed and stained with HE. Inlets show higher magnification (top row) or quantification of cell density in adipose tissue. Adipocyte circumference versus area (Cell density) in WAT as determined by HistoQuest software (bottom) was plotted on y-Axis. X-Axis data represent haematoxylin staining intensity and mean X values were arbitrarily set =1.

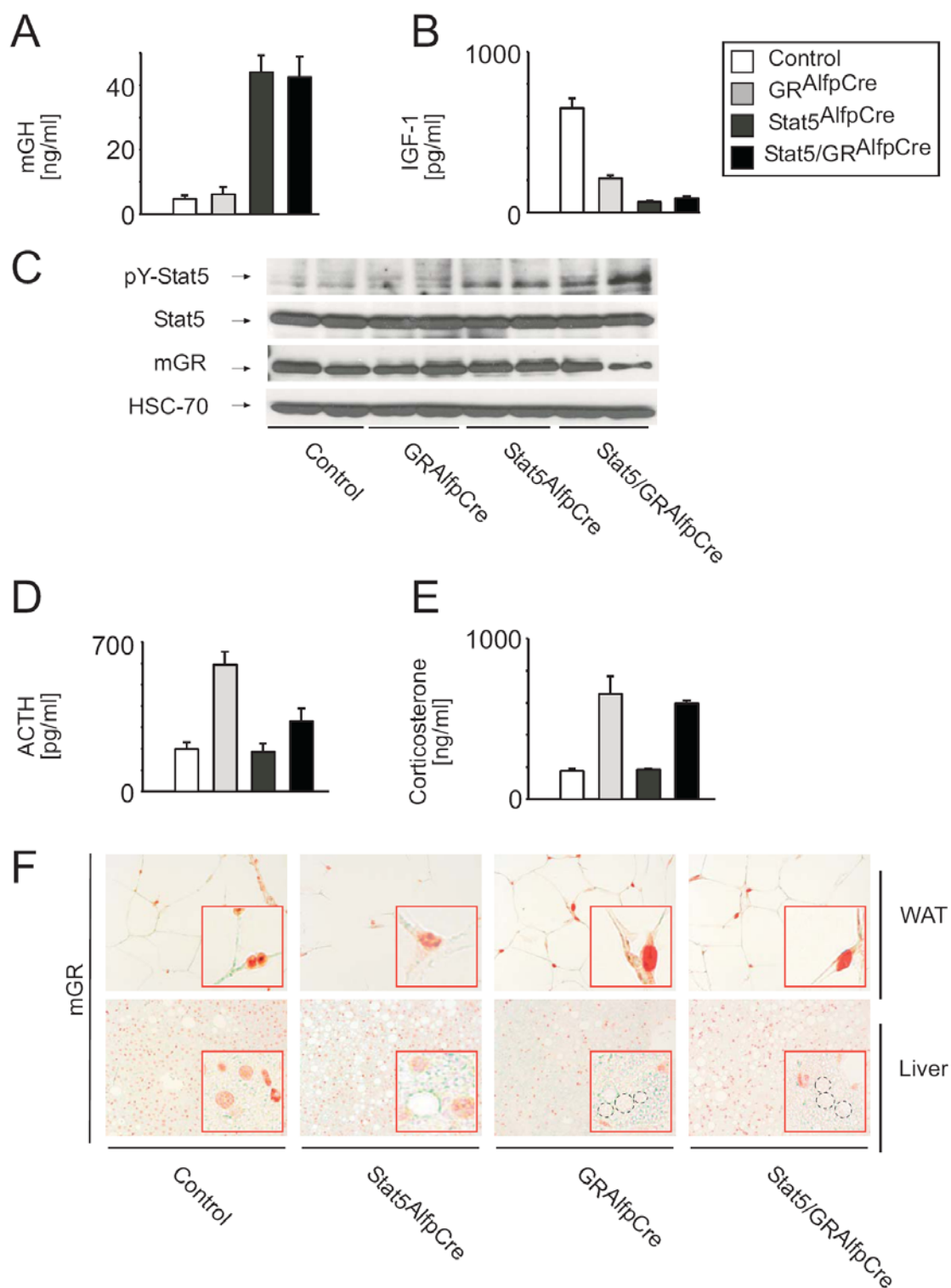


Figure 26. GH resistance and impaired GC negative feedback regulation in Stat5/GR^{AlpCre} mice
 For all subsequent panels, male mice at 12 months of age were taken. (A, B) Levels of GH (A) and IGF-1 (B) were determined by ELISA. For all subsequent serum analyses: n=8/genotype; *, p<0.05; **, p<0.01, ***, p<0.001. Error bars represent mean \pm SEM. (C) GH-mediated activation of Stat5 in epididymal WAT. Levels of phosphorylated Stat5 (pY-Stat5), total-Stat5 and total-GR were analysed using immunoblot analysis. (D, E) Levels of corticosterone (D) and ACTH (E) were determined by RIA. (F) Nuclear translocation of the GR in white adipose tissue (WAT) was analysed by immunohistochemistry.

3.2.4. Compound loss of hepatic Stat5 and Glucocorticoid Receptor signaling does not affect lipoprotein particle-mediated lipid distribution

Apart from imbalances in fatty acids synthesis and breakdown, liver steatosis can result from altered shuttling of lipids to and from the liver. Thus, we examined these processes in more detail. We isolated the hepatic organic phase, prepared density fractions using FPLC and determined the qualitative lipoprotein composition (see Methods). No apparent differences in lipoprotein particle-mediated shuttling of triglycerides were observed, although the triglyceride and cholesterol content in serum of GR^{AlfpCre} mice was generally lower (Figure 27). Thus, we concluded that the phenotypes observed in Stat5^{AlfpCre} and Stat5/GR^{AlfpCre} mutants were rather caused by induction of hepatic *de novo* lipid synthesis as shown above (Figure 22 and Figure 23) then by dysfunctional lipoprotein-mediated shuttling of lipids.

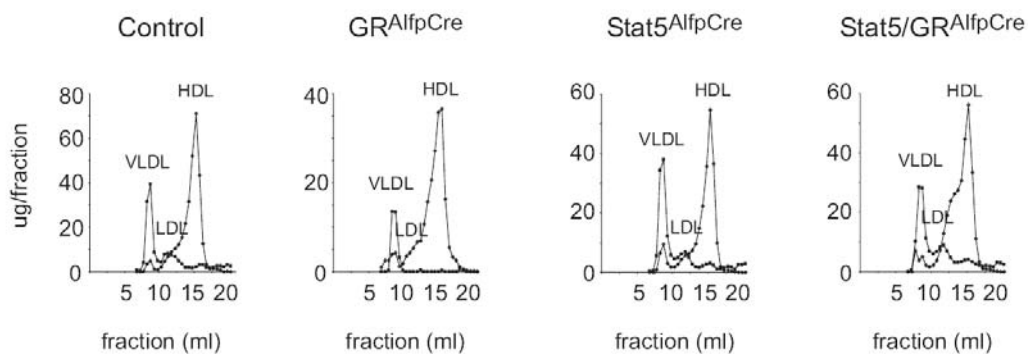


Figure 27. Unaltered lipoprotein particle profile in 8-weeks old male mice

Lipoprotein distribution was analysed by FPLC fractionation and subsequent TG and total cholesterol quantification in each fraction (n=5/genotype).

3.2.5. Loss of Stat5 is not compensatory counteracted by Stat1 and Stat3 activation

A recent publication reported the limited onset of liver steatosis in mice conditionally deleted for hepatic Stat5 signaling using Albumin Cre recombinase mediated excision of Stat5 alleles (Stat5^{AlbCre})¹²⁴. Compensatory activation of Stat1 and Stat3 transcription factors accompanied the fatty accumulation. Researchers proposed mechanistically that Stat1 and Stat3 proteins were compensatory recruited to the GHR without mechanistic proof. Moreover, aberrantly activated interferon signaling pathways normally associated with antiviral, immunomodulatory and antitumor activities were present in Stat5^{AlbCre} mutants. In contrast to the strategy followed by

Cui et al 2007, we warranted excision of floxed Stat5 alleles using AlfpCre recombinase which recombines more efficiently in liver hepatocytes and biliary cells^{114, 122}. Supportive of the findings observed by Cui et al., loss of hepatic Stat5 proteins mediated by AlfpCre recombinase led to significant increases in total Stat1 and a slight increase in total Stat3 levels (Figure 28; row 1, 3 and 5). In stark contrast to Cui et al., we observed no increased phosphorylation of Stat1 or Stat3 proteins in Stat5^{-AlfpCre} and Stat5/GR^{AlfpCre} mice (Figure 28, row 2 and 4). Thus, we explained the accumulation of lipids upon hepatic loss of Stat5 using AlfpCre as being a direct consequence of Stat5 deletion in the liver. The metabolic syndrome-like phenotype observed in Stat5^{-AlfpCre} and Stat5/GR^{AlfpCre} was thus irrespective of compensatory Stat1 and Stat3 signaling.

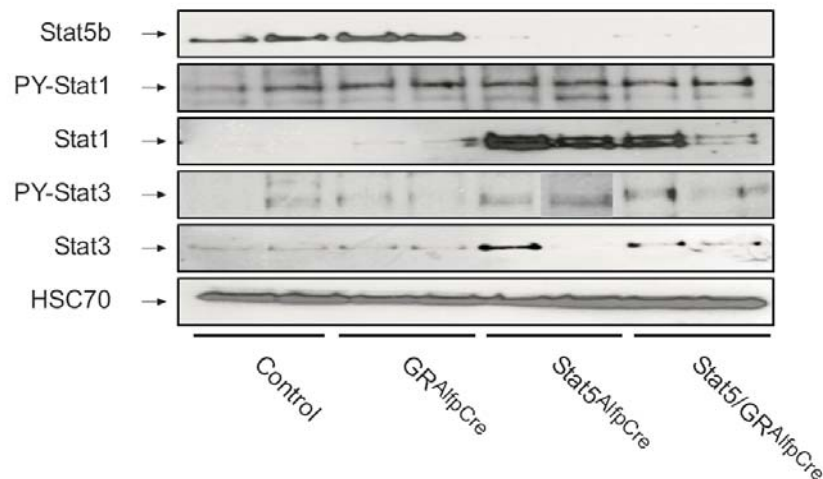


Figure 28. Loss of hepatic Stat5 is not compensatory counteracted by Stat1 and Stat3 activation

Representative immunoblots of liver homogenates from 8-weeks-old male mice. Amount of phosphorylation and total levels of Stat family members were determined using specific antibodies. HSC70 served as loading control.

3.2.6. Development of steatosis is independent of Jak2 upstream kinase

Upstream stimuli for Stat5 activation are conveyed by Janus kinases upon cytokine and growth factor stimulation; specifically Jak2 was shown to activate Stat5 upon GH action¹⁰⁹. As shown before, ablation of hepatic Stat5 signaling leads to inductions of hepatic *de novo* lipogenesis and concomitant onset of insulin resistance under steady-state conditions. We aimed to shed further light on the role of Jak2 in steatogenesis. To achieve hepatic losses of Jak2 proteins, we crossed mice harbouring floxed Jak2 alleles with mice expressing the AlfpCre recombinase

($Jak2^{AlfpCre}$). Interestingly, $Jak2^{AlfpCre}$ mutants had macroscopically normal livers (Figure 29A), exhibited neither increases in the LW/BW ratio (~5 % LW/BW) nor other obvious alterations upon macroscopic examination of livers. Histopathological analysis confirmed these observations: In contrast to $Stat5^{AlfpCre}$ and $Stat5/GR^{AlfpCre}$ animals, $Jak2^{AlfpCre}$ mutants exhibited no lipid accumulation in hepatic tissues. In addition, no fibrotic or necrotic processes could be observed (Figure 29B). Thus, we concluded that Jak2-dependent signal transduction is dispensable for the Stat5-mediated steatogenesis. Rather, this pinpointed towards direct repressive functions of Stat5 proteins on hepatic lipid biosynthesis. Interestingly, $Jak2^{AlfpCre}$ animals displayed perturbations in normal postnatal growth (not shown herein), further underpinning the importance of the GH-Jak2-Stat5-GR axis in regulation body growth.

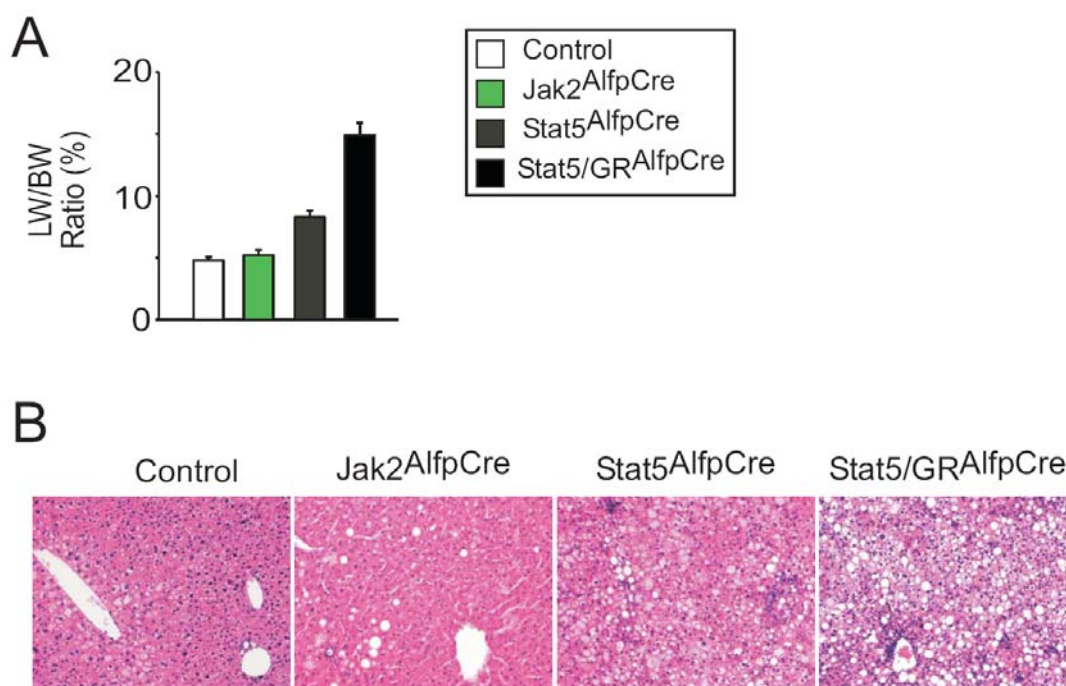


Figure 29. No liver steatosis upon loss of hepatic Jak2 signaling in $Jak2^{AlfpCre}$ mice
 (A) Liver/Body Weight (LW/BW) ratio in 6-months-old male mice. (B) Histological analyses of liver sections from 6-months old male mice. Tissue sections were fixed and stained with HE.

3.3. Loss of hepatic Stat5 leads to severe liver fibrosis in $MDR2^{-}$ mice

The transgenic $MDR2^{-}$ mouse line strain harbours genetics deletions of the multi-drug resistance protein 2 (MDR2), a liver-specific P-glycoprotein responsible for bile acid transport across the apical hepatocyte membrane¹⁷⁴. The $MDR2^{-}$ strain is widely used for studying the onset and progression of inflammatory liver cancer¹⁷⁵. To

investigate possible roles of hepatic Stat5 during liver carcinogenesis, we crossed MDR2⁻ mutants with mice specifically deleted for Stat5 in hepatocytes (Stat5^{AlfpCre}). By respective intercrossing we obtained four genotypes (Controls, MDR2⁻, Stat5^{AlfpCre} and MDR2⁻/Stat5^{AlfpCre}) which were born at Mendelian ratios. Postnatally, both Stat5-deficient lines, Stat5^{AlfpCre} and MDR2⁻/Stat5^{AlfpCre} exhibited profound defects in postnatal growth (Figure 30A, D), an effect caused by impairments in Stat5-mediated transcription of growth promoting genes such as IGF-1 (see section 3.1). In addition, livers of Stat5^{AlfpCre} and MDR2⁻/Stat5^{AlfpCre} mutants were yellowish and enlarged starting with four weeks of age (Figure 30B). Again this reflects the crucial role of Stat5 in hepatic lipid metabolism demonstrated earlier (see section 3.2). Strikingly, livers from MDR2⁻/Stat5^{AlfpCre} compound knockouts were texturized and sclerotic, pinpointing towards increased wound-healing and scar-formation processes leading to increased collagen deposition, a process widely observed during liver fibrogenesis (Figure 30B). Severe jaundice (Figure 30C) was observed in MDR2⁻/Stat5^{AlfpCre} double mutants and hinted towards perturbed bile flux across hepatocyte membranes or towards defective bile secretion into the intestine due to obliterated bile ducts (cholestasis). Serum levels of bile acids and bilirubin were increased dramatically (~19fold and ~23fold vs. controls). These are two parameters frequently elevated in cholestatic disorders such as PBC (primary biliary cirrhosis) and PSC (primary sclerosing cholangitis). Additional serum parameters indicative of extrahepatic cholestasis like high ALP and ALT (increased ~4.2fold and ~7fold respectively) were observed (Table 4). To investigate these processes in more detail, we undertook histopathological analyses of tissue specimens obtained from all four genotypes: HE staining of eight weeks old mice revealed no histopathologies in control animals and, interestingly, MDR2⁻ mutants. Stat5^{AlfpCre} knockout animals displayed significant steatosis as described earlier (see section 3.2). Interestingly, MDR2⁻/Stat5^{AlfpCre} mutant livers displayed marked perilobular fibrosis and a profound disruption of normal liver architecture (Figure 30E, top panel). Chromotrop Anilinblue (CAB) staining as collagen-specific marker revealed massive perivenular and perilobular collagen accumulation, indicative of severe liver fibrosis. Closer examination revealed marked pericellular collagen deposition (chicken wire fibrosis), an indicator for late-stage liver fibrosis (Figure 30E, bottom panel). Periodic acid-Schiff (PAS) staining as hepatic glycogen marked revealed defects in hepatocyte functions leading to defective synthesis and storage of glycogen in livers from MDR2⁻/Stat5^{AlfpCre} mutants.

Significant PAS negative areas were indicative of degenerative processes such as necrosis (Figure 30E, bottom panel). Thus, MDR2⁻/Stat5^{AlfpCre} knockouts exhibited severe liver fibrosis observed on the macroscopic and microscopic level. Fibrosis was accompanied by extensive extrahepatic cholestasis, jaundice and hepatomegaly. The respective single mutants exhibited mild histopathologies, in part reported before (see section 3.2).

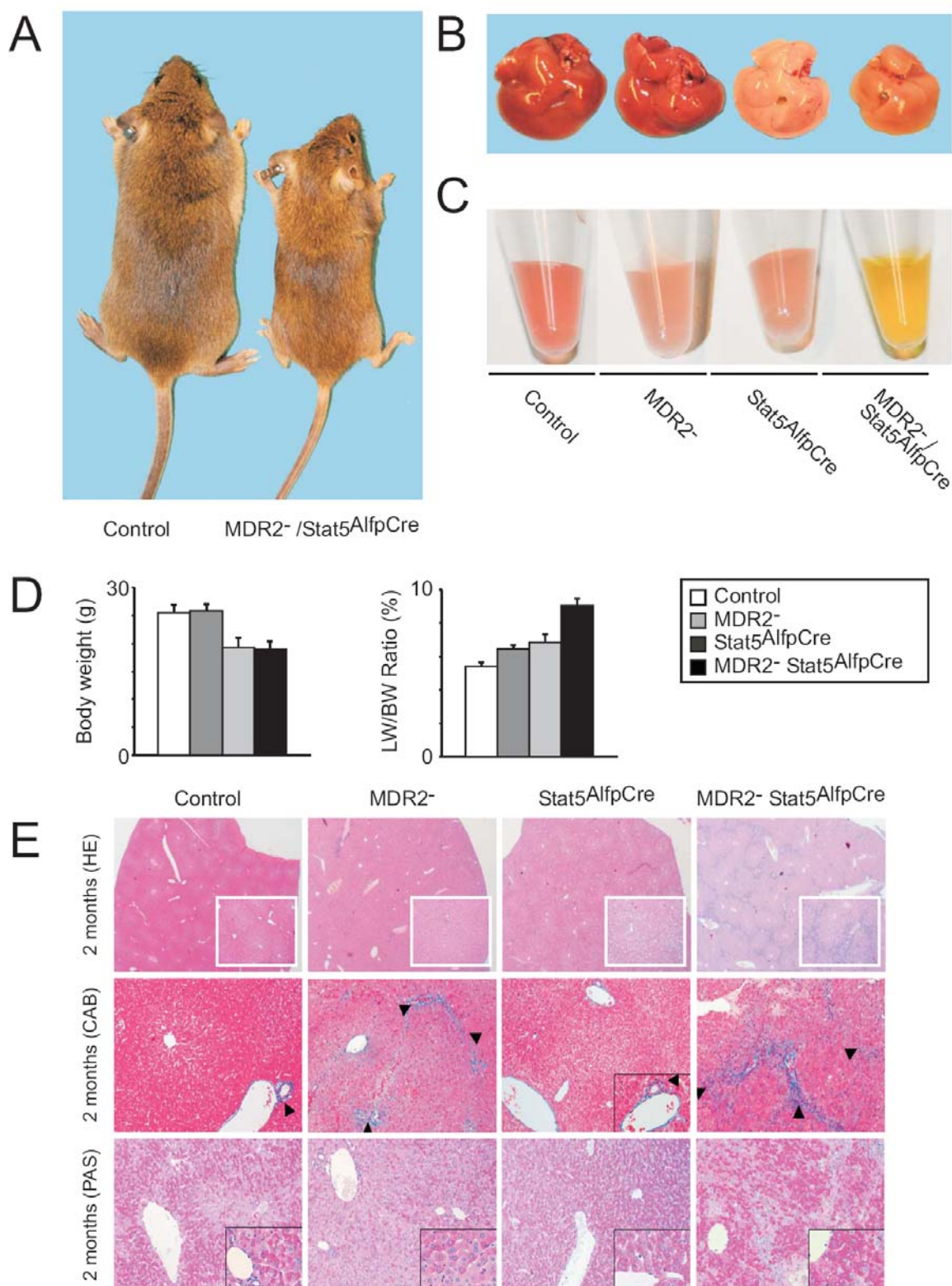


Figure 30. Loss of hepatic Stat5 in MDR2⁻ mice leads to cholestasis, jaundice and liver fibrosis (A) Macroscopic appearance and (B) Livers and (C) serum from 8-weeks-old male mice of the indicated genotypes. (D) Body Weight (left) and Liver/Body Weight (LW/BW) ratio (right) in 8-weeks-old male mice. Data represent mean ± SEM (n=8/genotype/timepoint). (E) Histological analyses of liver sections from 8-weeks old mutant mice. Tissue sections were fixed and stained with HE (row 1). Collagen deposition was visualized by CAB staining. Insets show higher magnification of vascular structures (row 2). Hepatic glycogen was visualized by PAS staining (row 3).

Table 4: Biochemical and metabolic serum parameters in male mutant mice

	n=	Controls	MDR2 ⁻	Stat5 ^{AlfpCre}	MDR2 ⁻ Stat5 ^{AlfpCre}
		8 weeks	8 weeks	8 weeks	8 weeks
Serum parameters					
ALT (U/l)	8	104 ± 13	284 ± 112 ^b	259 ± 38 ^b	690 ± 77 ^c
ALP (U/l)	8	160 ± 23	175 ± 18	181 ± 26	687 ± 76 ^c
TG (mg/dl)	8	176 ± 18	190 ± 17	221 ± 16 ^b	266 ± 11 ^c
Cholesterol (mg/dl)	9	142 ± 6	135 ± 10	117 ± 4	124 ± 10
Glucose (mg/dl) – fed	9	193 ± 7	197 ± 13	228 ± 20 ^a	221 ± 13 ^a
Bilirubin (mg/dl)	9	0.19 ± 0.02	0.16 ± 0.02	0.12 ± 0.01	4.34 ± 1.34 ^c
Bile acids (umol/l)	5	37 ± 3	42 ± 4 ^a	53 ± 5 ^b	687 ± 18 ^c

Eight weeks old male mice were fed with chow and sacrificed by carbon dioxide asphyxiation. Concentrations of given serum parameters are expressed as mean ± SEM for indicated number of mice from each genotype. ALT, alanine transaminase; ALP, alkaline phosphatase; TG, triglycerides. ^a = p-Value <0.05 vs. Control, ^b = p-Value <0.01 vs. Control, ^c = p-Value <0.001 vs. Controls.

3.3.1. Deletion of MDR2 proteins causes hepatic Stat5b activation

Tetrachloroethane (CCl₄) treatment leads to artificially induced liver fibrosis in mice. Recently, a report demonstrated important roles for hepatic Stat5 in CCl₄-induced fibrogenesis. Insensitivity to GH action (GH resistance) and blunted Stat5-mediated signal transduction accompanied the disease. Thus, Stat5 was claimed to constitute an importer repressor of liver fibrosis in mice.

To address the question whether Stat5 similarly counteracts MDR2-driven liver fibrogenesis, we isolated livers of all genotypes, prepared liver homogenates and determined the activation status of Stat5 and other important Stat family members using immunoblot analysis. Strikingly and in line with previous observations (section 3.2.5), loss of hepatic Stat5 leads to significant increases in basal Stat1 (strong) and Stat3 (mild) protein levels (Figure 31). Notably, no compensatory Stat1 or Stat3 hyperphosphorylation was observed. Interestingly, MDR2⁻ animals expressed significantly elevated levels of phosphorylated Stat5 (pY-Stat5). Thus, we reasoned that Stat5 might exhibit fibrogenesis-repressing functions during development or progression of liver fibroses.

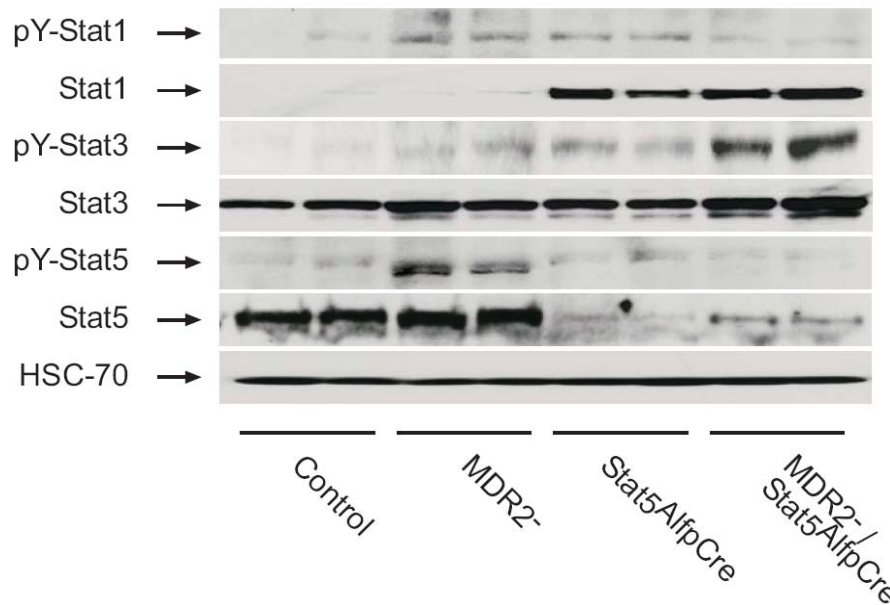


Figure 31. Loss of MDR2⁻ leads to compensatory hyperactivation of hepatic Stat5
 Representative immunoblots of liver homogenates from 8-weeks-old male mice. Amount of phosphorylation and total levels of Stat family members were determined using specific sera. HSC70 served as loading control.

3.3.2. MDR2⁻/Stat5^{AlfpCre} mice display autocrine growth factor loops

Hepatic stellate cells (HSC) under normal conditions perform important vitamin A storage functions, but upon a variety of liver insults transdifferentiate into pro-fibrogenic and pro-inflammatory myofibroblasts (MFB) ¹⁷⁶. MFB upon liver damage proliferate and accumulate at the site of tissue repair and synthesize ECM components like collagen. Kupffer cells, macrophage-like liver cells of mesenchymal origin secrete mitogenic PDGF and TGFb under fibrotic conditions, further favouring HSC transdifferentiation and ECM synthesis. To evaluate the impact of TGFb and/or PDGFb growth factor circuits in MDR2⁻/Stat5^{AlfpCre}-associated fibrosis, we isolated hepatic RNA and quantified TGFb and PDGFb mRNA levels by qPCR analysis. Interestingly, we observed only modest increases (~1.5fold vs. controls) of TGFb mRNA levels in MDR2⁻/Stat5^{AlfpCre} mutants. In contrast, TGFbR mRNA levels were drastically increased (~3.5fold vs. controls) in MDR2⁻/Stat5^{AlfpCre} mutants, thereby triggering potent TGFbR-dependent signal transduction even under conditions of moderately elevated TGFb (Figure 32, left). Unambiguously, PDGFb (~150fold vs. controls) and PGFbR mRNA (~40fold vs. controls) were elevated in MDR2⁻/Stat5^{AlfpCre} animals (Figure 32, right). Thus, autocrine PDGFb and, less pronounced

TGF β signaling is activated in fibrotic MDR2⁻/Stat5^{AlfpCre} double knockout animals. These observations reflect the current notion of an essential role of PDGF β and TGF β during hepatic fibrogenesis.

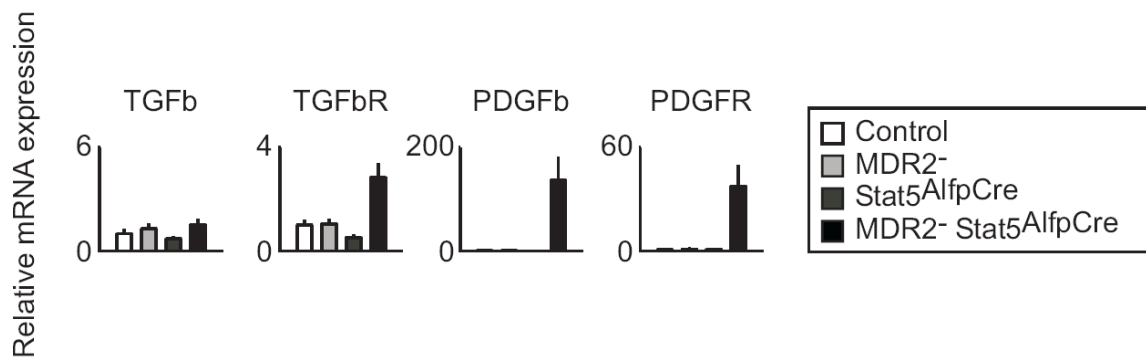


Figure 32. MDR2⁻/Stat5^{AlfpCre} mutants harbour hyperactive TGF β and PDGF β growth factor circuits

Quantitative PCR (qPCR) analysis of hepatic mRNA expression in male mice of indicated genotypes. For qPCR analysis, mice were sacrificed at eight weeks of age. Hepatic mRNA was isolated using Trizol, transcribed into cDNA and analysed by qPCR using intron–spanning, gene specific primers. Ct values were normalized to GAPDH mRNA levels using the Δ Ct method. Data represent mean \pm SEM. N=6/genotype were used.

3.3.3. Fibrogenesis in MDR2⁻/Stat5^{AlfpCre} mice is accompanied by ECM remodelling

Fibrosis is believed to secondarily occur due to repetitive liver insults and concomitant wound-healing processes. Following acute injury, the liver parenchyma undergoes intensive cellular proliferation in order to replace degenerative hepatocytes, accompanied by inflammatory processes and moderate deposition of collagen. Finally, the sum of liver insults leads to overt fibrosis, which can progress to late-stage liver pathologies such as cirrhosis, defined by the circumlobular deposition of collagen (Figure 30E). Molecularly, the massive build-up of ECM hails from imbalances between synthesis (predominantly collagen 1 and 3 (COL1 and COL3)) and proteolysis (predominantly Matrixmetalloproteases (MMP) members, especially MMP2, MMP3 and MMP13) of ECM components. Most MMPs are synthesized as latent pro-enzymes and require proteolytic activation by MMP14 and MMP15 to liberate their proteolytic properties. Tissue inhibitors of MMP1 and 2 (TIMP1 and TIMP2) effectively quench MMP proteolysis. Transcriptional activation of TIMPs and decrease of MMP mRNA synthesis is frequently observed during fibrotic processes. To assess the extend of ECM remodelling, we isolated hepatic mRNA of all four

genotypes and quantified transcript levels of important ECM modulators. The synthesis of collagen COL1 (~70fold vs. controls) and COL3 mRNA (~30fold vs. Controls) was massively induced in fibrotic MDR2⁻/Stat5^{AlfpCre} animals. TIMP1 (~30fold vs. controls) or TIMP2 (~5fold vs. Controls) mRNA transcription was concomitantly upregulated. Interestingly, MMP2 (~45fold), MMP3 (~10fold) and MMP13 (~25fold) mRNA transcript levels were severely upregulated compared to controls. The same was true for mRNA levels of membrane-tethered MMP activators MMP14 (~6fold vs. controls) and MMP15 (~3fold vs. Controls).

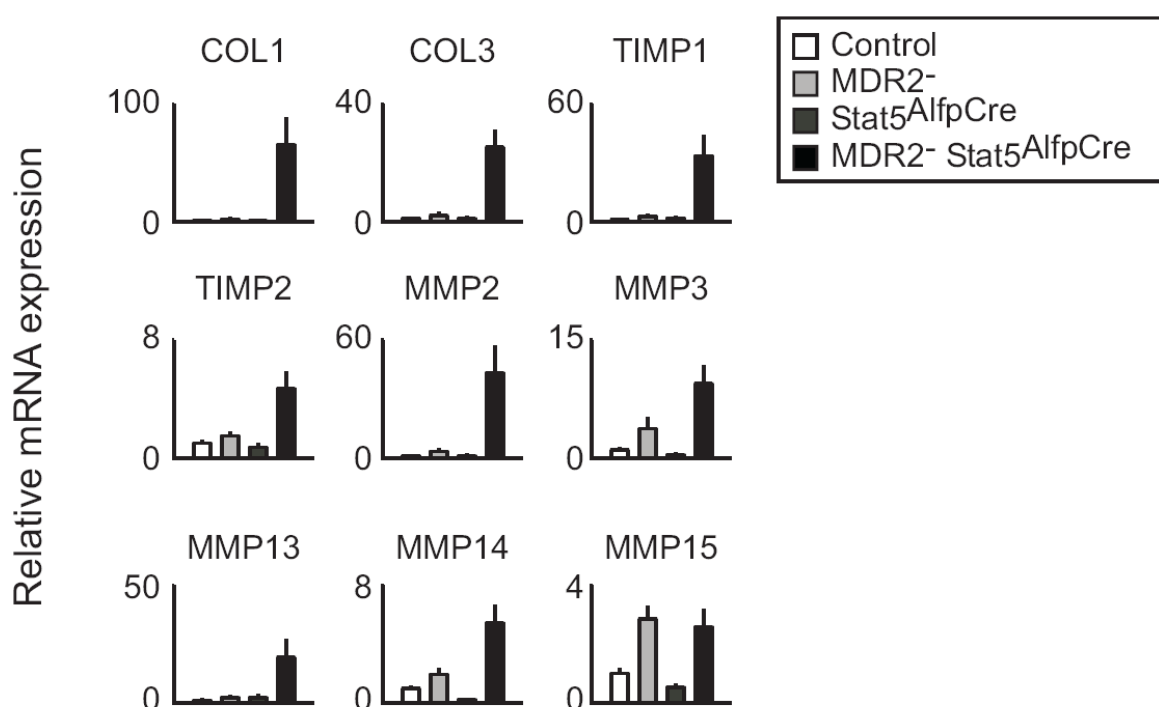


Figure 33. Fibrogenesis in MDR2⁻/Stat5^{AlfpCre} mice is accompanied by potent ECM remodelling
Quantitative PCR (qPCR) analysis of hepatic mRNA expression in male mice of indicated genotypes. For qPCR analysis, mice were sacrificed at eight weeks of age. Hepatic mRNA was isolated using Trizol, transcribed into cDNA and analysed by qPCR using intron-spanning, gene specific primers. Ct values were normalized to GAPDH mRNA levels using the Δ Ct method. Data represent mean \pm SEM. N=6/genotype were used.

Thus, fibrogenesis in MDR2⁻/Stat5^{AlfpCre} animals is accompanied by imbalances in ECM turnover. Potent synthesis of COL1 and COL3 in concert with strong inhibition of ECM proteolysis exerted by TIMP1 and TIMP2 was observed, leading to a massive build-up of collagen deposition. Interestingly, MDR2⁻/Stat5^{AlfpCre} mutant mice were also characterized by significant increases in MMP-dependent proteolysis. Notably, although MDR2⁻ animals exhibit modest liver fibrosis at eight

weeks of age, no significant remodelling of the ECM was observed on the transcript level.

3.3.4. Loss of hepatic Stat5 in MDR2⁻ mice leads to impaired bile acid circulation

An essential function for hepatocytes is the synthesis and recycling of bile. The underlying hepatobiliary transport processes are crucial for proper secretion and flux of bile^{177, 178}. These processes are regulated by an array of bile transporters located either on the basolateral (facing the hepatic sinusoids) or apical side (protruding into the bile canaliculi) of hepatocytes (reviewed in¹⁷⁹). Dysfunctional bile transporters expression is frequently observed in cholestatic diseases artificially induced by bile-duct ligation (BDL)¹⁸⁰. Common to animal models characterized by cholestatic-induced fibroses is the reduction of two major basolateral bile pumps; sodium independent organic anionic transporter (OATP1) and sodium dependent bile acid transporter (NTCP1). Dysregulation basolateral bile pump expression was also observed upon artificial induction of liver fibrosis¹⁸¹. Interestingly, NTCP1¹⁸² and OATP1¹⁸³ are experimentally confirmed Stat5 target genes; a finding pinpointing towards essential roles of Stat5 in bile circulation homeostasis. We thus addressed the question whether loss of hepatic Stat5 in MDR2⁻ mutants leads to dysfunctional bile acid flux due to aberrant NTCP1/OATP1 transporter expression. As shown in Figure 34A, NTCP1 and OATP1 transcript levels were severely downregulated in both Stat5-deficient mouse strains. In contrast, apical bile transporters (i.e. MRP2, MRP3, MDR1b and BSEP) did not differ significantly in their transcript levels, although modest reductions in OATP2 and BSEP mRNA could be observed (Figure 34B). To confirm our findings, we prepared liver homogenates and probed with antibodies specific for afore mentioned bile transporters (Figure 34C). In line with reduced mRNA levels, OATP1 protein levels were reduced to below the detection limit in mice devoid of Stat5 (Figure 34C, row 3). NTCP1 was residually expressed in Stat5^{AlfpCre} single mutants, yet significantly lower compared to control animals and undetectable in MDR2⁻/Stat5^{AlfpCre} animals (Figure 34C, row 4). Protein levels of MRP2 and MRP3 were unaltered (Figure 34C, row 1, 2). Thus, we could show that hepatic Stat5 loss in the MDR2⁻ background led to the downregulation of two major basolateral bile transporters, notably NTCP1 and OATP1 at the transcript and protein

level. This presumably results in impaired bile flux across the hepatocyte and retention of bile in the serum (Table 4). Residual NTCP1 expression in Stat5^{AlfpCre} animals might suffice to ensure physiological bile flux, reflected in the observation that serum bile acids are only moderately elevated (Table 4).

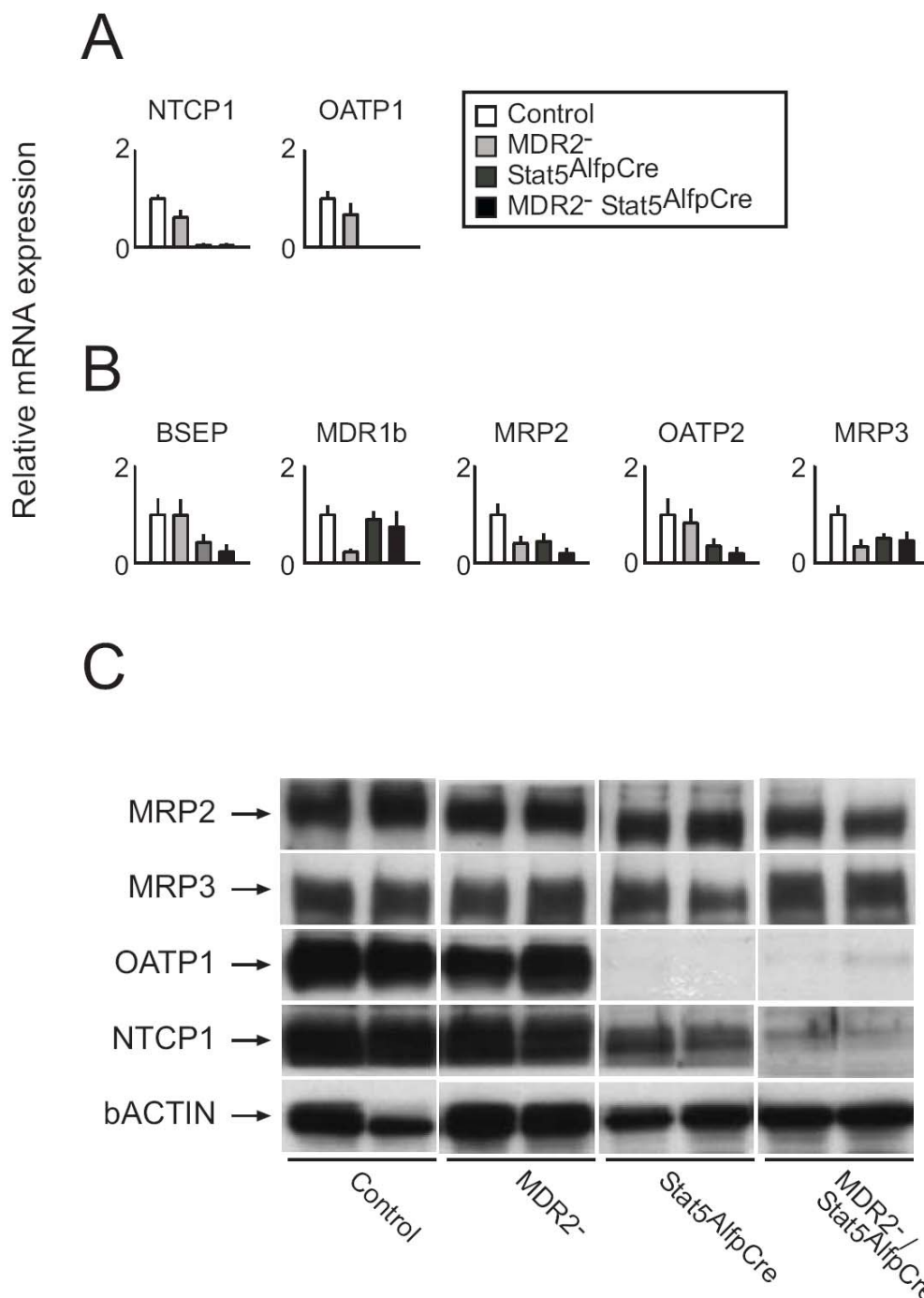


Figure 34. Loss of hepatic Stat5 defective NTCP1/OATP1-mediated bile flux

(A, B) Quantitative PCR (qPCR) analysis of hepatic mRNA expression in male mice of indicated genotypes. For qPCR analysis, mice were sacrificed at eight weeks of age. Hepatic mRNA was isolated using Trizol, transcribed into cDNA and analysed by qPCR using intron-spanning, gene specific primers. Ct values were normalized to GAPDH mRNA levels using the Δ Ct method. Data represent mean \pm SEM. N=6/genotype were used. (C) Immunoblot analysis of liver homogenates from

male mutant mice using specific antibodies. Endogenous beta Actin (bACTIN) served as loading control. Three livers of each genotype were analysed and representative images shown.

4. Discussion

4.1. A linear Stat5-GR axis controls postnatal body growth

We could demonstrate the critical role of GR–Stat5 protein interactions in regulating postnatal body growth and expression of maturation-related genes. Our hypothesis that this functional interaction is a direct consequence of physical Stat5-GR interaction is supported by the following results:

- (i) Affymetrix expression profiling revealed an extensive overlap of gene expression changes induced by the loss of either hepatic Stat5 or GR (Figure 9A).
- (ii) A tight correlation of the magnitude of expression changes for Stat5-GR coregulated genes was demonstrated for the single mutants ($\text{Stat5}^{\text{AlfpCre}}$ and $\text{GR}^{\text{AlfpCre}}$, Figure 9B).
- (iii) Combined ablation of GR and Stat5 transcription factors did not affect postnatal body growth or the expression of the Stat5-GR coregulated genes more than loss of Stat5 only (Figure 8).
- (iv) Aminoterminal truncation of Stat5 disrupted the protein–protein interaction of Stat5 with GR (Figure 11C,D) but led to similar growth retardations. Moreover, it resulted in abrogated transcription preferentially of those Stat5-responsive target genes that are also dependent on GR cofactor recruitment (Figure 12).

This is further supported by previous data, showing that GR is present on Stat5-dependent regulatory regions of growth hormone induced genes and that mice with a mutation in the dimerization domain of the GR (GR^{dim} mice) leading to defective DNA binding of GR, display normal growth and intact transcription of GH-responsive genes¹¹⁴. Collectively, these data support a model in which GH-activated Stat5 binds to Stat5 responsive DNA elements and uses the GR as a cofactor to promote body growth by inducing appropriate gene transcription. Our results have a clear implication for the long-standing discussion on the role of the liver in postnatal growth. According to the original “somatomedin hypothesis” from 1956, GH triggers the hepatocyte to secrete a secondary mediator (later suggested to be IGF-1) promoting postnatal growth. This hypothesis was later contradicted since it was shown that peripheral administration of GH promotes growth¹⁵⁴ and that deletion of IGF-1 in hepatocytes does not cause any major growth perturbations¹⁵⁷. It was also

shown recently that mice harbouring a muscle-specific loss of Stat5 show an approximate 20 % reduction in growth¹⁸⁴. However, researchers¹⁵⁵ showed that mice lacking ALS in all cells and IGF-1 exclusively in hepatocytes display abrogated growth behaviour. This suggested a role of the hepatocyte in somatic growth, although the conclusions of the study are somewhat limited since ALS was also deleted in non-hepatic tissues, such as in the developing cartilage. In addition, the confounding effect of IGF-1 deletion on general body growth was small and transient. We provide unequivocal evidence for the importance of Stat5 and GR in hepatocytes for postnatal growth. Thus, GH triggers growth both through endocrine factors secreted by the liver and through paracrine mediators produced in the target organs. In the study by Yakar et al., the blunted growth of the ALS/IGF-1 double-mutant mice was suggested to result from the fact that they had even lower levels of circulating IGF-1 than the liver-specific IGF-1 mutants. However, the growth disturbance of the mice in our study might depend on additional GH-target genes, further with actions different from simply regulating levels of circulating IGF-1. Thus, IGF-1 serum levels are only moderately reduced in the growth-retarded GR mutants (28 % reduction)¹¹⁴, while it is much lower in liver-specific IGF-1 mutants (75 % reduction), which show no overt growth defect. This implies that other genes found to be dependent on GR-Stat5 interactions in our study are actively involved in growth promotion. Identification of those additional hepatic GH-induced mediators of growth remains to be done and will probably be challenging since simultaneous and hepatocyte-specific deletions of several genes might be necessary. The second major finding was the unexpectedly high fraction of transcriptional activation mediated by GR and Stat5 dependent on a physical Stat5-GR interaction (42 % and 26 %, respectively). We could also demonstrate that the GR is not a mere general positive modulator of Stat5 action since the whole Stat5 transcriptome was divided in relatively clear sets of GR-dependent and GR independent genes. Interestingly, these sets fall into different functional groups. Thus, the genes dependent on Stat5-GR protein interactions were preferentially enriched in functional groups related to growth and maturation. However, a small group of Stat5-responsive genes are not totally, but still partially, dependent on GR. We show that the N-terminal domain of Stat5b constitutes the docking domain for the GR, while it is also involved in chromatin binding. Accordingly, it is required for the expression of genes dependent on physical Stat5-GR interaction *in vivo* and for maintaining physiological postnatal growth. We have recently

demonstrated that this domain is also important for the oligomerisation of Stat5¹⁸⁵. The AF-1 domain of GR may constitute its cognate binding partner, since it has been shown to be necessary for Stat5-GR interaction¹⁴⁰. In conclusion, we show an unexpectedly prominent role for the GR in acting as coactivator for Stat5 in hepatocytes. We provide *in vivo* evidence that this Stat5-GR interaction is not an unselective requirement for all Stat5 signaling processes but rather preferentially affects gene sets involved in growth and maturation. In line with this, we show that Stat5-GR protein interactions in hepatocytes are instrumental for maintaining physiological postnatal growth and that the coactivating action of GR involves the amino terminus of Stat5. This provided insight into the mechanism of growth control and we solved and supported the challenged somatomedin hypothesis at the transcriptional level, which postulated a critical role for hepatic GH signaling in postnatal growth.

As an example for Stat5-GR synergism in gene transactivation we chose Suppressor of Cytokine Signaling 2 (Socs2). Using Luciferase (LUC) reporter assays we could demonstrate that Stat5-mediated transactivation of the Socs2 promoter also necessitates GR signaling. We confirmed the dependence of synergistic Stat5- and GR signaling in a standard cell line (COS7) as well as in immortalized primary hepatocytes.

Generally, Stat5 signaling plays a key role in mediating cytokine and growth factor action. Constitutive signaling leads to malignant transformation and thus has to be tightly controlled. Stat5 feedback inhibition is in part mediated by transcription of Socs2 proteins leading to Jak2 or GHR degradation by ubiquitin-mediated proteolysis¹⁸⁶. No reports have so far demonstrated a role for GR signaling in modulating Stat5-mediated transactivation of Socs2. Interestingly, the estrogen receptor (ER), a closely related nuclear hormone receptor was shown to negatively regulate GH signaling by inducing Socs2 transcription¹⁸⁷. Although the findings presented in this study are reminiscent to results presented in the former report, no protein interaction between the ER and Stat5 were observed, putatively due to differences in the AF-1 domain, which is poorly conserved among nuclear hormone receptors, but it is crucial for Stat5-GR interaction¹⁴⁰. We thus conclude that Stat5-GR-dependent transactivation of the Socs2 promoter represents an unrelated finding. The significance of synergistic Stat5-GR co-dependent Socs2 transcription might open new avenues for keeping unbalanced Stat5 activity at bay. This is physiologically relevant, as hyperactivation

of Stat5 might lead to malignant transformation under certain conditions. Pharmacological activation of GR signaling in diseases, e.g. by established GR agonists (e.g. Prednisolone or Dex) would result in potent transactivation of the Socs2 promoter, leading to indirect suppression of Jak2-Stat5 signaling, presumably ameliorating disease.

4.2. Compound loss of hepatic Stat5 and GR signaling causes steatosis

Deletion of Stat5 in hepatocytes causes modest, non-progressive steatosis. Surprisingly, combined ablation of Stat5 and the GR induced severe, progressive steatosis, and steatohepatitis. Thus, we propose a two-step model of steatogenesis in Stat5^{AlfpCre} and Stat5/GR^{AlfpCre} mice.

(i) Hepatocyte-deletion of Stat5 leads to insulin resistance and steatosis due to induction of hepatic *de novo* lipogenesis. This is reflected by the phenotype observed in young Stat5^{AlfpCre} and Stat5/GR^{AlfpCre} mutants ('1st step'). Peripheral adipose tissues are unaltered at this time point.

(ii) Additional deletion of the GR mobilizes lipids from peripheral fat stores which eventually accumulate in the liver of older animals. This is reflected by the dramatic phenotype seen in older Stat5/GR^{AlfpCre} mice ('2nd step').

Triglyceride synthesis in the liver is mainly controlled by two transcription factors: Firstly, SREBP-1c controls cholesterol and fatty acid synthesis^{188, 189}. Secondly, the nuclear hormone receptor PPARgamma promotes lipogenesis in concert with C/EBPalpha^{43, 190}. In addition, SREBP-1c potentiates activation of the adipogenic PPARgamma/C/EBPalpha axis⁴⁸. Overexpression of SREBP-1c or PPARgamma factor induced steatosis in transgenic mice^{45, 46, 191}. Molecular signature analysis revealed a potent upregulation of SREBP-1c/PPARgamma-dependent *de novo* lipogenesis in Stat5^{AlfpCre} and Stat5/GR^{AlfpCre} animals. This was in line with a rising number of mouse models for liver steatosis which are characterized by SREBP-1c^{47, 192} and/or PPARgamma upregulation^{47, 193, 194}. The importance of PPARgamma and SREBP-1c has been underscored by their deletion in steatotic *ob/ob* mice. In both cases a reversion of hepatic fat accumulation was observed^{39, 44}. PPARalpha constitutes another important PPAR family member regulating beta-oxidation of fatty acids. High PPARgamma levels can lead to aberrant transactivation of the PPARalpha promoter¹⁹⁵. The induction of PPARalpha-dependent peroxisomal and

mitochondrial catabolism could be caused by this cross reactivity. Another, more speculative explanation for combined induction of PPARgamma and PPARalpha signaling pathways could be putative repressive functions of Stat5 in PPARalpha/gamma transcription. Indeed, Stat5 responsive elements were found in the human PPARgamma promoter¹⁹⁶ and an inhibitory function of Stat5 on PPARalpha/gamma-dependent transcription was demonstrated *in vitro*¹⁹⁷. Recently, a report underlined the significance of Stat5/PPARgamma interplay in hematopoietic disorders¹⁹⁸. Yet, the molecular nature of Stat5/PPAR interplay in epithelia remains enigmatic without further investigation.

In most cases, a tight correlation exists between steatosis and hepatic insulin resistance^{64, 199}. The hyperinsulinaemic conditions subsequently lead to increased *de novo* lipogenesis via SREBP-1c²⁰⁰ and a blunted suppression of FFA release from adipose tissues via HSL. High circulating levels of FFA can induce steatosis by aberrant deposition of lipids in hepatocytes. Increased plasma levels of FFA, resistin and insulin in Stat5^{AlfpCre} and Stat5/GR^{AlfpCre} mice suggested insulin resistance. This was confirmed by functional glucose and insulin tolerance tests. A molecular defect in phosphorylating the IR-adaptor proteins IRS-1 and IRS-2 upon insulin challenge was concomitantly observed. Two possible mechanisms might explain the insulin resistance observed in Stat5^{AlfpCre} and Stat5/GR^{AlfpCre} animals:

(i) The insulin resistance is secondary to the lipid accumulation caused by increased SREBP-1c/PPARgamma-dependent *de novo* lipogenesis. A similar effect is seen upon short term high-fat diet feeding of mice. These animals develop primary steatosis without concomitant insulin resistance²⁰¹. Hepatic insulin resistance develops later due to impaired IRS-1 and IRS-2 phosphorylation, as high levels of SREBP-1c are correlated to impaired transcription of IRS-2. Indeed, reduced levels of IRS-2 protein in concert with high SREBP-1c levels are observed in Stat5^{AlfpCre} and Stat5/GR^{AlfpCre} mice (Figure 24B and Figure 23A).

(ii) Hepatic insulin resistance in Stat5^{AlfpCre} and Stat5/GR^{AlfpCre} animals could be due to a putative IR-docking function of Stat5b. This was reported by multiple studies relying e.g. on Yeast 2-Hybrid screens^{52, 54}. Insulin-dependent activation of Stat5 was demonstrated to be independent of Jak2 upstream kinases²⁰². Our data support the latter notion, especially as mice harbouring conditional deletions of Jak2 in hepatocytes (Jak2^{AlfpCre}) did not develop steatosis (Figure 29A, B). Thus, conditional deletion of Stat5 in hepatocytes might lead to primary defects in IR-dependent signal

transduction. The aggravated insulin resistance phenotype of Stat/GR^{AlfpCre} mice compared with Stat5^{AlfpCre} animals was a reflection of the combination of both, pronounced insulin resistance (due to deletion of Stat5) and glucose intolerance (due to deletion of GR) (Figure 24A). This condition might be due to either increased internalisation or prolonged cytoplasmic retention of the IR, a compensatory mechanism described *in vitro*²⁰³. This was reflected in the reduced phosphorylation of the IR itself upon insulin action in Stat5/GR^{AlfpCre} animals. Surprisingly, we could not detect any significant *in vivo* tyrosine phosphorylation of Stat5b upon insulin injection over different time points and doses. Our data currently suggest a cytoplasmic role for Stat5b proteins in insulin signaling, but further proof would be required to clarify the role of Stat5b proteins in the IR signal transduction cascade.

Steatosis is not only found in obese but also in lean patients suffering under depletion of peripheral adipose tissues (lipodystrophy). The extent of hepatic fat accumulation correlates well with degeneration of peripheral fat depots²⁰⁴. The homeostasis of adipose tissues is usually tightly controlled. Among others, GH possesses potent lipolytic properties. High levels of GH reduce adipose tissue mass via increased basal lipolysis²⁰⁵ and leads to increased levels of FFA¹⁴⁸. This effect is dependent of Stat5 activation in adipose tissues²⁰⁶.

Glucocorticoids in contrast have anti-lipolytic properties and favour fat accumulation in adipose tissue via stimulation of LPL¹⁴⁵. Interestingly, a combination of both (GH+ glucocorticoids) leads to dramatic lipolysis exceeding the lipolysis induced by GH alone^{148, 149}. The secretion of GH is controlled via negative inhibition by IGF-1. Hepatic deletion of Stat5 reduced the synthesis of IGF-1 which was followed by high systemic levels of GH (GH resistance)¹²⁶. This liver-neuroendocrine feedback mechanism was reflected in the modest depletion of fat storages in Stat5^{AlfpCre} knock-outs^{123, 127} and was consistent with previous reports showing high levels of circulating GH levels upon hepatic Stat5 deletion²⁰⁷. The GH-mediated lipolysis was reflected in high phosphorylation of Stat5 in WAT of Stat5^{AlfpCre} and Stat5/GR^{AlfpCre} animals.

In contrast, GR^{AlfpCre} mice harboured enlarged fat pads and showed signs of hypercortisolism (preliminary data, not shown). We could show that high levels of corticosterone in GR^{AlfpCre} and Stat5/GR^{AlfpCre} animals were caused by elevated concentrations of ACTH. High levels of corticosterone subsequently led to increased nuclear translocation of the GR in WAT. A liver-mediated inhibitor of glucocorticoid

secretion (as seen for IGF-1 regulating GH secretion) was so far not described. Yet, mouse models with defects in hepatic gluconeogenesis (as seen in GR^{AlfpCre} mice¹³⁶) showed elevated levels of ACTH and corticosterone²⁰⁸. We excluded ectopic expression of the AlfpCre recombinase in the pituitary gland due to the reported obesity phenotype observed upon Stat5 deletion using Nestin-Cre., which deletes also in the pituitary²⁰⁹. We can currently not exclude that mechanisms upstream of the pituitary might contribute to ACTH release upon hepatic GR or Stat5/GR deletion. Taken together, Stat5/GR^{AlfpCre} animals harboured a hyperactive HPA axis leading to elevated levels of GH and glucocorticoids. This led to potent lipolysis of adipose tissues resulting in peripheral lipodystrophy. Increased mobilisation of triglycerides by combined GH and glucocorticoid action subsequently resulted in the massive flux of FFA into the liver of Stat5/GR^{AlfpCre} mice ('2nd hit'). This aggravated the mild steatosis caused by increased *de novo* lipogenesis upon Stat5 deletion in hepatocytes ('1st hit').

4.3. Loss of hepatic Stat5 signaling leads to severe liver fibrosis in the MDR2^{-/-} mouse model of inflammatory liver cancer

Liver fibrosis constitutes a severe liver pathology induced by constant liver damage and concomitant wound-healing processes. Repetitive liver insults such as chronic alcohol abuse or viral infections result in abundant collagen deposition around hepatic lobes, a process in which dynamics and magnitude of fibrotic damages are orchestrated by the nature of the damaging agent. It is widely established that bile flux perturbations and impairments in hepatic bile uptake result in cholestasis, in turn constituting a major risk factor for developing liver fibrosis. In various mouse models for cholestasis, the expression of NTCP1 and OATP1, two major basolateral bile pumps are severely compromised^{179, 180}. Whether these observations were causative for the development of cholestasis or mere compensatory consequences secondary to elevated serum bile levels could not be fully answered. NCTP1 and OATP1¹⁸³ are established Stat5 target genes, transcribed upon prolactin action. It was thus conceivable that loss of hepatic Stat5 would result in profound defects of bile flux across the hepatocyte. Interestingly, this did not induce cholestasis in Stat5^{AlfpCre} mutants alone. We hypothesized that additional insults due to loss of the apical MDR2 bile transporter are necessary to induce overt cholestasis as observed

in MDR2⁻/Stat5^{AlfpCre} double mutants. Generally, cholestasis and the concomitant retention of toxic bile in hepatocytes leads to constant hepatocyte damage, transdifferentiation of HSC, ECM remodelling and degeneration of hepatocytes. Thus, MDR2⁻/Stat5^{AlfpCre} mutants constitute a valuable murine model for liver fibrosis and could assist in further investigating molecular mechanisms underlying hepatic fibrogenesis. One especially intriguing aspect could be the pharmacologically induction of Stat5-dependent bile transporters putatively leading to alleviation of the disease.

In summary, my work on the Stat5GR transcription factor gene regulatory network contributes to our molecular understanding of postnatal body growth, the regulation of hepatic lipid metabolism and fibrogenesis in the liver. Hopefully, these results will lead to therapeutic inventions leading to amelioration of disease.

5. Materials and Methods

5.1. Materials

5.1.1. Chemicals and enzymes:

In general, chemicals, materials and enzymes were commercially obtained from the following companies:

Chemicals/Materials:

VWR international, Darmstadt, Germany
Sigma-Aldrich, Vienna, Austria
Lactan, Graz, Austria
Eppendorf, Vienna, Austria
Amersham, Vienna, Austria
Fisher Scientific, Vienna, Austria
Sarstedt, Wr. Neudorf, Austria
Qiagen, Vienna, Austria
Biorad, Vienna, Austria
PAA, Pasching, Austria
Applied Biosystems, Foster City, USA
Neolab, Heidelberg, Germany
BD Biosciences, Franklin Lakes, USA
Novo Nordisk Pharma, Vienna, Austria
MP Biomedicals, Illkirch, France
IBL Hamburg, Hamburg, Germany

Enzymes:

Invitrogen, Karlsruhe, Germany
 Roche, Mannheim, Germany
 New England Biolabs, Schwalbach, Germany
 Fermentas, St. Leon-Rot, Germany
 DAKO, Glostrup, Denmark

Radionucleotides:

Amersham, Vienna, Austria

5.1.2. Standard solutions10 x Phosphate buffered saline (PBS):

80 g	NaCl
2 g	KCl
14.4 g	Na ₂ HPO ₄
2.4 g	KH ₂ PO ₄

→ adjust pH to 7.4, fill up with H₂O_{dd} to 1 L and autoclave

10 x TBE (Tris borate EDTA) buffer :

108 g	Tris
55 g	boric acid
40 ml	0.5 M EDTA

→ fill up with H₂O_{dd} to 1 L and autoclave

50 x TAE (Tris acetate EDTA) buffer:

242 g	Tris
-------	------

57.1 ml Acetic acid
 100 ml 0.5 M EDTA (pH 8.0)
 → fill up with H₂O_{dd} to 1 L and autoclave

TE buffer:

10 mM	Tris/HCl pH 8.0
1 mM	EDTA pH 8.0

5.1.3. Media for bacterial cultivationLB medium:

10 g	Bacto-Trypto1
5 g	Yeast Extract
5 g	NaCl

--> fill up with H₂O_{dd} to 1 L, set pH =7.2 using NaOH and autoclave

LB agar:

1 x LB medium
 1.5 % (w/v) bacto agar

5.1.4. Plasmid constructs

pMSCV:

The pMSCV (Murine Stem Cell Virus) plasmids, originally designed as expressed vectors optimised for efficient protein expression in stem cell lines, are widely used in other mammalian cell lines. pMSCV plasmids harbour mutated MSCV-derived long terminal repeats (LTR) ensuring high transcriptional activity, driving abundant protein expression of cloned target genes. In addition, pMSCV plasmids harbour ampicillin resistance cassettes for selection of transformed bacteria. Hygromycin (hygro) resistance cassettes allow stable transfection of mammalian cell lines. A green fluorescent protein (GFP) is situated at the 3' end of the cloned target gene under the control of an internal ribosomal entry site (IRES) allowing for quantification of transfection efficiency using FACS (fluorescence activated cell sorting) analysis. The multiple cloning site (MCS) harbours restriction sites for standard restriction endonucleases used in molecular biology.

pE2F-Luc reporter plasmids:

pE2F-Luc was originally designed for monitoring E2F-promoter-dependent (a major target gene of the retinoblastoma (Rb) tumour suppressor, a critical cell-cycle regulator) transcriptional activation. To adapt the pE2F-Luc vector for quantifying Stat5-dependent transactivation of the Socs2 promoter, respective 5' promoter regions were cloned 3' of the TA minimal promoter (Figure 14). Thus, Luciferase transcription is driven by (i) the minimal TA promoter in concert with E2F enhancer elements and (ii) a variable Socs2 promoter region.

5.2. Molecular biology

5.2.1. Standard techniques

5.2.1.1. DNA electrophoresis

Routinely, DNA fragments were analysed by separation according to their molecular weight using agarose gel electrophoresis. Briefly, 1-2 % (w/v) low-melting agarose (Roche Cat. No. 1388991) was dissolved in 1 x TAE buffer, boiled in a microwave oven and allowed to cool down to approximately 40-50 °C. Five µl of ethidium bromide (10 mg/ml) was added per 100 ml agarose solution, the gel cast in plastic trays and allowed to solidify at RT. Depending on the size and agarose concentration of the gel a voltage between 80-130 V was applied. The migratory behaviour of the DNA fragments was visualised using a short-wave UV lamp.

5.2.1.2. Extraction of DNA fragments from agarose gels

Following size-separation by agarose gel electrophoresis, gel slices containing desired DNA fragments were excised under a UV lamp using a sterile blade. The DNA was separated from the agarose and purified using the QIAquick Gel Extraction Kit (Qiagen Cat. No. 28704) according to vendor's instructions. After column-based purification, the DNA was eluted with H₂O_{dd} and stored at -20 °C until needed.

5.2.1.3. Transformation of bacteria

Chemically competent E.coli DH5alpha Library efficiency (LE, Invitrogen Cat. No. 18263012) were used for standard plasmid amplification and transformation. For transformation, 200 µl of chemically competent LE were thawed on ice and 100 µl/reaction transferred to a prechilled 15 ml Falcon tube. Depending on the application either (i) 100 ng of plasmid DNA or (ii) 2 µl of ligation reaction mixture were added on ice and mixed gently. The reaction was incubated on ice for 20-30 min followed by a heat shock at 42 °C for exactly 90 s. Subsequently, the tube was allowed to chill on ice for 2 min and 900 µl of prewarmed LB medium added. The reaction was incubated at 37 °C for 60 min under shaking at 225 rpm and various dilutions of the reaction mixture plated on appropriated agar selection plates overnight. Positive single cell clones were picked using a sterile tip and transferred to a 15 ml Falcon tube containing 4 ml LB medium plus antibiotics.

5.2.2. Vector cloning

Cloning of truncated Socs2 promoter fragments (see Figure 14) into the pE2F-Luc Luciferase vector was performed using established protocols from Sambrook et al. (1989). Briefly, respective genomic sequences were amplified using primers containing appropriate restriction endonucleases sites. The PCR fragments were then cut by restriction enzymes, dephosphorylated using calf intestine phosphatase and ligated using T4 ligase into appropriately cut vectors. Purification of DNA fragments was carried out using the QIAquick Gel-Extraction Kit (Qiagen) according to supplier's protocol. Chemically competent DH5alpha E.coli was heatshock transformed and plated on agar selection plates. Positive clones were confirmed by restriction analysis and DNA sequencing.

5.2.2.1. Cloning strategy for Socs2 reporter constructs

In the following, DNA sequences of primers are given which were used for PCR amplification of Socs2 promoter regions for subsequent cloning into the pE2F-Luc Luciferase reporter vectors:

<u>PrimerID</u>	<u>Sequence (Localisation 5' of Socs2 mRNA transcription start)</u>
S2Clon1	GCG CGG CCA <u>CGC GTT</u> CTG TGC AAA GGC CCA GGA GGG (bp -4696 to -4675 5' of Socs2 mRNA ATG)
S2Clon2	GCG CGG CCA <u>CGC GTG</u> CAT CCT GCT AAG TTA CTC CC (bp -3402 to -3364 5' of Socs2 mRNA ATG)
S2Clon3b	GCG CGG CCA <u>GAT CTA</u> GTG TGC GCG CGA CTT CCC AG (bp -1845 to -1865 5' of Socs2 mRNA ATG)
S2Clon4b	GCG CGG CCA <u>GAT CTG</u> GGA GAT GAG TCA ACA CGT CC (bp 1 to -20 5' of Socs2 mRNA ATG)
	<u>Mlu I site</u>

Bgl II site**5.2.3. DNA isolation and analysis****5.2.3.1. Isolation of plasmid DNA from bacteria**

Plasmid DNA was isolated using commercially available plasmid isolation kits (Qiagen Cat. No. 27106) according to vendor's manual. Briefly, bacteria were lysed, cellular debris removed and the supernatant given onto a DNA-binding matrix column. The column was rinsed extensively with ethanol and the DNA eluted using nuclease-free H₂O_{dd}. The DNA concentration was determined using UV/VIS spectrophotometry: The OD at 260 nm was used for calculation of DNA concentration and the OD ratio of 260 nm/280 nm served as indicator of DNA purity. Generally, DNA exhibiting a 260 nm/280 ratio = 1.8-2.0 were used for subsequent experiments. The DNA was used instantly for cloning purposes or stored at -20 °C for long-term storage.

5.2.3.2. Isolation of tail DNA for genotyping

Pups were weaned between day 17-21 post natum and identified using ear tags. In addition, a 1-2 mm tail piece was clipped using sterile scissors, transferred into a 1.5 ml reaction tube and digested in 200 µl of NID buffer containing 2 µl of Proteinase K (stock solution 10 mg/ml) overnight at 56 °C. The next morning, the proteolytic activity was inactivated by heating to 95 °C for 10 min. Two µl of supernatant used as template for genotyping the mice using gene-specific genotyping PCR.

NID buffer:

50 mM	KCl
10 mM	Tris-HCl (pH 8.3)
2 mM	MgCl ₂
0.1 mg/ml	Gelatine
0.45 %	NP-40
0.45 %	Tween-20

5.2.3.3. Genotyping PCR

To determine the allele status of specific genes, 2 µl of tail DNA were analysed by gene-specific PCR using *Taq*-polymerase (Roche) following manufacturer's instructions. The cycling conditions used for all genotyping PCR were as follows:

<u>95 °C</u> (1 cycle)	<u>5 min</u>	<u>Initial denaturation</u>
95 °C	20 s	Denaturation
55 °C	20 s	Annealing
<u>72 °C</u>	<u>90 s</u>	<u>Elongation</u>

(40 cycles)

72°C	10 min	Final elongation
(1 cycle)		

Following PCR amplification, the reaction mixture was diluted with DNA loading buffer and analysed using 2 % agarose gel electrophoresis containing 5 µl ethidium bromide (10 mg/ml) per 100 ml gel.

In the following, DNA sequences of primers used for gene-specific genotyping PCR are given. All oligonucleotides were obtained commercially (MWG Biotech, Munich).

<u>Primer ID</u>	<u>Sequence</u>
GR flox1	5' – GGC ATG CAC ATT ACG GCC TTC T – 3'
GR flox4	5' – GTG TAG CAG CCA GCT TAC AGG A – 3'
GR flox8	5' – CCT TCT CAT TCC ATG TCA GCA TGT – 3'

Amplicons:

GR ^{wt}	225 bp,
GR ^{flox}	275 bp
GR ^{null}	390 bp

<u>Primer ID</u>	<u>Sequence</u>
S5del1685	5' – GAA AGC ATG AAA GGG TTG GAG – 3'
S5f11686	5' – AGC AGC AAC CAG AGG ACT AC – 3'
S5f11842	5' – AAG TTA TCT CGA GTT AGT CAG G – 3'

Amplicons:

Stat5 ^{wt}	450 bp
Stat5 ^{flox}	200 bp

<u>Primer ID</u>	<u>Sequence</u>
Cre1	5' – CGG TCG ATG CAA CGA GTG ATG AGG – 3'
Cre2	5' – CCA GAG ACG GAA ATC CAT CGC TCG – 3'

Amplicons:

AlfpCre ⁺	700 bp
----------------------	--------

<u>Primer ID</u>	<u>Sequence</u>
MDR2for	5' – GCT GAG ATG GAT CTT GAG – 3'
MDR2rev	5' – GTC GAG TAG CCA GAT GAT GG – 3'

Amplicons:

MDR2 ^{wt}	362 bp
--------------------	--------

<u>Primer ID</u>	<u>Sequence</u>
NEOgeno1	5' – ATC CAA AGC CAG AGC ACC GG – 3'
NEOgeno4	5' – TTT GTC ACG TCC TGC ACG ACG C – 3'

Amplicons:

MDR2 ⁻	700 bp
-------------------	--------

5.2.4. RNA isolation and analysis

5.2.4.1. Isolation of messenger RNA from murine livers

High quality mRNA was isolated from frozen organs (e.g. liver, adipose tissues). Approximately 50 mg of frozen tissue were transferred into a prechilled 14 ml round bottom Falcon tube containing 5 ml of Trizol reagent (Fisher Scientific Cat. No. VX15596018). Tissue specimens were homogenized directly in Trizol using a rotating blade homogenator. The resulting homogenate was incubated for 2-3 min at RT to sequester RNA from bound nucleoprotein complexes and transferred into a new nuclease-free reaction tube. Chloroform was added (200 μ l per initial 1 ml of Trizol reagent), vigorously shaken and centrifuged at 12,000 rpm for 15 min at 4 °C. The upper aqueous phase, containing hydrophilic RNA was transferred into a new tube, carefully ensuring no cross-contamination with the lower organic phase. For precipitation, 0.7 x (v/v) 2-propanol was added and incubated for 10 min at RT. Two μ l of glycogen were added to facilitate pellet handling at later stages. Centrifugation at 12,000 for 10 min led to pelleting of precipitated RNA, which was washed two times with 75 % DEPC-Ethanol. Finally, the solvent was removed, remaining ethanol droplets carefully removed using a pipette and 100 μ l of DEPC-H₂O added for solubilization of the RNA. The solubilization was facilitated by incubating the tube at 37 °C for 10 min. Isolated RNA was used for Affymetrix expression profiling or reversely transcribed into cDNA for quantitative RT-PCR (qPCR) analysis. Samples were stored at -80 °C and repeated freeze-thawing avoided by appropriate aliquoting. The RNA quality and quantity was determined using agarose 1 % RNase-free 1x MOPS gel electrophoresis: For this, 500 ng of isolated RNA were diluted in 10 μ l RNA denaturation buffer and incubated at 65 °C for 10 min. Following denaturation, samples were loaded onto the gel and separated at low voltage (< 80 V). High RNA quality could be ascertained by three clearly discriminable bands for 28 S, 18 S and 5.8 S of ribosomal RNA (rRNA). The ratio between 28 S to 18 S RNA bands should be approximately 2:1.

H₂O/DEPC

1 l

H₂O_{dd}

1 ml

Diethylpyrocarbonate (DEPC)

→ The mixture was stirred, incubated overnight at RT and autoclaved

RNA denaturation buffer:

5 μ l

Ethidium bromide

0.5 μ l

10x MOPS buffer

5 μ l

Formamide

1.75 μ l

Formaldehyde

0.55 μ lNuclease-Free H₂O

MOPS buffer:

41.8 g

[N-Morpholino] propanesulfonic acid (MOPS)

6.8 g

Sodium Acetate

20 ml

0.5 M EDTA

→ fill up with DEPC-H₂O to 1 L, autoclave and store at 4 °C in the dark.

In addition, the concentration of isolated RNA was quantified using UV/VIS spectrophotometry at 260 nm. The 260 nm/ 280 nm ratio was an indicator of RNA purity and should be >1.8.

5.2.4.2. Reverse transcription

For synthesis of complementary DNA (cDNA) from respective mRNA samples, 1 µg of total RNA were used. The cDNA synthesis was carried out using commercially available kits (Applied Biosystems). Total RNA was diluted to 2 µl and incubated with MuLV reverse transcriptase (Applied Biosystems Cat. No. N8080018) buffer, oligo-dT primers (Applied Biosystems Cat. No. N8080128), RNase inhibitor (Applied Biosystems Cat. No. N8080119) and DEPC-H₂O for 5 min at 70 °C for annealing of oligo-dT primers onto poly-A sequences of the mRNA. Afterwards, the samples were incubated on ice for > 2 min and 1 µl MuLV reverse transcriptase (Applied Biosystems Cat. No. N8080018) were added, followed by an incubation for 60 min at 42 °C. A final heat inactivation step at 70 °C for 10 min removed residual reverse transcriptase activity. The cDNA was diluted 1:5 and was used instantly or stored at -20 °C.

5.2.4.3. Quantitative RT-PCR (qPCR)

Five µl of diluted cDNA samples (section 5.2.4.2) were used for quantification of gene-specific transcript levels via quantitative RT-PCR (qPCR). For this, the diluted cDNA was amplified using commercially available *Taq* polymerase kits (Eppendorf Cat. No. 0032007724) according to manufacturer's instructions. Intron-spanning primers ensured amplification of specific mRNA transcripts. Cross-contamination of genomic DNA (gDNA) was excluded by regular testing of mRNA samples not reversely transcribed. The SYBR green method was applied for determining concentrations of double stranded PCR products obtained after PCR using intron-spanning primers. The PCR cycle in which a given mRNA specific fluorescent signal crossed an arbitrary threshold was defined as C_T .cycle. The difference of a gene-specific C_T value to that of an endogenous housekeeping gene (GAPDH) was called ΔC_T value. Individual ΔC_T for all genotypes were calculated and compared relatively to controls. The primer sequences were designed manually and DNA oligonucleotides obtained from a commercial supplier (MWG Biotech, München). The DNA sequences of primers used for qPCR analysis are given in (Table 5).

Gene symbol	Accession No.	Sequence
Srebp-1	NM_011480	for: GCG TGG TTT CCA ACA TGA CC rev: CTC CAG CTC AGC TGT AGT GC
Fasn	NM_007988	for: TGT CTG ACA CTG GCA ATC TGA T rev: CGG TCA CAC GGG TAG GTA GC
Scd1	NM_009127.3	for: CGC TCT TTA CCC TTT GCT G rev: ATA GTC AGT TGC TCG CCT CAC
Scd2	NM_009128.1	for: ATC TGC AGG ATT GCC TCT GGG rev: TCT CAT GCT CAC ACC TAC CCG
Acaca	NM_133360.2	for: GGA CTT CAT GAA TTT GCT GAT TCT CAG TT rev: GTC ATT ACC ATC TTC ATT ACC TCA ATC TC

Acacb	NM_133904.1	for: AGT GTG TAA GAA GCT CGT GGG rev: CCT CCA GTA GAA GAA GGT GCG
Pparg	NM_011146.2	for: ACC CAA TGG TTG CTG ATT AC rev: CGG GAA GGA CTT TAT GTA TGA G
Dgat1	NM_010046.2	for: TGT GGT GAT GCT GAT CCT GAG rev: GGA TAG GAT CCA CCA GGA TGC
Dgat2	NM_026384.3	for: TGG CAT AAG GCC CTA TTT GG rev: ATG GTG TCT CGG TTG ACA GG
Cd36	NM_007643.3	for: CCT TAC TTG GGA TTG GAG TGG rev: CGG CTT TAC CAA AGA TGT AGC C
Fabp4	NM_024406.1	for: TTC GAT GAA ATC ACC GCA GA rev: AGG GCC CCG CCA TCT
Mod1	NM_008615.1	for: AGT TGC TCT TGG GGT GGT GGC rev: TAG TGC TGT ACA TCT GGG AGG
Ppara	NM_011144.3	for: ATC GCG TAC GGC AAT GGC TTT A rev: GCC TCG GAG GTC CCT GAA CAG
Acox1	NM_015729.2	for: CCG CCT ATG CCT TCC ACT TTC TC rev: CGC CAC TTC CTT GCT CTT CCT GT
Ehhadh	NM_023737.2	for: CCG GTC AAT GCC ATC AGT CC rev: GGT AGA AGC TGC GTT CCT CTT GC
Acadm	NM_007382.2	for: ATG ACG GAG CAG CCA ATG A rev: ATG GCC GCC ACA TCA GA
Acadl	NM_007381.3	for: AGC TGA TCG CAA GAC AGA TCG rev: AGA ATC CGC ATG AGC TGC ATG
Acavdl	NM_017366.2	for: CCC GGT TCT TTG AGG AAG TGA A rev: AGT GTC GTC CTC CAC CTT CTG
Cpt1	NM_009948.1	for: CGA GGA TTC TCT GGA ACT GC rev: GGT CGC TTC TTC AAG GTC TG
Pgc1a	NM_008904.1	for: CCG ATC ACC ATA TTC CAG GT rev: GTG TGC GGT GTC TGT AGT GG
Cebpa	NM_007678	for: ATG GAG TAC AGC GGT GAG TAT TC rev: GTT GCC ACT GGA CAT CTC TTC
Cebpb	NM_009883.2	for: GGT GGA CAA GCT GAG CGA CGA GTA rev: AAC AAG TTC CGC AGG GTG CTG AG
Hnf1a	NM_009327.2	for: CCA CGT TCA CGA ACA CGG GCG CC rev: TGG AGG CCT CTG TGT CTG AGG TG
Rxra	NM_011305.3	for: CGA GCC ATT GTC CTG TTC AAC CC rev: TGG CTT GAT GTG GTG CCT CCA GC
Tgfb1	NM_011577.1	for: GGC ACC GGA GAG CCC TGG ATA CC rev: CGG CAC GCA GCA CGG TGA CGC CG
Tgfbr	NM_009370.2	for: TTG CCA GGA CCA TTG TGT TA rev: GGA ACC ATG AAC GCT CTT CT
Pdgf1	NM_011057.3	for: CCC ACA GTG GCT TTT CAT TT rev: GTG GAG GAG CAG ACT GAA GG
Pdgfr	NM_008809.1	for: TCA ACG ACT CAC CAG TGC TC rev: TTC AGA GGC AGG TAG GTG CT
Col1	NM_007742.3	for: CAC CCT CAA GAG CCT GAG TC rev: TGG CGG GCT GAT GTA CCA GT
Col3	NM_009930.1	for: GGG GAC CAG GGC GAC CAC T rev: CAG GTG AAC CCG GCA AGA ACG
Timp1	NM_011593.2	for: TCC TCT TGT TGC TAT CAC TGA TAG CTT rev: CGC TGG TAT AAG GTG GTC TCG TT
Timp2	NM_011594.3	for: GGG ACA CGC TTA GCA TCA CCC rev: GAA GAA CTT GGC CTG GTG CCC
Mmp2	NM_008610.2	for: TCC CTG ATA ACC TGG ATG CCG rev: GCA GCG ATG AAG ATG ATA GGG C
Mmp3	NM_010809.1	for: CAT TCA CAC CCT GGG TCT CCC rev: GCT TCA AAG ACA GCA TCC ACC C
Mmp13	NM_008607.1	for: TCT TCT CTG AGA ACC ACG TGT GG rev: GAC TCT CAC AAT GCG ATT ACT CC

Mmp14	NM_008608.2	for: GGG TGT TTG ACG AAG CCT CCC rev: GCT GAC TTG GGA TAC CCT GGC
Mmp15	NM_008609.3	for: ATC CCC ACC TCT CCC AAA GGG rev: TCC CGC AGG ATG GAT TTG GGG
Ntcp1	NM_011387.1	for: ACC TTC CCC CCT GAA GTC ATT GG rev: GGA TTA TTC CCG TTG TGG GTA CC
Oatp1	NM_013797.2	for: GTT TCA TCT TCT CAC TCG CAG CC rev: TTG ATC CTC TCA CTG CTG CAG GC
Bsep	NM_021022.3	for: CAA CAC CAA AGA GAT CTC CGT GG rev: CAA TGA CAA TAC AGG TCC GAC CC
Mdr1b	NM_011075.1	for: TTG TGA GGG CAG CCA AGG AGG CC rev: CAC AAT GCA GGT GCG GCC TTC CC
Mrp2	NM_013806.2	for: TTG TGG CTG GCC TGC AAC TTG GG rev: CAA TCT TGC CGC TGT CTA GGA CC
Oatp2	NM_178235.2	for: GAA TTG AAA TCA CTT GGA ATG GG rev: TTA AAG CTA TAC TCA AAC CCA CG
Mrp3	NM_029600.3	for: GCA GGC CTG GAT TTC CAG TGC GC rev: ATT CAG CTA CTA CTC CTT TGT CC

Table 5. Primer sequences used for qPCR experiments

5.2.4.4. Whole genome expression profiling (Affymetrix) and bioinformatics

For each microarray, three livers were pooled. Total RNA was isolated using RNeasy kits with DNaseI digest on column (Qiagen). RNA quality was assessed using the Bioanalyzer 2100 Lab-on-chip system (Agilent Technologies). Ten μg of isolated RNA were labelled and hybridised onto mouse U74Av2 arrays (Affymetrix), containing 12,500 sequences. We used three arrays for each mutant group ($\text{Stat5}^{\text{AlfpCre}}$, $\text{GR}^{\text{AlfpCre}}$, $\text{Stat5/GR}^{\text{AlfpCre}}$ and $\text{Stat5}^{\Delta\text{N}}$) and nine arrays for the control group (littermates to the mutant mice). Arrays were normalized using GCRMA. Genes with a mean expression of <25 in all of the groups were excluded. Significance levels were calculated in affyImGUI. As criterion for calling a gene significantly changed we used $p < 0.001$, or the combined criterion of $p < 0.0025$ and a log ratio >1 or less than -1 (fold change >2 or <0.5). Investigation of coordinated changes in functional gene sets was done using MAPPfinder. We limited the analysis to approximately 100 predefined groups, of which some were custom made. The two criteria for inclusion of genes were $p < 0.01$ and $p < 0.05$. Gene sets with p -value <0.05 after correction for multiple comparisons were considered significant.

5.2.4.5. Molecular signature analysis of Affymetrix expression data

We performed a specific molecular signature analysis for genes involved in lipid metabolism on raw data from microarray analysis previously described (section 5.2.4.4). In order to find molecular signatures in the data we looked for coordinated changes in functional gene-sets using MAPPFinder¹⁵⁹. We limited the analysis to around one hundred hand-picked, pre-defined groups, of which some were custom-made from papers describing profiles from the livers of mice lacking different transcription factors or administered with specific agonists or antagonists. Many lists were also taken from the GSEA software and consist of genes with certain motifs in their promoter regions as identified in a systematic study of regulatory motifs in mammals²¹⁰. The two criteria for inclusion of genes in the MAPPFinder-analysis were $p < 0.001$ or $p < 0.05$. This was done to pick up high magnitude changes of small

groups of genes and low-amplitude changes in large groups, respectively. Gene-sets with p-value <0.05 after correction for multiple comparisons were considered as significant.

5.3. Protein chemistry

5.3.1. Protein isolation

5.3.1.1. Preparation of liver homogenates

For preparation of murine liver homogenates, approximately 100 mg of tissue were transferred to a 15 ml round-bottom tube loaded with 1 ml of IP buffer containing Proteinase/phosphatase inhibitors (IP+ buffer). Using a tissue homogenator with rotating blades, liver specimens were solubilised directly in IP+ buffer until no tissues clumps were visible. Foam generation should be avoided to minimize protein denaturation. The homogenate was transferred to a fresh 1.5 ml reaction tube and cellular debris removed by centrifugation at maximum speed for 15 min at 4 °C in a table micro centrifuge. The supernatant was again transferred to a new tube and centrifugation repeated until the solutions turned translucent. The supernatant was either mixed instantly with 4xSB (reducing sample buffer) for SDS-PAGE, incubated with antibodies for immunoprecipitation purification or shock frozen in liquid N₂ and stored at -80 °C.

IP buffer:

25 mM	HEPES pH 7.5
150 mM	NaCl
10 mM	EDTA
0.1 %	Tween-20
0.5 %	NP-40
10 mM	beta-Glycerophosphate

IP+ buffer = IP buffer containing:

1 mM	Na ₃ VO ₄
1 mM	NaF
10 µg/ml	Leupeptin
10 µg/ml	Aprotinin
1 mM	PMSF
1 tablet	Complete protease inhibitor cocktail (Boehringer Cat. No. 1697498)

4 x SDS sample buffer (reducing):

240 mM	Tris/HCl pH 6.8
40 mM	DTT
8 %	SDS
0.01 %	Bromphenol blue
40 %	Glycerol
→ aliquoted and stored at -20 °C	

5.3.1.2. Preparation of cell line extracts

Cellular extracts from HEK293 cells used for EMSA analysis were prepared using whole cell extract (WCE) buffer. If not indicated otherwise, cells were harvested from Petri dishes using a sterile blade. Cells were washed two times with ice-cold PBS, followed by centrifugation at 12,000 rpm for 15 min at 4 °C and solubilisation in twice the cell pellet volume in WCE buffer. Disruption of cells was facilitated by incubation for 1 h at 4 °C under vigorous shaking using a horizontal shaker. Subsequently, cellular debris was removed by centrifugation at maximum speed for 15 min at 4 °C using a tabletop micro centrifuge. The supernatant was either directly used in EMSA analysis or shock frozen in liquid N₂ and stored at -80 °C.

WCE buffer:

20 mM	Hepes pH 7.9
20 %	Glycerol
50 mM	KCl
1 mM	EDTA
1 mM	DTT
400 mM	NaCl
5 µg/ml	Leupeptin
5 mM	Beta-Glycerophosphate
1 mM	PMSF
5 µg/ml	Aprotinin
10 mM	NaF
5 mM	Na ₃ VO ₄
→ aliquot and store at -20°C	

5.3.1.3. Protein quantification with the Bradford method

Protein concentration in liver homogenates were quantified using Bradford reagent (Bio-Rad Cat. No. 500-0006). Briefly, a standard curve including protein concentrations ranging from 1 to 20 µg/µl was prepared in microcuvettes according to manufacturer's instructions. The unknown protein sample was pipetted into a separate cuvette. When necessary, 1/10 dilutions of the unknown samples were prepared in the respective homogenisation buffer. Finally, the standards and samples were diluted in 1 ml of a 1:5 mixture of water and Bradford reagent, incubated for 5 min and the absorption of measured at 550 nm. The protein concentration of unknown samples was calculated using the OD values of the standard curve.

5.3.2. Immunoprecipitation

For certain applications, enrichment of proteins was necessary prior to immunoblot analysis due to low expression of the respective protein. Immunoprecipitation utilised high-affinity binding of Sepharose bead-bound antibodies to the respective protein epitope. Briefly, 1000-2000 µg of tissue homogenate in IP+ buffer were diluted with IP+ buffer to a final volume of 600 µl. One µg of antibody/antiserum was added and antibody-antigen complexes allowed to form overnight under constant agitation using a wheel shaker. Subsequently, 40 µl of pre-swollen protein A Sepharose beads (GE Healthcare Cat. No. 17-0780-01) were added and incubated for 1 h at 4 °C on the

wheel shaker. The Fc region of the utilised antibody was bound with high affinity by the Protein A and stable Bead-Antibody-Epitope complexes were formed. After incubation, the Sepharose beads were rinsed three times with 700 µl of IP+ buffer and spun down in a micro centrifuge at 2,000 rpm for 1 min at 4 °C. After a final spin at 12,000 rpm for 5 min at 4 °C, the supernatant was discarded and pelleted Sepharose beads dissolved in 40µl of reducing SDS sample buffer. Finally, the mixture was heated to 95 °C for 5 min and the supernatant transferred into a new 1.5 reaction tube. It was subsequently analysed instantly using Western Blot analysis or stored at -20 °C. Antibodies were used for immunoprecipitation as indicated in

Antibody	Source	Species
IRS-1	Up (#06248)	Rabbit polyclonal
IRS-2	Up (#06506)	Rabbit polyclonal
IR beta chain (IRb)	SC (sc-711)	Rabbit polyclonal

Abbreviations: Sc, Santa Cruz Biotechnologies; Up, Upstate Biotech.

Table 6. Antibodies used for immunoprecipitation of respective proteins

5.3.3. Western Blot

5.3.3.1. Sodium Dodecylsulfate Polyacrylamide Gel Electrophoresis

Cellular extracts or tissue homogenates diluted in 4x SDS sample buffer were boiled for 5 min prior to SDS-PAGE analysis including 5 % (v/v) of fresh beta-Mercaptoethanole. According to original protocols introduced by Laemmli, proteins were separated in a discontinuous gel consisting of

(i) A stacking gel with a low acrylamide percentage for focussing of migratory bands.

Stacking gel (4 % acrylamide, 4 ml for two gels):

0.5 ml	1.0 M Tris (pH 6.8)
0.67 ml	30 % Acrylamide Mix
20 µl	20 % SDS
40 µl	10 % APS
4 µl	TEMED
2.7 ml	H ₂ O _{dd}

(ii) A separation gel with variable acrylamide percentages for separation of proteins according to molecular weight. To facilitate polymerisation, the gel is overlaid with 2-Propanol. Routinely, a 6 cm Minigel system was used (Bio-Rad Cat. No. 170-3940). The following separation gels were routinely casted:

8 % gel (20 ml for 2 x 1.5 mm gels):

5 ml	1.5 M Tris (pH 8.8)
5.3 ml	30 % Acrylamide
100 µl	20 % SDS
200 µl	10 % APS
12 µl	TEMED
9.3 ml	H ₂ O _{dd}

<u>10 % gel (20 ml for 2 x 1.5 mm gels):</u>	
6.7 ml	1.5 M Tris (pH 8.8)
5 ml	30 % Acrylamide
100 µl	20 % SDS
200 µl	10 % APS
8 µl	TEMED
7.9 ml	H ₂ O _{dd}

<u>10 x Laemmli buffer:</u>	
25 mM	Tris-HCl (pH 8.3)
192 mM	Glycine
1 % (w/v)	SDS
→ fill up with H ₂ O _{dd} to 1 L and store at RT	

SDS-PAGE was carried out in 1 x Laemmli buffer running at 20-30 mA/gel until the dye in the loading buffer was running out of the gel. After electrophoretic separation gels were subjected to immunoblotting (section 5.3.3.2).

5.3.3.2. Protein transfer onto Nylon membranes

Protein transfer was carried out using Bio-Rad semi-dry blotting or wet blotting devices and proteins blotted onto 0.45 µm nitrocellulose membranes (GE Healthcare Cat. No. RPN303E) pre-equilibrated in transfer buffer. A current of 0.8 mA/cm² was applied and proteins were allowed to transfer for 90 min (semi-dry transfer, RT) or 3 h (wet transfer, 4 °C). Following protein transfer, the membranes were rinsed with H₂O_{dd} and transfer efficiency controlled via staining with Ponceau S solution for 5 min. Excess Ponceau staining was removed with multiple washes o H₂O_{dd}.

<u>Ponceau S solution:</u>	
0,1 %	Ponceau S dye
5 %	Acetic Acid

<u>Transfer buffer:</u>	
48 mM	Tris
39 mM	Glycine
0.037 % (v/v)	SDS
20 %	Methanol

5.3.3.3. Immunoblot analysis (antibody staining)

Following Ponceau S staining, nitrocellulose membranes were washed twice with H₂O_{dd} and blocked for 1 h in blocking solution (5 % BSA in 1x TBST). The membrane was sealed in plastic foil and incubated overnight with respective primary antibodies diluted in TBST + 1 % BSA. Subsequently, the membrane was rinsed three times for 10 min in 1x TBST and incubated for 30-45 min with an appropriate species-specific antibody conjugated to horseradish-peroxidase (HRP) in a dilution of 1:2000 to 1:5000. Afterwards, membranes were washed three times with 1x TBST. For specific

detection of bands corresponding to the utilized antibody, an enhanced chemiluminescence (ECL) system (Amersham Biosciences Cat. No. RPN 2132) was used to expose ECL films (THP Pierce Cat. No. PI-34091). The exposition times varied between the antibodies used. Primary antibodies were utilised as indicated in (Table 7). Membranes could be stripped of the primary antibody by immersion in stripping buffer for 30 min at 55 °C under constant agitation. Afterwards, the membrane could be blocked and re-incubated using different antibodies.

Stripping buffer:

6.25 ml 1 M Tris-HCl pH 6.8
 0.675 ml beta-Mercaptoethanol
 10 ml 20 % SDS
 → fill up with H₂O_{dd} to 100 ml

10 x TBST:

500 mM Tris-HCl
 1.5 M NaCl
 0.5 % Tween-20
 → adjust to pH 8 and fill up with H₂O_{dd} to 2 L

Antibody	Source	Species	Dilution
Anti HSC-70	SC (sc-7298)	Mouse monoclonal	1:20,000
Anti AKT	SC (sc-8312)	Rabbit polyclonal	1:2,000
Anti pS-AKT	CS (#9271S)	Rabbit polyclonal	1:250
Anti phosphotyrosine	Up (12-302)	Mouse monoclonal	1:1,000
Anti PPARgamma	SC (sc-7273)	Mouse monoclonal	1:2,000
Anti SREBP-1c	SC (sc-13551)	Mouse monoclonal	1:2,000
Anti Stat1	BD (#610115)	Mouse monoclonal	1:1,000
Anti pY-Stat1	CS (#9167)	Rabbit monoclonal	1:1,000
Anti Stat3	BD (#610189)	Mouse monoclonal	1:5,000
Anti pY-Stat3	CS (9131)	Rabbit polyclonal	1:1,000
Anti Stat5	Anti Stat5 aa775-788	Rabbit polyclonal	1:5,000
Anti GR	SC (sc-1004)	Rabbit monoclonal	
Anti MRP2	Kindly provided by Dr. James Boyer, Yale		1:2,000
Anti MRP3	University, New Haven, USA		1:2,000
Anti NTCP1	Kindly provided by Dr. Bruno Stieger, Zurich,		1:2,000
Anti OATP1	Switzerland		1:2,000
Anti beta Actin	Sigma AC-15	Mouse monoclonal	1:2,000
Anti mouse-HRP	Dako (P0447)	Goat polyclonal	1:5,000
Anti rabbit-HRP	Dako (P0217)	Swine polyclonal	1:5,000

Abbreviations: BD, Becton Dickinson; CS, Cell Signaling; Dako, DakoCytomation; SC, Santa Cruz Biotechnologies; Up, Upstate Biotech.

Table 7. Primary and secondary antibodies used in immunoblot analysis

5.3.4. EMSA

Electromobility shift assays (EMSA) constitute a widely utilised technique for studying *in vitro* the interaction between DNA binding proteins (e.g. transcription factors) and respective DNA elements. Briefly, radiolabeled DNA oligomers migrate along an electric current. The migration behaviour is influenced by interaction of DNA-binding protein interacting with respective DNA sequences and decelerating their migratory velocity ('shift'). Additional binding of specific antibodies leads to further deceleration of the DNA-binding protein velocity ('supershift'). For analysis of the DNA binding properties of full-length and N-terminally truncated Stat5 isoforms *in vivo*, we

prepared liver homogenates from PBS and GH-treated control as well as Stat5^{ΔN} mice directly in IP+ buffer. The binding properties of GH-activated Stat5 were tested on classical Stat5 responsive DNA elements from the bovine beta Casein promoter. Similarly, the putative binding properties of GH-activated Stat5 on three putative Stat5 responsive elements found in the Socs2 promoter (Socs2 Stat5 RE #1-3) were assessed. To verify our findings in cell culture, we transfected HEK293 cells with pMSCV expression plasmids encoding for Stat5 and the erythropoietin receptor (EpoR). Subsequent Epo stimulation for 30 min led to potent activation and phosphorylation of cytoplasmic Stat5 molecules. The binding properties of Epo-activated Stat5 on putative Stat5 responsive elements in the Socs2 were assessed using EMSA analysis. Single stranded DNA oligonucleotides applied for EMSA analysis (Table 8) were annealed at equimolar concentrations (~100 μM/oligomer) in 200 μl annealing buffer (10 x = 0.625 x PCR buffer II (Roche); 9.4 mM MgCl₂) by heating to 95 °C for 10 min, followed by slow cooling to RT and subsequent incubation on ice for > 15 min. Annealed double stranded DNA oligos were diluted to 2.5 μM for radiolabeling. The labelling reaction (5 pmol of annealed dsDNA incubated with 10 U of polynucleotide kinase (PNK) and 5 μl of ATP ³²P (Amersham Biosciences; 8,000 cpm/μl) were incubated at 37 °C for 1 h. Radiolabeled oligonucleotides were purified on size exclusion columns (Bio-Rad Cat. No. 7326221) and stored at -20 °C until needed. For analysis of Stat5-DNA binding interaction using EMSA, 20 μl reaction mixtures were prepared for each sample, containing 2 μl BSA solution, 2 μl poly-dI-dC (Roche Cat. No. 108812), 4 μl 5x binding buffer and 1 μl of radiolabeled oligonucleotides. Usually 20-30 μg of liver homogenate or cellular extract were used per reaction. Protein extracts were incubated for > 5 min at RT before loading of the gel. For supershift analysis, the reaction mixture was incubated for >10 min with 1 μl of a rabbit polyclonal anti Stat5 specific antiserum. Complexes were separated on non-denaturing 4 % acrylamide gels containing 0.25 x TBE and run in 0.25 x TBE running buffer at 200 V for 2-3 h. The reaction was stopped after the Orange G dye, which migrates with a comparable velocity as unbound oligos, was running out of the gel. The gel was dried on a vacuum drier at 80 °C for 2 h and subjected to autoradiography. Coated Kodak MR films (Sigma Cat. No. Z350370) were exposed > 1 d at -80°C.

BSA solution:

10 mg/ml	BSA in 20 mM KPO ₄
50 mM	NaCl
0.1 mM	EDTA
5 %	Glycerol

5 x Binding buffer:

50 mM	Tris
5 mM	DTT
1 mM	PMSF
0.5 mM	EDTA
25 %	Glycerol
250 mM	NaCl
0.5 %	KPO ₄

DNA oligomer	Promoter	Sequence
Beta Casein Stat5 RE	Bovine beta Casein	AGATTTCTAGGAATTCAAATC (sense) GATTTGAATTCCTAGAAATCT (antisense)
Socs2 Stat5 2xRE #1	Murine Socs2	AAGATTCCAGGAAAACA (sense) TGTTTTCTGGAATCTT (antisense)
Socs2 Stat5 2xRE #2	Murine Socs2	GTATTTCAAAGAAAAT (sense) ATTTTTCTTTGAAATAC (antisense)
Socs2 Stat5 2xRE #3	Murine Socs2	CGGATTCCTGGAAAGTT (sense) AACTTTCCAGGAATCCG (antisense)

Abbreviations: RE, responsive element

Table 8. DNA sequence of Stat5 responsive oligonucleotides used in EMSA analysis

5.3.5. Tissue analysis and paraffin embedding

Experimental mice were killed by asphyxiation or cervical dislocation and isolated organs cut in 2-3 mm thick slides, fixed for 48 h in phosphate-buffer 10 % formaldehyde solution and dehydrated using graded ethanol. The dehydrated organs were washed three times with xylene, replaced with liquid paraffin and finally cast into metal moulds and let solidify. Solid paraffin blocks were stored at RT until needed for histological or immunohistochemical analyses. Two μm thick sections of paraffin blocks were generated using a microtome (Leica) and subsequent smoothing in a 50 °C water bath. Finally, the tissue sections were transferred onto poly-Lysine coated Superfrost glass slides (Lacton Cat. No. 193515000) and let dry at RT overnight. Tissue sections can be stored at RT for several weeks until needed for histological or immunohistochemical analyses.

5.3.5.1. Histopathology

For standard histology using haematoxylin/eosin (HE) staining, paraffin sections of 2 μm thickness were prepared, deparaffinised by incubation for 2x5 min in xylene and dehydrated using a decreasing ethanol (EtOH) gradient (2x2 min 100 % EtOH; 20 dips in each 95 % EtOH, 95 % EtOH, 70 % EtOH, 50 % EtOH, $\text{H}_2\text{O}_{\text{dd}}$, $\text{H}_2\text{O}_{\text{dd}}$). Subsequently, sections were incubated in Mayer's haematoxylin solution (VWR Cat. No. 1092490500) and rinsing with tap for 5-10 min to differentiate the staining intensity. Slides were counterstained with eosin solution (Roth Cat. No. 7089.2), dipped in $\text{H}_2\text{O}_{\text{dd}}$ rehydrated using the aforementioned graded ethanol in reverse order. After a final incubation in xylene, tissue sections were mounted on Superfrost glass slides using Eukitt mounting medium (Lactan Cat. No. 361894G).

Eosin solution:

30 ml	1 % Eosin
270 ml	70 % Ethanol
3 ml	Glacial acetic acid

5.3.5.2. Immunohistochemistry

For immunohistochemical analysis of PPAR γ and GR protein expression, overnight-dried paraffin sections were heated for 2 h at 60 °C or 30 min at 70 °C to

remove excess paraffin. Finally paraffin slides were rehydrated using graded ethanol (2x2 min 100 % EtOH; 20 dips in each 95 % EtOH, 95 % EtOH, 70 % EtOH, 50 % EtOH, H₂O_{dd}, H₂O_{dd}). Subsequently, the sections treated with 3 % Tris-buffered hydrogen peroxide for 15 min to block endogenous peroxide activity. Endogenous avidin- and biotin-activity was masked using a commercially available blocking kit (Eubio Cat. No. SP-2001). Slides were blocked with 5 % Tris-buffered BSA and incubated overnight with an antibody recognising mouse/human PPAR γ (sc-7273, dilution 1:100, Santa Cruz Biotech.) or murine GR (sc-1004; dilution 1:1000, Santa Cruz Biotech.). The slides were rinsed three times using 1x TBST and incubated with a polyvalent biotinylated antibody and streptavidin-HRP each for 10 min (both ID labs Cat. No. IDST1007). Specific signals were detected using a AEC-substrate detection kit (IDLabs Cat. No. IDST1007). After appropriate staining intensity had developed the reaction was stopped by immersion in H₂O_{dd} and mounted on Superfrost glass slides using aqueous Aquatex mounting medium (Lactan Cat. No. 1085620050).

5.3.6. Electron microscopy

For electron microscopy, mouse livers were cut into 1-2 mm thin pieces and fixed overnight in 1.6 % glutaraldehyde. Images were recorded using various magnifications (1,500 x – 4,000 x) using a standard transmission electron microscope (TEM).

5.4. Cell biology

5.4.1. Cell lines

Cultivation of cell lines was carried out in incubators maintaining a temperature of 37 °C, humidity of 95 % and 5 % CO₂. Cells were passaged and handled under sterile conditions.

5.4.2. Handling of cell lines and transient transfection

The following cell lines were routinely used for *in vitro* transfection experiments:

HEK 293 cells

Human embryonic kidney cells (HEK 293 cells) were cultivated and propagated in Dulbecco's Modified Eagle Medium with high glucose (DMEM; Invitrogen Cat. No. 41965-062); 10 % fetal calf serum (FCS; PAA Cat. No. 41965-062), 1 mM L-Glutamine and 1 % penicillin / streptomycin. Transient transfection were carried using a modified version of the Sambrook Ca₃(PO₄)₂ method: Briefly, HEK 293 cells were seeded out at a final concentration of 1x10⁵ cells/ml medium in 100 mm Petri dishes and were allowed to adhere to the dish for 2-6 h. 10 μ g of total plasmid DNA were diluted in 450 μ l sterile water. Subsequently, 50 μ l of 2.5M CaCl₂ solution were added, followed by drop wise addition of 500 μ l 2x HBS buffer under constant vortexing. The solutions were incubated for 1 min until precipitation of calcium phosphate crystals was observed by a foggy appearance of the reaction mixture,

which was given onto the adherent cells in a swirling manner. Proper precipitation of crystals was confirmed by microscopy. After 18 h, the medium was replaced and transfected cells from one 100 mm Petri dish were distributed onto 2x 6well dishes to allow for multiple cytokine stimulation conditions. Cells were allowed to adhere overnight and were stimulated with various cytokines. Subsequently, culture dishes were rinsed two times with ice-cold PBS, scraped off using a sterile blade and pelleted by centrifugation for 1 min at 6,000 rpm. Finally, cells were taken up in WCE buffer for EMSA analysis.

2 x HBS buffer:

50 mM	Hepes pH 7.05
10 mM	KCl
280 mM	NaCl
1.5 mM	Na ₂ PO ₄

→ dissolve in 950ml H₂O_{dd} and adjust pH to 7.1 with 1 N HCl. Fill up with H₂O to 1 L and sterilize using 0.22 µg filters. Aliquot in 50 ml reaction tubes and store at -20 °C.

MIMp16/19ARF^{-/-}-Ras and MIMp16/19ARF^{-/-} cells

MIMp16/19ARF^{-/-} and MIMp16/19ARF^{-/-}-Ras cells are primary hepatocytes isolated from mice deleted for p16/19ARF proteins and exhibited sustained proliferative capabilities in cell culture. Both cell lines were maintained and extended in RPMI medium (Sigma Cat. No. R0883-6x500ml), supplemented with 10 % FCS, 1 mM L-Glutamine and 1 % penicillin / streptomycin in Petri dishes coated with rat collagen (BD Cat. No. 354236). Moreover, MIMp16/19ARF^{-/-} were dependent on growth factor stimulation with 80 ng/ml TGFalpha (Sigma Cat. No. # T-7924), 60 ng/ml IGF-II (Sigma Cat. No # I-2526) and 2.8 µM insulin (Novo Nordisk). MIMp16/19ARF^{-/-}-Ras were stably transfected with the Ras proto-oncogene to allow for factor-independent growth. Both MIMp16/19^{-/-} cell lines were transiently transfected with the Lipofectamine 2000[®] reagent (Invitrogen Cat. No. 11668-027) using a modified version of the vendor's instructions: Briefly, cells were seeded out a final concentration of 1x10⁵ cells/ml medium one day prior to transfection. Before transfection the medium was removed and replaced with RPMI containing only 1 mM L-Glutamine (RPMI+). The next morning, 8 µg of total plasmid DNA were mixed with 750 µl of RPMI+ and 40 µl Plus[®] reagent (Mix I). Simultaneously, 60 µl of Lipofectamine 2000[®] reagent was diluted in 800 µl RPMI+ and incubated for 15 min (Mix II). Subsequently, Mix I and Mix II were pooled, mixed gently and incubated at room temperature (RT) for 15 min. The pooled reaction mixture was added to the cells under constant agitation. After 3 h, RPMI+ was removed and replaced with RPMI containing FCS, L-Glutamine and penicillin / streptomycin. After 18 h, the medium was replaced and transfected cells from one 100 mm Petri dish were distributed onto 2x6well dishes to allow for multiple cytokine stimulation conditions. Cells were allowed to adhere overnight and were stimulated with various cytokines after 48 h. Subsequently, culture dishes were rinsed two times with ice-cold PBS, scraped off using a sterile blade and pelleted by centrifugation for 1 min at 6,000 rpm. Finally, cells were taken up in potassium phosphate buffer for reporter assay analysis.

COS7 cells

COS7 are epithelial african green monkey kidney cells immortalized using an origin-defective mutant of SV40. COS7 are widely used in reporter assay analyses due to their rather basal transcription machinery. COS7 cells were maintained and propagated in DMEM (high glucose) supplemented with FCS, L-Glutamine and penicillin / streptomycin. For transient transfection experiment, one fully growth T75 cell culture flask was trypsinised and detached cells allocated onto five 100 mm Petri dishes one day prior to transfection. At the day of transfection, 544 μ l of DMEM was pipetted into a 1.5 ml reaction tube and mixed with 48 μ l of Fugene reagent (Roche Cat. No. 11814443001), flicked once and allowed to incubate for 5 min. Subsequently, 8 μ g of total plasmid DNA was added to the reaction mixture, flicked and incubated for 5 min. The transfected reagent:DNA complex was given onto the cells in a swirling and drop wise manner. After 18 h, cells from one transfected 100 mm Petri dish were distributed onto one 24 well dish to allow for multiple cytokine stimulations. COS7 cells were allowed to adhere overnight and were stimulated with various cytokines after 48 h. Subsequently, culture dishes were rinsed two times with ice-cold PBS, scraped off using a sterile blade and pelleted by centrifugation for 1 min at 6,000 rpm. Finally, cells were taken up in KH_2PO_4 lysis buffer for reporter assay analysis.

5.4.3. Luciferase reporter assay

Luciferase reporter assays are used to quantify the ability of a given promoter sequence to drive the transcription of the firefly Luciferase gene. Luciferase itself is an enzyme catalysing the reaction a reaction in which Luciferin is transformed into its decarboxylated isoform leading to emission of photons. As under standard conditions the amount of luciferin is supplied in excess, the amount of emitted light is proportional to the amount of Luciferase and constitutes an indirect measurement for the transactivation capability of a cloned promoter sequence. To determine the Luciferase activity in transfected cell lines, the pelleted cells were taken up in 50-100 μ l of potassium chloride lysis buffer. The pellets were pipetted up and down repeatedly and put on a horizontal shaker for 30 min to facilitate lysis of cells. Insoluble debris was removed by centrifugation for 15 min at 12,000 rpm in a cooled micro centrifuge. The supernatant was shock-frozen and stored at -80°C or used instantly. For measuring Luciferase activity, 20 μ l of supernatant was transferred to a opaque 96 well microtiter plate and diluted with 50 μ l of assay buffer (4 mM ATP, 200 mM MgSO_4 in Gly-Gly buffer). The plate was transferred into a luminometer equipped with a dispenser, automatically adding 50 μ l of injection buffer (0.25 mM luciferin in Gly-Gly buffer) into each well. The subsequent light emission was detected at 560nm and counted for 2 s.

The efficiency of each transfection was quantified via co-transfection of 0.5 μ g plasmid vector DNA constitutively expressing beta Galactosidase. To assess the enzymatic Galactosidase activity as an indicator for efficiency of DNA transfection into cells, the complete Luciferase reaction mixture (120 μ l) was transferred onto a fresh, translucent microtiter plate and 50 μ l of CPRG (chlorophenolred-beta-D-galactopyranoside, Sigma Cat. No. 59767100MGF) solution, a chromogenic beta Galactosidase substrate, pipetted into each well. Upon beta Galactosidase activity, the colourless CPRG solution turned yellow. The absorption was then measured in a spectrophotometer at 405 nm as an indicator of beta Galactosidase enzyme activity. For relative quantification of the transactivation activity of a given promoter elements

each sample the Luciferase values were measured and normalised against the beta Galactosidase values as an indicator of transfection efficiency.

KH₂PO₄ lysis buffer:

13.6 g KH₂PO₄
 0.1 % Triton X-100
 → fill up with H₂O_{dd} to 1 L, adjust pH to 7.8 using NaOH

CPRG solution:

27,1 mg CPRG
 0.5 % BSA
 → fill up with 20 ml PBS, aliquot and store at -20 °C

5.5. Colony breeding and management

Mice were kept at the Decentralized Biomedical Facilities, Medical University of Vienna (MUW) under standardized conditions. All animal experiments were carried out according to an ethical animal license protocol and contract approved by the MUW and the Austrian Ministry BMBWK authorities. Mice are maintained on a 12 h light-dark cycle.

5.5.1. Transgenic mouse lines

(i) Mice harbouring a hepatocyte-specific deletion of the glucocorticoid receptor ($GR^{AlfpCre}$) were generated by intercrossing with animals with a floxed third exon of the GR²¹¹ with mutants carrying the Cre recombinase under the control of the albumin promoter and alpha-fetoprotein enhancer sequences¹⁵⁸. Animals deleted for hepatic Stat5 were generated by crossing mice harbouring the AlfpCre recombinase with mutants carrying a floxed Stat5a/b allele ($Stat5^{AlfpCre}$)¹¹⁹. $Stat5/GR^{AlfpCre}$ compound knockout animals were generated by respective intercrossing. $Stat5^{\Delta N}$ mice were generated as described¹²⁷. All animals were maintained on a mixed C57/BL6 and 129SvEv background and genotyped as indicated.

(ii) Mice deleted for MDR2 ($MDR2^-$) were purchased from Jackson Laboratories. $MDR2^-$ mice were initially maintained on a FVB/N background. Due to appropriate intercrossing $MDR2^{+/-}$, $MDR2^-$, $Stat5^{AlfpCre}$ and $MDR2/Stat5^{AlfpCre}$ animals were generated and experimental mice were regarded to be on a mixed background.

5.5.2. Metabolic function tests

5.5.2.1. Glucose tolerance test

To assay the capability of transgenic mice to metabolize orally administered glucose, we performed oral glucose tolerance tests (OGTT). For this, mice were fasted overnight in a fresh cage prior to glucose gavage to obtain comparable basal glucose levels. The next morning, the body weight was determined and basal glucose levels analysed. For this, the tail vein was nicked and one droplet venous blood measured

using a glucometer (OneTouch Ultra, LifeScan). Glucose was orally administered at a concentration of 10 $\mu\text{l/g}$ body weight using a gavage syringe. The measurement of glucose levels was done by sampling venous tail blood at indicated time points. Immediately after the experiment, mice were transferred into a fresh cage and provided with food *ad libitum*.

5.5.2.2. Insulin tolerance test

Insulin tolerance tests were performed with animals initially fasted for 4 h in a fresh cage. Subsequently, the body weight was determined and insulin (Novo Nordisk) injected peritoneally at a final concentration of 0.75 U/kg body weight. Blood samples were taken from the tail vein at indicated time points and glucose levels determined using a glucometer (OneTouch Ultra, LifeScan). Plasma insulin concentrations were analysed using a rat insulin ELISA (Crystal Chem Cat. No. INSKR020) following vendor's instruction manual.

5.5.3. Blood sampling and serum parameter quantification

To determine serum concentration of cytokines and growth factors or biochemical parameters, blood was harvested from mice using heart puncture and collected in tubes precoated with EDTA. Blood samples were subsequently centrifuged at 5,000 rpm for 5 min at RT to remove insoluble, coagulated blood components. The plasma (supernatant) was transferred into a new tube and analysed instantly using various techniques or shock frozen in liquid N_2 and stored at -80°C .

Concentrations of important biochemical and metabolic serum parameters were determined using a Reflotron Plus analyser (Roche). Briefly, 30 μl of serum or plasma were pipetted onto an analyte-specific strip and inserted into the machine. Final concentration of were calculated taken possible pre-dilutions into account.

5.5.3.1. Lipoprotein profile

Plasma samples of five fed mice of each genotype were pooled and compared with five control littermates. Lipoproteins were isolated by FPLC. 200 μl pooled plasma samples were subjected to FPLC analysis and lipoproteins were eluted with 10 mM Tris-HCl, 1 mM EDTA, 0.9 % NaCl, and 0.02 % NaN_3 (pH 7.4). Fractions of 0.5 ml each were collected and lipids (triglycerides and total cholesterol) assayed enzymatically using commercially available kits. To enhance sensitivity, reaction buffers were supplemented by the addition of sodium 3, 5-dichloro-2-hydroxy-benzenesulfonate.

5.5.4. Immuno assays

Immuno assays (particularly enzyme linked immuno sorbent assays (ELISA) and radio immunoassay (RIA)) detect the concentration of an antigen in serum samples with high reproducibility and accuracy. Briefly, an antigen-specific antibody was immobilised and scavenges the desired antigen. Finally, the amount of trapped

antigen was converted to a signal using radiolabel led secondary antibodies (RIA) or a chromogenic enzyme activity coupled to the secondary antibody (ELISA).

5.5.4.1. Radio Immunoassay (RIA)

Serum corticosterone (MP Biochemicals Cat. No. 07-120102) and ACTH (MP Biochemicals Cat. No. 07-106102) levels were determined using commercially available RIA following instructions from the vendor. Briefly, a standard curve was prepared and subsequently the displacement of Corticosterone/ACTH-specific antibodies bound to radiolabel led Corticosterone/ACTH (Cort^{*}/ACTH^{*}) by serum Corticosterone/ACTH quantified using a gamma counter (Beckmann). Thus, extensive displacement of Corticosterone/ACTH antibodies from Cort^{*}/ACTH^{*} due to high levels of serum Corticosterone/ACTH led to a low radioactivity. The exact concentrations of serum Corticosterone/ACTH was deduced using the previously prepared standard curve.

5.5.4.2. Enzyme Linked Immuno Sorbent Assay (ELISA)

Plasma GH (Millipore Cat. No. EZRMGH-45K), IGF-1 (IBL Hamburg Cat. No. UK45021), Leptin, TNFalpha and Resistin concentrations (all Millipore Cat. No. MADPK-71K-04) were determined using ELISA kits. Briefly, plastic dishes precoated with the respective growth factor/cytokine specific antibody were incubated with serum samples according to manufacturer's instructions. A secondary antibody coupled to an enzymatic function was added. Finally, the development of the chromogenic reaction was stopped and the concentration of the respective analyte in the serum determined measuring the OD at 450 nm using a spectrophotometer. The exact concentrations were calculated using an analyte standard curve.

5.5.5. Colorimetric assays

5.5.5.1. Quantification of free fatty acids (FFA)

The concentration of serum FFA was determined using a colorimetric assay system (Wako Cat. No. 999-65406). Briefly, the assay relied on the catalytic oxidation of free carbonic acids such as FFA (R-COOH) by (i) Acyl-CoA synthase, (ii) Acyl-CoA oxidase and (iii) peroxidase:

- (i) $R-COOH + ATP + CoA-SH \rightarrow \rightarrow Acyl-CoA + AMP + PP_i$
- (ii) $Acyl-CoA + O_2 \rightarrow \rightarrow 2,3-Enoyl-CoA + H_2O_2$
- (iii) $H_2O_2 + 4 H_2N-phenanzon + 3-CH_3-N-Ethyl-N (beta-hydroxyethyl)-aniline \rightarrow \rightarrow quinoneimine (color) + 4 H_2O$

A standard curve of oleic acid was prepared and 4 μ l serum sample used for quantification. The experiment was carried out as given in the vendor's instructions. The OD was measured at 550 nm and the final concentration of FFA calculated taken possible pre-dilutions into account.

5.5.5.2. Isolation and quantification of hepatic triglycerides

Hepatic lipids were isolated from frozen liver tissues using the original method of Stanley and Folch. For this, approximately 100 mg were weighted and transferred into a 15 ml reaction tube pre-equipped with 2 ml of a chloroform/methanol (2:1 v/v) mixture. The tissue was homogenized until no tissues clumps were visible, followed by incubation for 20-25 min on a rotating wheel at RT. Cell debris and insoluble fragments were removed by centrifugation at 4,000 rpm for 10 min. The resulting supernatant was transferred into a fresh reaction tube and the organic phase extracted two times 0.9 % NaCl solution, followed by careful aspiration of the aqueous phase. Then, 50 μ l of the lipophilic phase were incubated with 10 μ l of a TX-100/chloroform (1:1 v/v) mixture in a fresh reaction tube. Vigorous shaking was followed by evaporation of the solvent in a Speed vac. The remaining pellet, containing the organic phase of the liver was taken up in 50 μ l of H₂O_{dd} and stored at -20 °C.

To determine the concentration of triglycerides in hepatic tissues, this colorimetric assay (Sigma Cat. No. TR0100) relied on the enzymatic quantification of glycerol liberated from cleaved triglycerides (tricarboxylic acid esters of glycerol) since the stoichiometric ratio between triglycerides and glycerol equals one. Four μ l of isolated triglycerides from liver tissues were pipetted onto a 96 well microtiter plate. Glycerol at a concentration of 2.5 mg/ml (Sigma Cat. No. G7793) was included as positive control whereas blank values include water. 100 μ l Free Glycerol Reagent is pipetted into each well and incubated for 5 min at 37 °C. The amount of glycerol not incorporated into triglycerides was determined by spectrophotometry measured at 540 nm. A second 96 well plate containing the same samples was pipetted and 100 μ l of Triglyceride Reagent added. The plate was incubated for 5 min at 37 °C and the OD at 540 nm measured again. This time, the OD 540 nm was proportional to the total amount of glycerol (free glycerol and glycerol incorporated in triglycerides) in the respective sample. Subtraction of the two values and normalization blank values yielded the concentration of triglycerides in the respective sample.

6. Literature:

References:

1. Kopelman PG: Obesity as a medical problem, *Nature* 2000, 404:635-643
2. Mokdad AH, Bowman BA, Ford ES, Vinicor F, Marks JS, Koplan JP: The continuing epidemics of obesity and diabetes in the United States, *JAMA* 2001, 286:1195-1200
3. Bray GA, Nielsen SJ, Popkin BM: Consumption of high-fructose corn syrup in beverages may play a role in the epidemic of obesity, *Am J Clin Nutr* 2004, 79:537-543
4. Petrie JR, Cleland SJ, Small M: The metabolic syndrome: overeating, inactivity, poor compliance or 'dud' advice?, *Diabet Med* 1998, 15 Suppl 3:S29-31
5. Canbay A, Bechmann L, Gerken G: Lipid metabolism in the liver, *Z Gastroenterol* 2007, 45:35-41
6. Weigand K, Alpert E: Human albumin synthesis via an albumin precursor in liver tissue slices, *Experientia* 1981, 37:1145-1147
7. McCuskey RS, McCuskey PA, Urbaschek R, Urbaschek B: Kupffer cell function in host defense, *Rev Infect Dis* 1987, 9 Suppl 5:S616-619
8. Pohl J, Ring A, Eehalt R, Herrmann T, Stremmel W: New concepts of cellular fatty acid uptake: role of fatty acid transport proteins and of caveolae, *Proc Nutr Soc* 2004, 63:259-262
9. Timlin MT, Barrows BR, Parks EJ: Increased dietary substrate delivery alters hepatic fatty acid recycling in healthy men, *Diabetes* 2005, 54:2694-2701
10. Bradbury MW: Lipid metabolism and liver inflammation. I. Hepatic fatty acid uptake: possible role in steatosis, *Am J Physiol Gastrointest Liver Physiol* 2006, 290:G194-198
11. Lambert MS, Avella MA, Berhane Y, Shervill E, Botham KM: The fatty acid composition of chylomicron remnants influences their binding and internalization by isolated hepatocytes, *Eur J Biochem* 2001, 268:3983-3992
12. Coleman RA, Lewin TM, Muoio DM: Physiological and nutritional regulation of enzymes of triacylglycerol synthesis, *Annu Rev Nutr* 2000, 20:77-103
13. Lorch Y, Zhang M, Kornberg RD: Histone octamer transfer by a chromatin-remodeling complex, *Cell* 1999, 96:389-392
14. Janknecht R, Hunter T: Transcription. A growing coactivator network, *Nature* 1996, 383:22-23
15. Janknecht R, Hunter T: Versatile molecular glue. Transcriptional control, *Curr Biol* 1996, 6:951-954
16. Collingwood TN, Urnov FD, Wolffe AP: Nuclear receptors: coactivators, corepressors and chromatin remodeling in the control of transcription, *J Mol Endocrinol* 1999, 23:255-275
17. Saltiel AR, Kahn CR: Insulin signalling and the regulation of glucose and lipid metabolism, *Nature* 2001, 414:799-806
18. Issemann I, Green S: Activation of a member of the steroid hormone receptor superfamily by peroxisome proliferators, *Nature* 1990, 347:645-650
19. Ferre P: The biology of peroxisome proliferator-activated receptors: relationship with lipid metabolism and insulin sensitivity, *Diabetes* 2004, 53 Suppl 1:S43-50

20. Kliewer SA, Forman BM, Blumberg B, Ong ES, Borgmeyer U, Mangelsdorf DJ, Umesono K, Evans RM: Differential expression and activation of a family of murine peroxisome proliferator-activated receptors, *Proc Natl Acad Sci U S A* 1994, 91:7355-7359
21. Chawla A, Repa JJ, Evans RM, Mangelsdorf DJ: Nuclear receptors and lipid physiology: opening the X-files, *Science* 2001, 294:1866-1870
22. Evans RM, Barish GD, Wang YX: PPARs and the complex journey to obesity, *Nat Med* 2004, 10:355-361
23. Desvergne B, Wahli W: Peroxisome proliferator-activated receptors: nuclear control of metabolism, *Endocr Rev* 1999, 20:649-688
24. Rao MS, Reddy JK: PPARalpha in the pathogenesis of fatty liver disease, *Hepatology* 2004, 40:783-786
25. Kersten S, Seydoux J, Peters JM, Gonzalez FJ, Desvergne B, Wahli W: Peroxisome proliferator-activated receptor alpha mediates the adaptive response to fasting, *J Clin Invest* 1999, 103:1489-1498
26. Mandard S, Muller M, Kersten S: Peroxisome proliferator-activated receptor alpha target genes, *Cell Mol Life Sci* 2004, 61:393-416
27. Fan CY, Pan J, Usuda N, Yeldandi AV, Rao MS, Reddy JK: Steatohepatitis, spontaneous peroxisome proliferation and liver tumors in mice lacking peroxisomal fatty acyl-CoA oxidase. Implications for peroxisome proliferator-activated receptor alpha natural ligand metabolism, *J Biol Chem* 1998, 273:15639-15645
28. Hashimoto T, Cook WS, Qi C, Yeldandi AV, Reddy JK, Rao MS: Defect in peroxisome proliferator-activated receptor alpha-inducible fatty acid oxidation determines the severity of hepatic steatosis in response to fasting, *J Biol Chem* 2000, 275:28918-28928
29. Ip E, Farrell GC, Robertson G, Hall P, Kirsch R, Leclercq I: Central role of PPARalpha-dependent hepatic lipid turnover in dietary steatohepatitis in mice, *Hepatology* 2003, 38:123-132
30. Kashireddy PV, Rao MS: Lack of peroxisome proliferator-activated receptor alpha in mice enhances methionine and choline deficient diet-induced steatohepatitis, *Hepatol Res* 2004, 30:104-110
31. Browning JD, Horton JD: Molecular mediators of hepatic steatosis and liver injury, *J Clin Invest* 2004, 114:147-152
32. Koo SH, Dutcher AK, Towle HC: Glucose and insulin function through two distinct transcription factors to stimulate expression of lipogenic enzyme genes in liver, *J Biol Chem* 2001, 276:9437-9445
33. Brown MS, Goldstein JL: The SREBP pathway: regulation of cholesterol metabolism by proteolysis of a membrane-bound transcription factor, *Cell* 1997, 89:331-340
34. Horton JD, Goldstein JL, Brown MS: SREBPs: transcriptional mediators of lipid homeostasis, *Cold Spring Harb Symp Quant Biol* 2002, 67:491-498
35. Horton JD, Goldstein JL, Brown MS: SREBPs: activators of the complete program of cholesterol and fatty acid synthesis in the liver, *J Clin Invest* 2002, 109:1125-1131
36. Lam TK, van de Werve G, Giacca A: Free fatty acids increase basal hepatic glucose production and induce hepatic insulin resistance at different sites, *Am J Physiol Endocrinol Metab* 2003, 284:E281-290
37. Shimomura I, Bashmakov Y, Ikemoto S, Horton JD, Brown MS, Goldstein JL: Insulin selectively increases SREBP-1c mRNA in the livers of rats with streptozotocin-induced diabetes, *Proc Natl Acad Sci U S A* 1999, 96:13656-13661

38. Shimano H, Horton JD, Shimomura I, Hammer RE, Brown MS, Goldstein JL: Isoform 1c of sterol regulatory element binding protein is less active than isoform 1a in livers of transgenic mice and in cultured cells, *J Clin Invest* 1997, 99:846-854
39. Yahagi N, Shimano H, Hasty AH, Matsuzaka T, Ide T, Yoshikawa T, Amemiya-Kudo M, Tomita S, Okazaki H, Tamura Y, Iizuka Y, Ohashi K, Osuga J, Harada K, Gotoda T, Nagai R, Ishibashi S, Yamada N: Absence of sterol regulatory element-binding protein-1 (SREBP-1) ameliorates fatty livers but not obesity or insulin resistance in Lep(ob)/Lep(ob) mice, *J Biol Chem* 2002, 277:19353-19357
40. Yamashita H, Takenoshita M, Sakurai M, Bruick RK, Henzel WJ, Shillinglaw W, Arnot D, Uyeda K: A glucose-responsive transcription factor that regulates carbohydrate metabolism in the liver, *Proc Natl Acad Sci U S A* 2001, 98:9116-9121
41. Iizuka K, Bruick RK, Liang G, Horton JD, Uyeda K: Deficiency of carbohydrate response element-binding protein (ChREBP) reduces lipogenesis as well as glycolysis, *Proc Natl Acad Sci U S A* 2004, 101:7281-7286
42. Lowell BB: PPARgamma: an essential regulator of adipogenesis and modulator of fat cell function, *Cell* 1999, 99:239-242
43. Tontonoz P, Hu E, Spiegelman BM: Stimulation of adipogenesis in fibroblasts by PPAR gamma 2, a lipid-activated transcription factor, *Cell* 1994, 79:1147-1156
44. Matsusue K, Haluzik M, Lambert G, Yim SH, Gavrilova O, Ward JM, Brewer B, Jr., Reitman ML, Gonzalez FJ: Liver-specific disruption of PPARgamma in leptin-deficient mice improves fatty liver but aggravates diabetic phenotypes, *J Clin Invest* 2003, 111:737-747
45. Zhang YL, Hernandez-Ono A, Siri P, Weisberg S, Conlon D, Graham MJ, Crooke RM, Huang LS, Ginsberg HN: Aberrant hepatic expression of PPARgamma2 stimulates hepatic lipogenesis in a mouse model of obesity, insulin resistance, dyslipidemia, and hepatic steatosis, *J Biol Chem* 2006, 281:37603-37615
46. Yu S, Matsusue K, Kashireddy P, Cao WQ, Yeldandi V, Yeldandi AV, Rao MS, Gonzalez FJ, Reddy JK: Adipocyte-specific gene expression and adipogenic steatosis in the mouse liver due to peroxisome proliferator-activated receptor gamma1 (PPARgamma1) overexpression, *J Biol Chem* 2003, 278:498-505
47. Horie Y, Suzuki A, Kataoka E, Sasaki T, Hamada K, Sasaki J, Mizuno K, Hasegawa G, Kishimoto H, Iizuka M, Naito M, Enomoto K, Watanabe S, Mak TW, Nakano T: Hepatocyte-specific Pten deficiency results in steatohepatitis and hepatocellular carcinomas, *J Clin Invest* 2004, 113:1774-1783
48. Kim JB, Wright HM, Wright M, Spiegelman BM: ADD1/SREBP1 activates PPARgamma through the production of endogenous ligand, *Proc Natl Acad Sci U S A* 1998, 95:4333-4337
49. Patti ME, Kahn CR: The insulin receptor--a critical link in glucose homeostasis and insulin action, *J Basic Clin Physiol Pharmacol* 1998, 9:89-109
50. Pessin JE, Saltiel AR: Signaling pathways in insulin action: molecular targets of insulin resistance, *J Clin Invest* 2000, 106:165-169
51. Taniguchi CM, Ueki K, Kahn R: Complementary roles of IRS-1 and IRS-2 in the hepatic regulation of metabolism, *J Clin Invest* 2005, 115:718-727
52. Chen J, Sadowski HB, Kohanski RA, Wang LH: Stat5 is a physiological substrate of the insulin receptor, *Proc Natl Acad Sci U S A* 1997, 94:2295-2300
53. Le MN, Kohanski RA, Wang LH, Sadowski HB: Dual mechanism of signal transducer and activator of transcription 5 activation by the insulin receptor, *Mol Endocrinol* 2002, 16:2764-2779
54. Sawka-Verhelle D, Tartare-Deckert S, Decaux JF, Girard J, Van Obberghen E: Stat 5B, activated by insulin in a Jak-independent fashion, plays a role in glucokinase gene transcription, *Endocrinology* 2000, 141:1977-1988

55. De Meyts P: Insulin and its receptor: structure, function and evolution, *Bioessays* 2004, 26:1351-1362
56. Haigh RJ, Shepherd PR, Nave BT, Siddle K: The role of phosphatidylinositol 3-kinase activity in insulin-stimulated mitogenesis in 3T3-L1 adipocytes, *Biochem Soc Trans* 1995, 23:179S
57. Michael MD, Kulkarni RN, Postic C, Previs SF, Shulman GI, Magnuson MA, Kahn CR: Loss of insulin signaling in hepatocytes leads to severe insulin resistance and progressive hepatic dysfunction, *Mol Cell* 2000, 6:87-97
58. Araki E, Lipes MA, Patti ME, Bruning JC, Haag B, 3rd, Johnson RS, Kahn CR: Alternative pathway of insulin signalling in mice with targeted disruption of the IRS-1 gene, *Nature* 1994, 372:186-190
59. Withers DJ, Gutierrez JS, Towery H, Burks DJ, Ren JM, Previs S, Zhang Y, Bernal D, Pons S, Shulman GI, Bonner-Weir S, White MF: Disruption of IRS-2 causes type 2 diabetes in mice, *Nature* 1998, 391:900-904
60. Withers DJ, Burks DJ, Towery HH, Altamuro SL, Flint CL, White MF: Irs-2 coordinates Igf-1 receptor-mediated beta-cell development and peripheral insulin signalling, *Nat Genet* 1999, 23:32-40
61. Yamauchi T, Tobe K, Tamemoto H, Ueki K, Kaburagi Y, Yamamoto-Honda R, Takahashi Y, Yoshizawa F, Aizawa S, Akanuma Y, Sonenberg N, Yazaki Y, Kadowaki T: Insulin signalling and insulin actions in the muscles and livers of insulin-resistant, insulin receptor substrate 1-deficient mice, *Mol Cell Biol* 1996, 16:3074-3084
62. Clark JM, Brancati FL, Diehl AM: Nonalcoholic fatty liver disease, *Gastroenterology* 2002, 122:1649-1657
63. Yki-Jarvinen H: Fat in the liver and insulin resistance, *Ann Med* 2005, 37:347-356
64. Marchesini G, Brizi M, Bianchi G, Tomassetti S, Bugianesi E, Lenzi M, McCullough AJ, Natale S, Forlani G, Melchionda N: Nonalcoholic fatty liver disease: a feature of the metabolic syndrome, *Diabetes* 2001, 50:1844-1850
65. Monetti M, Levin MC, Watt MJ, Sajan MP, Marmor S, Hubbard BK, Stevens RD, Bain JR, Newgard CB, Farese RV, Sr., Hevener AL, Farese RV, Jr.: Dissociation of hepatic steatosis and insulin resistance in mice overexpressing DGAT in the liver, *Cell Metab* 2007, 6:69-78
66. Utzschneider KM, Kahn SE: Review: The role of insulin resistance in nonalcoholic fatty liver disease, *J Clin Endocrinol Metab* 2006, 91:4753-4761
67. Reitman ML, Arioglu E, Gavrilova O, Taylor SI: Lipoatrophy revisited, *Trends Endocrinol Metab* 2000, 11:410-416
68. Angulo P: Obesity and nonalcoholic fatty liver disease, *Nutr Rev* 2007, 65:S57-63
69. Browning JD, Szczepaniak LS, Dobbins R, Nuremberg P, Horton JD, Cohen JC, Grundy SM, Hobbs HH: Prevalence of hepatic steatosis in an urban population in the United States: impact of ethnicity, *Hepatology* 2004, 40:1387-1395
70. Angulo P: Nonalcoholic fatty liver disease, *N Engl J Med* 2002, 346:1221-1231
71. Bellentani S, Saccoccio G, Masutti F, Croce LS, Brandi G, Sasso F, Cristanini G, Tiribelli C: Prevalence of and risk factors for hepatic steatosis in Northern Italy, *Ann Intern Med* 2000, 132:112-117
72. Luyckx FH, Desai C, Thiry A, Dewe W, Scheen AJ, Gielen JE, Lefebvre PJ: Liver abnormalities in severely obese subjects: effect of drastic weight loss after gastroplasty, *Int J Obes Relat Metab Disord* 1998, 22:222-226

73. Silverman JF, O'Brien KF, Long S, Leggett N, Khazanie PG, Pories WJ, Norris HT, Caro JF: Liver pathology in morbidly obese patients with and without diabetes, *Am J Gastroenterol* 1990, 85:1349-1355
74. Powell EE, Jonsson JR, Clouston AD: Steatosis: co-factor in other liver diseases, *Hepatology* 2005, 42:5-13
75. Schwimmer JB, Behling C, Newbury R, Deutsch R, Nievergelt C, Schork NJ, Lavine JE: Histopathology of pediatric nonalcoholic fatty liver disease, *Hepatology* 2005, 42:641-649
76. Adams LA, Angulo P, Lindor KD: Nonalcoholic fatty liver disease, *CMAJ* 2005, 172:899-905
77. Petersen KF, Shulman GI: Etiology of insulin resistance, *Am J Med* 2006, 119:S10-16
78. Seppala-Lindroos A, Vehkavaara S, Hakkinen AM, Goto T, Westerbacka J, Sovijarvi A, Halavaara J, Yki-Jarvinen H: Fat accumulation in the liver is associated with defects in insulin suppression of glucose production and serum free fatty acids independent of obesity in normal men, *J Clin Endocrinol Metab* 2002, 87:3023-3028
79. Matsumoto M, Ogawa W, Akimoto K, Inoue H, Miyake K, Furukawa K, Hayashi Y, Iguchi H, Matsuki Y, Hiramatsu R, Shimano H, Yamada N, Ohno S, Kasuga M, Noda T: PKC λ in liver mediates insulin-induced SREBP-1c expression and determines both hepatic lipid content and overall insulin sensitivity, *J Clin Invest* 2003, 112:935-944
80. Shimomura I, Matsuda M, Hammer RE, Bashmakov Y, Brown MS, Goldstein JL: Decreased IRS-2 and increased SREBP-1c lead to mixed insulin resistance and sensitivity in livers of lipodystrophic and ob/ob mice, *Mol Cell* 2000, 6:77-86
81. Skelly MM, James PD, Ryder SD: Findings on liver biopsy to investigate abnormal liver function tests in the absence of diagnostic serology, *J Hepatol* 2001, 35:195-199
82. Mayer J, Bates MW, Dickie MM: Hereditary diabetes in genetically obese mice, *Science* 1951, 113:746-747
83. Chen H, Charlat O, Tartaglia LA, Woolf EA, Weng X, Ellis SJ, Lakey ND, Culpepper J, Moore KJ, Breitbart RE, Duyk GM, Tepper RI, Morgenstern JP: Evidence that the diabetes gene encodes the leptin receptor: identification of a mutation in the leptin receptor gene in db/db mice, *Cell* 1996, 84:491-495
84. Coburn CT, Knapp FF, Jr., Febbraio M, Beets AL, Silverstein RL, Abumrad NA: Defective uptake and utilization of long chain fatty acids in muscle and adipose tissues of CD36 knockout mice, *J Biol Chem* 2000, 275:32523-32529
85. Shimano H, Horton JD, Hammer RE, Shimomura I, Brown MS, Goldstein JL: Overproduction of cholesterol and fatty acids causes massive liver enlargement in transgenic mice expressing truncated SREBP-1a, *J Clin Invest* 1996, 98:1575-1584
86. Shimomura I, Shimano H, Korn BS, Bashmakov Y, Horton JD: Nuclear sterol regulatory element-binding proteins activate genes responsible for the entire program of unsaturated fatty acid biosynthesis in transgenic mouse liver, *J Biol Chem* 1998, 273:35299-35306
87. Feldstein AE, Canbay A, Guicciardi ME, Higuchi H, Bronk SF, Gores GJ: Diet associated hepatic steatosis sensitizes to Fas mediated liver injury in mice, *J Hepatol* 2003, 39:978-983
88. Weltman MD, Farrell GC, Liddle C: Increased hepatocyte CYP2E1 expression in a rat nutritional model of hepatic steatosis with inflammation, *Gastroenterology* 1996, 111:1645-1653

89. Gao D, Wei C, Chen L, Huang J, Yang S, Diehl AM: Oxidative DNA damage and DNA repair enzyme expression are inversely related in murine models of fatty liver disease, *Am J Physiol Gastrointest Liver Physiol* 2004, 287:G1070-1077
90. Weiler-Normann C, Herkel J, Lohse AW: Mouse models of liver fibrosis, *Z Gastroenterol* 2007, 45:43-50
91. Friedman SL: Seminars in medicine of the Beth Israel Hospital, Boston. The cellular basis of hepatic fibrosis. Mechanisms and treatment strategies, *N Engl J Med* 1993, 328:1828-1835
92. Bedossa P, Paradis V: Liver extracellular matrix in health and disease, *J Pathol* 2003, 200:504-515
93. Knittel T, Schuppan D, Meyer zum Buschenfelde KH, Ramadori G: Differential expression of collagen types I, III, and IV by fat-storing (Ito) cells in vitro, *Gastroenterology* 1992, 102:1724-1735
94. Olaso E, Friedman SL: Molecular regulation of hepatic fibrogenesis, *J Hepatol* 1998, 29:836-847
95. Parsons CJ, Takashima M, Rippe RA: Molecular mechanisms of hepatic fibrogenesis, *J Gastroenterol Hepatol* 2007, 22 Suppl 1:S79-84
96. Gressner OA, Weiskirchen R, Gressner AM: Evolving concepts of liver fibrogenesis provide new diagnostic and therapeutic options, *Comp Hepatol* 2007, 6:7
97. Pinzani M, Marra F, Carloni V: Signal transduction in hepatic stellate cells, *Liver* 1998, 18:2-13
98. Friedman SL, Arthur MJ: Activation of cultured rat hepatic lipocytes by Kupffer cell conditioned medium. Direct enhancement of matrix synthesis and stimulation of cell proliferation via induction of platelet-derived growth factor receptors, *J Clin Invest* 1989, 84:1780-1785
99. Marshall CJ: Specificity of receptor tyrosine kinase signaling: transient versus sustained extracellular signal-regulated kinase activation, *Cell* 1995, 80:179-185
100. Marra F, Arrighi MC, Fazi M, Caligiuri A, Pinzani M, Romanelli RG, Efsen E, Laffi G, Gentilini P: Extracellular signal-regulated kinase activation differentially regulates platelet-derived growth factor's actions in hepatic stellate cells, and is induced by in vivo liver injury in the rat, *Hepatology* 1999, 30:951-958
101. Kawada N, Ikeda K, Seki S, Kuroki T: Expression of cyclins D1, D2 and E correlates with proliferation of rat stellate cells in culture, *J Hepatol* 1999, 30:1057-1064
102. Schnabl B, Bradham CA, Bennett BL, Manning AM, Stefanovic B, Brenner DA: TAK1/JNK and p38 have opposite effects on rat hepatic stellate cells, *Hepatology* 2001, 34:953-963
103. Marra F, Pinzani M, DeFranco R, Laffi G, Gentilini P: Involvement of phosphatidylinositol 3-kinase in the activation of extracellular signal-regulated kinase by PDGF in hepatic stellate cells, *FEBS Lett* 1995, 376:141-145
104. Reif S, Lang A, Lindquist JN, Yata Y, Gabele E, Scanga A, Brenner DA, Rippe RA: The role of focal adhesion kinase-phosphatidylinositol 3-kinase-akt signaling in hepatic stellate cell proliferation and type I collagen expression, *J Biol Chem* 2003, 278:8083-8090
105. Kim AH, Khursigara G, Sun X, Franke TF, Chao MV: Akt phosphorylates and negatively regulates apoptosis signal-regulating kinase 1, *Mol Cell Biol* 2001, 21:893-901
106. Pinzani M, Knauss TC, Pierce GF, Hsieh P, Kenney W, Dubyak GR, Abboud HE: Mitogenic signals for platelet-derived growth factor isoforms in liver fat-storing cells, *Am J Physiol* 1991, 260:C485-491

107. Zhu J, Wu J, Frizell E, Liu SL, Bashey R, Rubin R, Norton P, Zern MA: Rapamycin inhibits hepatic stellate cell proliferation in vitro and limits fibrogenesis in an in vivo model of liver fibrosis, *Gastroenterology* 1999, 117:1198-1204
108. Massague J: TGF-beta signal transduction, *Annu Rev Biochem* 1998, 67:753-791
109. Levy DE, Darnell JE, Jr.: Stats: transcriptional control and biological impact, *Nat Rev Mol Cell Biol* 2002, 3:651-662
110. Schulze H, Ballmaier M, Welte K, Germeshausen M: Thrombopoietin induces the generation of distinct Stat1, Stat3, Stat5a and Stat5b homo- and heterodimeric complexes with different kinetics in human platelets, *Exp Hematol* 2000, 28:294-304
111. Miyoshi K, Cui Y, Riedlinger G, Robinson P, Lehoczyk J, Zon L, Oka T, Dewar K, Hennighausen L: Structure of the mouse Stat 3/5 locus: evolution from *Drosophila* to zebrafish to mouse, *Genomics* 2001, 71:150-155
112. Paukku K, Yang J, Silvennoinen O: Tudor and nuclease-like domains containing protein p100 function as coactivators for signal transducer and activator of transcription 5, *Mol Endocrinol* 2003, 17:1805-1814
113. Gewinner C, Hart G, Zachara N, Cole R, Beisenherz-Huss C, Groner B: The coactivator of transcription CREB-binding protein interacts preferentially with the glycosylated form of Stat5, *J Biol Chem* 2004, 279:3563-3572
114. Tronche F, Opherck C, Moriggl R, Kellendonk C, Reimann A, Schwake L, Reichardt HM, Stangl K, Gau D, Hoefflich A, Beug H, Schmid W, Schutz G: Glucocorticoid receptor function in hepatocytes is essential to promote postnatal body growth, *Genes Dev* 2004, 18:492-497
115. Hoelbl A, Kovacic B, Kerenyi MA, Simma O, Warsch W, Cui Y, Beug H, Hennighausen L, Moriggl R, Sexl V: Clarifying the role of Stat5 in lymphoid development and Abelson-induced transformation, *Blood* 2006, 107:4898-4906
116. Schwaller J, Parganas E, Wang D, Cain D, Aster JC, Williams IR, Lee CK, Gerthner R, Kitamura T, Frantsve J, Anastasiadou E, Loh ML, Levy DE, Ihle JN, Gilliland DG: Stat5 is essential for the myelo- and lymphoproliferative disease induced by TEL/JAK2, *Mol Cell* 2000, 6:693-704
117. Yao Z, Kanno Y, Kerenyi M, Stephens G, Durant L, Watford WT, Laurence A, Robinson GW, Shevach EM, Moriggl R, Hennighausen L, Wu C, O'Shea JJ: Nonredundant roles for Stat5a/b in directly regulating Foxp3, *Blood* 2007, 109:4368-4375
118. Gatzka M, Piekorz R, Moriggl R, Rawlings J, Ihle JN: A role for STAT5A/B in protection of peripheral T-lymphocytes from postactivation apoptosis: insights from gene expression profiling, *Cytokine* 2006, 34:143-154
119. Cui Y, Riedlinger G, Miyoshi K, Tang W, Li C, Deng CX, Robinson GW, Hennighausen L: Inactivation of Stat5 in mouse mammary epithelium during pregnancy reveals distinct functions in cell proliferation, survival, and differentiation, *Mol Cell Biol* 2004, 24:8037-8047
120. Grebien F, Kerenyi MA, Kovacic B, Kolbe T, Becker V, Dolznig H, Pfeffer K, Klingmuller U, Muller M, Beug H, Mullner EW, Moriggl R: Stat5 activation enables erythropoiesis in the absence of EpoR and Jak2, *Blood* 2008, 111:4511-4522
121. Kieslinger M, Woldman I, Moriggl R, Hofmann J, Marine JC, Ihle JN, Beug H, Decker T: Antiapoptotic activity of Stat5 required during terminal stages of myeloid differentiation, *Genes Dev* 2000, 14:232-244
122. Engblom D, Kornfeld JW, Schwake L, Tronche F, Reimann A, Beug H, Hennighausen L, Moriggl R, Schutz G: Direct glucocorticoid receptor-Stat5 interaction in hepatocytes controls body size and maturation-related gene expression, *Genes Dev* 2007, 21:1157-1162

123. Udy GB, Towers RP, Snell RG, Wilkins RJ, Park SH, Ram PA, Waxman DJ, Davey HW: Requirement of STAT5b for sexual dimorphism of body growth rates and liver gene expression, *Proc Natl Acad Sci U S A* 1997, 94:7239-7244
124. Cui Y, Hosui A, Sun R, Shen K, Gavrillova O, Chen W, Cam MC, Gao B, Robinson GW, Hennighausen L: Loss of signal transducer and activator of transcription 5 leads to hepatosteatosis and impaired liver regeneration, *Hepatology* 2007, 46:504-513
125. Hennighausen L, Robinson GW: Interpretation of cytokine signaling through the transcription factors STAT5A and STAT5B, *Genes Dev* 2008, 22:711-721
126. Zhou Y, Xu BC, Maheshwari HG, He L, Reed M, Lozykowski M, Okada S, Cataldo L, Coschigamo K, Wagner TE, Baumann G, Kopchick JJ: A mammalian model for Laron syndrome produced by targeted disruption of the mouse growth hormone receptor/binding protein gene (the Laron mouse), *Proc Natl Acad Sci U S A* 1997, 94:13215-13220
127. Teglund S, McKay C, Schuetz E, van Deursen JM, Stravopodis D, Wang D, Brown M, Bodner S, Grosveld G, Ihle JN: Stat5a and Stat5b proteins have essential and nonessential, or redundant, roles in cytokine responses, *Cell* 1998, 93:841-850
128. Laron Z, Mannheimer S, Guttman S: Plasma disappearance of various 131-I-labelled growth hormone preparations in man and rabbit, *Nature* 1965, 207:298-299
129. Kofoed EM, Hwa V, Little B, Woods KA, Buckway CK, Tsubaki J, Pratt KL, Bezrodnik L, Jasper H, Tepper A, Heinrich JJ, Rosenfeld RG: Growth hormone insensitivity associated with a STAT5b mutation, *N Engl J Med* 2003, 349:1139-1147
130. Woelfle J, Billiard J, Rotwein P: Acute control of insulin-like growth factor-I gene transcription by growth hormone through Stat5b, *J Biol Chem* 2003, 278:22696-22702
131. Flint DJ, Binart N, Kopchick J, Kelly P: Effects of growth hormone and prolactin on adipose tissue development and function, *Pituitary* 2003, 6:97-102
132. Kornfeld JW, Grebien F, Kerenyi MA, Friedbichler K, Kovacic B, Zankl B, Hoelbl A, Nivarti H, Beug H, Sexl V, Muller M, Kenner L: The different functions of Stat5 and chromatin alteration through Stat5 proteins, *Front Biosci* 2008, 13:6237-6254
133. Donahue LR, Beamer WG: Growth hormone deficiency in 'little' mice results in aberrant body composition, reduced insulin-like growth factor-I and insulin-like growth factor-binding protein-3 (IGFBP-3), but does not affect IGFBP-2, -1 or -4, *J Endocrinol* 1993, 136:91-104
134. Beato M, Herrlich P, Schutz G: Steroid hormone receptors: many actors in search of a plot, *Cell* 1995, 83:851-857
135. Tronche F, Kellendonk C, Reichardt HM, Schutz G: Genetic dissection of glucocorticoid receptor function in mice, *Curr Opin Genet Dev* 1998, 8:532-538
136. Opherck C, Tronche F, Kellendonk C, Kohlmuller D, Schulze A, Schmid W, Schutz G: Inactivation of the glucocorticoid receptor in hepatocytes leads to fasting hypoglycemia and ameliorates hyperglycemia in streptozotocin-induced diabetes mellitus, *Mol Endocrinol* 2004, 18:1346-1353
137. Hanson RW, Reshef L: Regulation of phosphoenolpyruvate carboxykinase (GTP) gene expression, *Annu Rev Biochem* 1997, 66:581-611
138. Grange T, Cappabianca L, Flavin M, Sassi H, Thomassin H: In vivo analysis of the model tyrosine aminotransferase gene reveals multiple sequential steps in glucocorticoid receptor action, *Oncogene* 2001, 20:3028-3038
139. Garrapa GG, Pantanetti P, Arnaldi G, Mantero F, Faloia E: Body composition and metabolic features in women with adrenal incidentaloma or Cushing's syndrome, *J Clin Endocrinol Metab* 2001, 86:5301-5306

140. Stoecklin E, Wissler M, Moriggl R, Groner B: Specific DNA binding of Stat5, but not of glucocorticoid receptor, is required for their functional cooperation in the regulation of gene transcription, *Mol Cell Biol* 1997, 17:6708-6716
141. Reichardt HM, Kaestner KH, Tuckermann J, Kretz O, Wessely O, Bock R, Gass P, Schmid W, Herrlich P, Angel P, Schutz G: DNA binding of the glucocorticoid receptor is not essential for survival, *Cell* 1998, 93:531-541
142. Stocklin E, Wissler M, Gouilleux F, Groner B: Functional interactions between Stat5 and the glucocorticoid receptor, *Nature* 1996, 383:726-728
143. Bengtsson BA, Eden S, Lonn L, Kvist H, Stokland A, Lindstedt G, Bosaeus I, Tolli J, Sjostrom L, Isaksson OG: Treatment of adults with growth hormone (GH) deficiency with recombinant human GH, *J Clin Endocrinol Metab* 1993, 76:309-317
144. Mayo-Smith W, Hayes CW, Biller BM, Klibanski A, Rosenthal H, Rosenthal DI: Body fat distribution measured with CT: correlations in healthy subjects, patients with anorexia nervosa, and patients with Cushing syndrome, *Radiology* 1989, 170:515-518
145. Bjorntorp P: Visceral obesity: a "civilization syndrome", *Obes Res* 1993, 1:206-222
146. Dunshea FR, Harris DM, Bauman DE, Boyd RD, Bell AW: Effect of porcine somatotropin on in vivo glucose kinetics and lipogenesis in growing pigs, *J Anim Sci* 1992, 70:141-151
147. Etherton TD, Bauman DE: Biology of somatotropin in growth and lactation of domestic animals, *Physiol Rev* 1998, 78:745-761
148. Ottosson M, Lonnroth P, Bjorntorp P, Eden S: Effects of cortisol and growth hormone on lipolysis in human adipose tissue, *J Clin Endocrinol Metab* 2000, 85:799-803
149. Djurhuus CB, Gravholt CH, Nielsen S, Pedersen SB, Moller N, Schmitz O: Additive effects of cortisol and growth hormone on regional and systemic lipolysis in humans, *Am J Physiol Endocrinol Metab* 2004, 286:E488-494
150. Yip RG, Goodman HM: Growth hormone and dexamethasone stimulate lipolysis and activate adenylyl cyclase in rat adipocytes by selectively shifting Gi alpha2 to lower density membrane fractions, *Endocrinology* 1999, 140:1219-1227
151. Kuhn R, Schwenk F, Aguet M, Rajewsky K: Inducible gene targeting in mice, *Science* 1995, 269:1427-1429
152. Gu H, Marth JD, Orban PC, Mossmann H, Rajewsky K: Deletion of a DNA polymerase beta gene segment in T cells using cell type-specific gene targeting, *Science* 1994, 265:103-106
153. Nagy A: Cre recombinase: the universal reagent for genome tailoring, *Genesis* 2000, 26:99-109
154. Isaksson OG, Jansson JO, Gause IA: Growth hormone stimulates longitudinal bone growth directly, *Science* 1982, 216:1237-1239
155. Yakar S, Rosen CJ, Beamer WG, Ackert-Bicknell CL, Wu Y, Liu JL, Ooi GT, Setser J, Frystyk J, Boisclair YR, LeRoith D: Circulating levels of IGF-1 directly regulate bone growth and density, *J Clin Invest* 2002, 110:771-781
156. Tronche F, Opherck C*, Moriggl R*, Kellendonk C, Reichardt H, Gau D, Stangl K, Schwake L, Höflich A, Schmid W, Gröne H, Beug H, Schütz G.: Glucocorticoid receptor function in hepatocytes is essential for post-natal body growth., *Genes Dev* 2004, in press:
157. Yakar S, Liu JL, Stannard B, Butler A, Accili D, Sauer B, LeRoith D: Normal growth and development in the absence of hepatic insulin-like growth factor I, *Proc Natl Acad Sci U S A* 1999, 96:7324-7329

158. Kellendonk C, Opherck C, Anlag K, Schutz G, Tronche F: Hepatocyte-specific expression of Cre recombinase, *Genesis* 2000, 26:151-153
159. Doniger SW, Salomonis N, Dahlquist KD, Vranizan K, Lawlor SC, Conklin BR: MAPPFinder: using Gene Ontology and GenMAPP to create a global gene-expression profile from microarray data, *Genome Biol* 2003, 4:R7
160. Rowland JE, Lichanska AM, Kerr LM, White M, d'Aniello EM, Maher SL, Brown R, Teasdale RD, Noakes PG, Waters MJ: In vivo analysis of growth hormone receptor signaling domains and their associated transcripts, *Mol Cell Biol* 2005, 25:66-77
161. Clodfelter KH, Holloway MG, Hodor P, Park SH, Ray WJ, Waxman DJ: Sex-dependent liver gene expression is extensive and largely dependent upon signal transducer and activator of transcription 5b (STAT5b): STAT5b-dependent activation of male genes and repression of female genes revealed by microarray analysis, *Mol Endocrinol* 2006, 20:1333-1351
162. Moriggl R, Sexl V, Kenner L, Duntsch C, Stangl K, Gingras S, Hoffmeyer A, Bauer A, Piekorz R, Wang D, Bunting KD, Wagner EF, Sonneck K, Valent P, Ihle JN, Beug H: Stat5 tetramer formation is associated with leukemogenesis, *Cancer Cell* 2005, 7:87-99
163. Hanada T, Kinjyo I, Inagaki-Ohara K, Yoshimura A: Negative regulation of cytokine signaling by CIS/SOCS family proteins and their roles in inflammatory diseases, *Rev Physiol Biochem Pharmacol* 2003, 149:72-86
164. Greenhalgh CJ, Bertolino P, Asa SL, Metcalf D, Corbin JE, Adams TE, Davey HW, Nicola NA, Hilton DJ, Alexander WS: Growth enhancement in suppressor of cytokine signaling 2 (SOCS-2)-deficient mice is dependent on signal transducer and activator of transcription 5b (STAT5b), *Mol Endocrinol* 2002, 16:1394-1406
165. Greenhalgh CJ, Rico-Bautista E, Lorentzon M, Thaus AL, Morgan PO, Willson TA, Zervoudakis P, Metcalf D, Street I, Nicola NA, Nash AD, Fabri LJ, Norstedt G, Ohlsson C, Flores-Morales A, Alexander WS, Hilton DJ: SOCS2 negatively regulates growth hormone action in vitro and in vivo, *J Clin Invest* 2005, 115:397-406
166. Hansen JA, Lindberg K, Hilton DJ, Nielsen JH, Billestrup N: Mechanism of inhibition of growth hormone receptor signaling by suppressor of cytokine signaling proteins, *Mol Endocrinol* 1999, 13:1832-1843
167. Soldaini E, John S, Moro S, Bollenbacher J, Schindler U, Leonard WJ: DNA binding site selection of dimeric and tetrameric Stat5 proteins reveals a large repertoire of divergent tetrameric Stat5a binding sites, *Mol Cell Biol* 2000, 20:389-401
168. Zhang X, Darnell JE, Jr.: Functional importance of Stat3 tetramerization in activation of the alpha 2-macroglobulin gene, *J Biol Chem* 2001, 276:33576-33581.
169. Mikula M, Fuchs E, Huber H, Beug H, Schulte-Hermann R, Mikulits W: Immortalized p19ARF null hepatocytes restore liver injury and generate hepatic progenitors after transplantation, *Hepatology* 2004, 39:628-634
170. Fischer AN, Herrera B, Mikula M, Proell V, Fuchs E, Gotzmann J, Schulte-Hermann R, Beug H, Mikulits W: Integration of Ras subeffector signaling in TGF-beta mediated late stage hepatocarcinogenesis, *Carcinogenesis* 2005, 26:931-942
171. Bradbury MW, Berk PD: Lipid metabolism in hepatic steatosis, *Clin Liver Dis* 2004, 8:639-671, xi
172. Miyaoka Y, Tanaka M, Naiki T, Miyajima A: Oncostatin M inhibits adipogenesis through the RAS/ERK and STAT5 signaling pathways, *J Biol Chem* 2006, 281:37913-37920
173. Yeh WC, Cao Z, Classon M, McKnight SL: Cascade regulation of terminal adipocyte differentiation by three members of the C/EBP family of leucine zipper proteins, *Genes Dev* 1995, 9:168-181

174. Smit JJ, Schinkel AH, Oude Elferink RP, Groen AK, Wagenaar E, van Deemter L, Mol CA, Ottenhoff R, van der Lugt NM, van Roon MA, et al.: Homozygous disruption of the murine *mdr2* P-glycoprotein gene leads to a complete absence of phospholipid from bile and to liver disease, *Cell* 1993, 75:451-462
175. Katzenellenbogen M, Mizrahi L, Pappo O, Klopstock N, Olam D, Jacob-Hirsch J, Amariglio N, Rechavi G, Domany E, Galun E, Goldenberg D: Molecular mechanisms of liver carcinogenesis in the *mdr2*-knockout mice, *Mol Cancer Res* 2007, 5:1159-1170
176. Marra F: Hepatic stellate cells and the regulation of liver inflammation, *J Hepatol* 1999, 31:1120-1130
177. Geier A, Gartung C, Matern S: [Regulation of hepatobiliary transporters in cholestatic liver disease], *Med Klin (Munich)* 2004, 99:7-17
178. Meier PJ, Stieger B: Bile salt transporters, *Annu Rev Physiol* 2002, 64:635-661
179. Trauner M, Boyer JL: Bile salt transporters: molecular characterization, function, and regulation, *Physiol Rev* 2003, 83:633-671
180. Geier A, Dietrich CG, Trauner M, Gartung C: Extrahepatic cholestasis downregulates *Oatp1* by TNF-alpha signalling without affecting *Oatp2* and *Oatp4* expression and sodium-independent bile salt uptake in rat liver, *Liver Int* 2007, 27:1056-1065
181. Geier A, Kim SK, Gerloff T, Dietrich CG, Lammert F, Karpen SJ, Stieger B, Meier PJ, Matern S, Gartung C: Hepatobiliary organic anion transporters are differentially regulated in acute toxic liver injury induced by carbon tetrachloride, *J Hepatol* 2002, 37:198-205
182. Ganguly TC, O'Brien ML, Karpen SJ, Hyde JF, Suchy FJ, Vore M: Regulation of the rat liver sodium-dependent bile acid cotransporter gene by prolactin. Mediation of transcriptional activation by Stat5, *J Clin Invest* 1997, 99:2906-2914
183. Wood M, Ananthanarayanan M, Jones B, Wooton-Kee R, Hoffman T, Suchy FJ, Vore M: Hormonal regulation of hepatic organic anion transporting polypeptides, *Mol Pharmacol* 2005, 68:218-225
184. Klover P, Hennighausen L: Postnatal body growth is dependent on the transcription factors signal transducers and activators of transcription 5a/b in muscle: a role for autocrine/paracrine insulin-like growth factor I, *Endocrinology* 2007, 148:1489-1497
185. Moriggl R, Sexl V., Kenner L., Duntsch C., Stangl K., Gingras S., Hoffmeyer A., Bauer A., Piekorz R., Wang D., Bunting K.D., Wagner E.F., Sonneck K., Valent P., Ihle J.N. Beug H.: Stat5 tetramer formation is associated with leukemogenesis, *Cancer Cell* 2005, in press:
186. Alexander WS: Suppressors of cytokine signalling (SOCS) in the immune system, *Nat Rev Immunol* 2002, 2:410-416
187. Leung KC, Doyle N, Ballesteros M, Sjogren K, Watts CK, Low TH, Leong GM, Ross RJ, Ho KK: Estrogen inhibits GH signaling by suppressing GH-induced JAK2 phosphorylation, an effect mediated by SOCS-2, *Proc Natl Acad Sci U S A* 2003, 100:1016-1021
188. Stoeckman AK, Towle HC: The role of SREBP-1c in nutritional regulation of lipogenic enzyme gene expression, *J Biol Chem* 2002, 277:27029-27035
189. Tontonoz P, Kim JB, Graves RA, Spiegelman BM: ADD1: a novel helix-loop-helix transcription factor associated with adipocyte determination and differentiation, *Mol Cell Biol* 1993, 13:4753-4759

190. Rosen ED, Hsu CH, Wang X, Sakai S, Freeman MW, Gonzalez FJ, Spiegelman BM: C/EBPalpha induces adipogenesis through PPARgamma: a unified pathway, *Genes Dev* 2002, 16:22-26
191. Shimomura I, Shimano H, Horton JD, Goldstein JL, Brown MS: Differential expression of exons 1a and 1c in mRNAs for sterol regulatory element binding protein-1 in human and mouse organs and cultured cells, *J Clin Invest* 1997, 99:838-845
192. Deng QG, She H, Cheng JH, French SW, Koop DR, Xiong S, Tsukamoto H: Steatohepatitis induced by intragastric overfeeding in mice, *Hepatology* 2005, 42:905-914
193. Inoue M, Ohtake T, Motomura W, Takahashi N, Hosoki Y, Miyoshi S, Suzuki Y, Saito H, Kohgo Y, Okumura T: Increased expression of PPARgamma in high fat diet-induced liver steatosis in mice, *Biochem Biophys Res Commun* 2005, 336:215-222
194. Nomoto K, Tsuneyama K, Abdel Aziz HO, Takahashi H, Murai Y, Cui ZG, Fujimoto M, Kato I, Hiraga K, Hsu DK, Liu FT, Takano Y: Disrupted galectin-3 causes non-alcoholic fatty liver disease in male mice, *J Pathol* 2006, 210:469-477
195. Marcus SL, Miyata KS, Zhang B, Subramani S, Rachubinski RA, Capone JP: Diverse peroxisome proliferator-activated receptors bind to the peroxisome proliferator-responsive elements of the rat hydratase/dehydrogenase and fatty acyl-CoA oxidase genes but differentially induce expression, *Proc Natl Acad Sci U S A* 1993, 90:5723-5727
196. Meirhaeghe A, Fajas L, Gouilleux F, Cotel D, Helbecque N, Auwerx J, Amouyel P: A functional polymorphism in a STAT5B site of the human PPAR gamma 3 gene promoter affects height and lipid metabolism in a French population, *Arterioscler Thromb Vasc Biol* 2003, 23:289-294
197. Zhou YC, Waxman DJ: Cross-talk between janus kinase-signal transducer and activator of transcription (JAK-STAT) and peroxisome proliferator-activated receptor-alpha (PPARalpha) signaling pathways. Growth hormone inhibition of pparalpha transcriptional activity mediated by stat5b, *J Biol Chem* 1999, 274:2672-2681
198. Prost S, Le Dantec M, Auge S, Le Grand R, Derdouch S, Auregan G, Deglon N, Relouzat F, Aubertin AM, Maillere B, Dusanter-Fourt I, Kirszenbaum M: Human and simian immunodeficiency viruses deregulate early hematopoiesis through a Nef/PPARgamma/STAT5 signaling pathway in macaques, *J Clin Invest* 2008, 118:1765-1775
199. Bugianesi E, Gastaldelli A, Vanni E, Gambino R, Cassader M, Baldi S, Ponti V, Pagano G, Ferrannini E, Rizzetto M: Insulin resistance in non-diabetic patients with non-alcoholic fatty liver disease: sites and mechanisms, *Diabetologia* 2005, 48:634-642
200. Tamura S, Shimomura I: Contribution of adipose tissue and de novo lipogenesis to nonalcoholic fatty liver disease, *J Clin Invest* 2005, 115:1139-1142
201. Samuel VT, Liu ZX, Qu X, Elder BD, Bilz S, Befroy D, Romanelli AJ, Shulman GI: Mechanism of hepatic insulin resistance in non-alcoholic fatty liver disease, *J Biol Chem* 2004, 279:32345-32353
202. Storz P, Doppler H, Pfizenmaier K, Muller G: Insulin selectively activates STAT5b, but not STAT5a, via a JAK2-independent signalling pathway in Kym-1 rhabdomyosarcoma cells, *FEBS Lett* 1999, 464:159-163
203. Bertacca A, Ciccarone A, Cecchetti P, Vianello B, Laurenza I, Del Prato S, Benzi L: High insulin levels impair intracellular receptor trafficking in human cultured myoblasts, *Diabetes Res Clin Pract* 2007, 78:316-323
204. Garg A: Lipodystrophies, *Am J Med* 2000, 108:143-152

-
205. Johannsson G, Marin P, Lonn L, Ottosson M, Stenlof K, Bjorntorp P, Sjostrom L, Bengtsson BA: Growth hormone treatment of abdominally obese men reduces abdominal fat mass, improves glucose and lipoprotein metabolism, and reduces diastolic blood pressure, *J Clin Endocrinol Metab* 1997, 82:727-734
206. Fain JN, Ihle JH, Bahouth SW: Stimulation of lipolysis but not of leptin release by growth hormone is abolished in adipose tissue from Stat5a and b knockout mice, *Biochem Biophys Res Commun* 1999, 263:201-205
207. Holloway MG, Cui Y, Laz EV, Hosui A, Hennighausen L, Waxman DJ: Loss of sexually dimorphic liver gene expression upon hepatocyte-specific deletion of Stat5a-Stat5b locus, *Endocrinology* 2007, 148:1977-1986
208. Rogoff D, Ryder JW, Black K, Yan Z, Burgess SC, McMillan DR, White PC: Abnormalities of glucose homeostasis and the hypothalamic-pituitary-adrenal axis in mice lacking hexose-6-phosphate dehydrogenase, *Endocrinology* 2007, 148:5072-5080
209. Lee JY, Muenzberg H, Gavrilova O, Reed JA, Berryman D, Villanueva EC, Louis GW, Leininger GM, Bertuzzi S, Seeley RJ, Robinson GW, Myers MG, Hennighausen L: Loss of cytokine-STAT5 signaling in the CNS and pituitary gland alters energy balance and leads to obesity, *PLoS ONE* 2008, 3:e1639
210. Xie X, Lu J, Kulbokas EJ, Golub TR, Mootha V, Lindblad-Toh K, Lander ES, Kellis M: Systematic discovery of regulatory motifs in human promoters and 3' UTRs by comparison of several mammals, *Nature* 2005, 434:338-345
211. Tronche F, Kellendonk C, Kretz O, Gass P, Anlag K, Orban PC, Bock R, Klein R, Schutz G: Disruption of the glucocorticoid receptor gene in the nervous system results in reduced anxiety, *Nat Genet* 1999, 23:99-103.

7. Abbreviations

μ	micro (10 ⁻⁶)
ACC	acetyl-CoA carboxylase
ADP	adenosine diphosphate
AF	activating function
AF-1	Activation function 1 (
AflpCre	Albumin alpha fetoprotein Cre
ALS	acid-labile subunit
ATP	adenosine triphosphate
bp	base pairs
BDL	bile-duct ligation
BSA	bovine serum albumin
BSEP	bile salt export pump
CAB	chromotrope anilinblue
cAMP	cyclic adenosine monophosphate
CCD	coiled-coil domain
cDNA	complementary DNA
ChIP	chromatin immunoprecipitation
CoA	coenzyme A
COL	collagen
CPRG	chlorophenolred-beta-D-galactopyranoside
Cre	cyclization recombination (Cre) recombinase
CbP	CREB binding protein
CYP	cytochrome p450
DEPC	diethylpyrocarbonate
DMEM	Dulbecco's modified eagle medium
DTT	dithiothreitol
EDTA	ethylenediaminetetraacetic acid
ELISA	enzyme-linked immuno sorbent assay
EMT	epithelial-mesenchymal transition
ER	estrogen receptor
ERK	extracellular signal regulated kinase
ET-1	endothelin 1
FA	fatty acids
FAD	flavin adenine dinucleotide
FAK	focal adhesion kinase
FAS	fatty acid synthases
FFA	free fatty acid
G6P	glucose-6-phosphatase
GAPDH	glyceraldehyde-3-phosphate- dehydrogenase
GC	glucocorticoid
GFP	green fluorescent protein
GH	growth hormone
GHR	growth hormone receptor
GR	glucocorticoid receptor
GRE	GR responsive element
HAT	histone acetylase

HCC	hepatocellular carcinoma
HDAC	histone deacetylase
HDL	high density lipoprotein
HL	hepatic lipase
HLH	helix-loop-helix
HPA	hypothalamic-pituitary-adrenal
HRP	horseradish peroxidase
HSC	heat shock complex
HSC	hepatic stellate cells
HSL	hormone sensitive lipase
IGF	insulin-like growth factor
IR	insulin receptor
IRES	internal ribosomal entry site
IRS	insulin receptor substrate
ITT	insulin tolerance test
LBD	ligand binding domain
LBD	ligand-binding domain
LDL	low density lipoprotein
Leu-Zip	leucine zipper
loxP	Cre recombinase recognition site
LPL	lipoprotein lipase
LTR	long terminal repeats
m	meter
m	milli (10^{-3})
M	molar
MAPK	mitogen activated protein kinase
MCS	multiple cloning site
MDR	multi-drug-resistant protein
MEK	mitogen induced extracellular kinase
MFB	myo-fibroblasts
min	minute
MMP	matrix metalloprotease
MOPS	[N-Morpholino] propanesulfonic acid
mRNA	messenger RNA
MRP	multidrug resistance protein
n	number
n	nano (10^{-9})
NADH	nicotinamide adenine dinucleotide
NAFLD	non-alcoholic fatty liver disease
NEFA	non-esterified fatty acids
NID	non ionic detergent (buffer)
NP40	nonidet P40
NTCP	sodium dependent bile acid transporter
OATP	sodium independent organic anionic transporter
OD	optical density
OGTT	oral glucose tolerance test
p	pico (10^{-12})
p	p-value (Student's test)
PBC	primary biliary cirrhosis
PBS	phosphate buffered saline

PDGFb	platelet derived growth factor beta
PDGFbR	platelet derived growth factor beta receptor
PEPCK	phosphoenol pyruvate carboxykinase
pH	pH value
PI3K	phosphatidylinositol-3-kinase
PIP ₃	phosphatidylinositol 3, 4, 5 trisphosphate
PK	pyruvate kinase
PL	pancreatic lipase
PPAR	peroxisome proliferator-activated receptor
PSC	primary sclerosing cholangitis
RE	responsive element
RIA	radioimmunoassay
RNA	ribonucleic acid
ROS	reactive oxygen species
rpm	rotations per minute
RT	room temperature
RXR	retinoic acid receptor
SDS	sodium dodecylsulfate
SH2	src homology domain
SMA	smooth muscle actin
SOCS	Suppressor of cytokine signaling
SREBP	sterol regulatory element binding protein
Stat	signal transducer and activator of transcription
ss	supershift
T2D	type II diabetes
TAD	transactivation domain
TAE	tris acetate EDTA buffer
TBE	tris borate EDTA buffer
TE	tris EDTA
TG	triglycerides
TGFb	tumor growth factor beta
TGFbR	tumor growth factor beta receptor
TIMP	tissue inhibitor of matrix metalloprotease
U	enzymatic unit
UV	ultraviolet
V	volt
VLDL	very-low density lipoprotein

8. Bibliography

Kornfeld JW, Kutschera S, Wohlberg M, Friedrich RE, Riethdorf L, Löning T, Klaus Pantel and Riethdorf S

Overexpression of TACE and TIMP3 in squamous cell carcinomas of the head and neck: Association with tumor development and progression (in preparation)

Baumgartner C, Sonneck C, Mayerhofer M, Gleixner KV, Fritz R, Cerny-Reiterer S, Kerényi MA, **Kornfeld JW**, Sillaber C, Moriggl R and Valent P

Expression of activated STAT5 in neoplastic mast cells in systemic mastocytosis: subcellular distribution and role of the transforming oncoprotein KIT D816V (in preparation)

Kornfeld JW, Pospisilik A, Friedbichler K, Esterbauer H, Hasselblatt P, Kerényi MA, Wagner KU, Engblom D, Haemmerle G, Kratky D, Kenner L, Terracciano L, Zechner R, Schütz G, Heim M and Moriggl R

Loss of transcription factors Stat5 and GR in hepatocytes leads to severe steatosis and peripheral lipodystrophy *Cell Metab* (submitted)

Engblom D*, **Kornfeld JW***, Schwake L, Tronche F, Reimann A, Beug H, Hennighausen L, Moriggl R[#] and Schutz G[#]

Direct glucocorticoid receptor-Stat5 interaction in hepatocytes controls body size and maturation-related gene expression. *Genes Dev* 10: 1157-62 (2007) (***=equal contribution and [#]=equal contribution**)

Kornfeld JW, Grebien F, Kerényi MA, Friedbichler K, Kovacic B., Zankl B, Hoelbl A, Nivarti H, Beug H, Muller M, Kenner L, Mullner EW, Gouilleux F and Moriggl R

The different functions of Stat5 and chromatin alteration through Stat5 proteins. *Front Biosci* 13: 6237-54 (2008)

Riethdorf S, Reimers N, Assmann V, **Kornfeld JW**, Terracciano L, Sauter G and Pantel K

High incidence of EMMPRIN expression in human tumors. *Int J Cancer* 15;119(8):1800-10 (2006)

9. Acknowledgements

First of all, I would like to express my gratitude to Dr. Richard Moriggl for providing me with the possibility to work in high-quality scientific projects and an access to state-of-the-art technology. Several interesting, fruitful discussions and his enthusiasm for science and biology contributed significantly to the completion of my thesis. I also would like to thank cordially Prof. Dr. Holger Kalthoff and Prof. Dr. Dr. Thomas C.G. Bosch for taking over the supervision of my thesis. Especially Prof. Kalthoff always supported me and his enthusiasm for research was one major motivation to pursue a career in science.

I would like to thank my collaborators without whom this work would not have been possible, notably Dr. Robert Eferl, Dr. Andrew Pospisilik, Prof. Dr. Harald Esterbauer, Dr. Peter Hasselblatt. Their expertise and motivation always helped me to endure times of hardships. In addition I want to merit Prof. Andrey Kozlov and Susanne Haindl which supported me technically. Working with them was a pleasure.

A special cheer goes to my group members, colleagues and friends at the LBI-CR, especially Mag. Hans-Peter Kantner, Mag. Leander Blaas, Dr. Emilio Casanova, Mag^a. Olivia Simma, Mag^a. Monica Musteanu and Dr. Pia-Maria Maurer. Lots of fun and laughter in the lab made the LBI a pleasant place to work. Coming or leaving from work was always with a smile.

I am very grateful for my family, they always supported me with spirit and the right perspective towards life. Showing me the real values often made science easier to bear. Of course without Judith, this work would not have existed. She supported me with unconditioned love, a different perspective and the right words in the right moment.

10. Curriculum Vitae



Personal information

Name Jan-Wilhelm Kornfeld, Ph.D.
Molecular biologist

.....
.....

Contact Wurlitzergasse 13/21
1160 Vienna, Austria

Phone: + 43 – 1 – 4277 – 64105
Mobile: + 43 – 664 – 6523289

Email: jan-wilhelm.kornfeld@lbicr.lbg.ac.at

.....
.....

Date and place of birth 10.08.1976 in Guetersloh, Germany

.....
.....

Nationality German

.....
.....

Languages German – mother tongue
French – fluently
English – fluently
Russian – basic skills

Academic degrees

July 2003

Biochemistry (Diploma)
University Hannover, Germany

Research institutions

2006-

Graduate Studies

Ludwig Boltzmann Institute for Cancer Research (LBI-CR)

Supervisor: Prof. Richard Moriggl, PhD

Project: The Role of Signal Transducer and Activator of transcription (Stat5) and the glucocorticoid receptor (GR) in hepatocyte function

2003-
2006

Fulltime Research Associate

Department of Tumor Biology, Hamburg, Germany

Supervisor: Sabine Riethdorf, PhD

Project: The Role of Tumor Necrosis Factor alpha Cleaving Enzyme (TACE) in squamous cell carcinoma of the Head and Neck

2003-
2002

Diploma studies (masters equivalent)

Hannover Medical School (MHH)

Supervisor: Prof. Reinhard Schwinzer, PhD

Project: Glycosylation and compartmentalisation of variantly expressed isoforms of the protein tyrosine phosphatase CD45RA

Further research experience

2003-
2005

Graduate Study Program in Molecular Biology

Center for molecular neurobiology (ZMNH), Hamburg

Supervisor: Prof. Melitta Schachner, PhD

October 2000-

Scientific Internship at the Siberian Institute of Plant

January 2001

Physiology and Biochemistry (SIFIBR), Irkutsk,

ussia

Supervisor: Prof. Natalya Igorevna, PhD

June 2001-

Scientific Internship at the University of Montreal

October 2001

School of Medicine (CHUM), Montréal, Canada

Supervisor: Prof. Yves Raymond, PhD

Invited talks

Symposium of the Medical University of Vienna (MUW), Vienna, Austria, 2007

Laboratoire d'Immunologie, CHU d'Amiens, Amiens, France, 2007

Ludwig Boltzmann Institute for traumatology, Vienna, Austria, 2007

Institute for zoology and developmental biology, Kiel, Germany, 2007

Internal Seminars of the special research council (SFB), Vienna, Austria 2006–2007

Internal Seminars of the department of tumor biology (SFB), 2003–2006

Poster presentations

Hepatocyte-Specific deletion of Stat5 and GR leads to severe fatty liver disease and liver cancer

Kornfeld, JW, Friedbichler K, Kozlov A, Haindl S, Zechner R and Moriggl R

- International conference: "Invasion and Metastasis", Berlin, Germany, 2008

Hepatocyte-Specific Deletion of Stat5 and GR leads to severe fatty liver disease and liver cancer

Kornfeld, JW, Friedbichler K, Kozlov A, Haindl S, Zechner R and Moriggl R

- Recess of the Medical university of Vienna (MUW), Vienna, Austria, 2007

Scientific publications

Mair M, Gumhold J, Schneller D, Fuchsbichler A, Zollner G, Fickert P, Kenner L, Poli V, **Kornfeld JW**, Blaas L, Casanova E, Mikulits W, Trauner M and Eferl R

STAT3 PROTECTS FROM BILE ACID-INDUCED LIVER INJURY AND CIRRHOSIS *Nature Med* (submitted)

Kornfeld JW, Kutschera S, Wohlberg M, Friedrich RE, Riethdorf L, Löning T, Klaus Pantel and Riethdorf S

Overexpression of TACE and TIMP3 in squamous cell carcinomas of the head and neck: Association with tumor development and progression (in preparation)

Baumgartner C, Sonneck C, Mayerhofer M, Gleixner KV, Fritz R, Cerny-Reiterer S, Kerenyi MA, **Kornfeld JW**, Sillaber C, Moriggl R and Valent P

Expression of activated STAT5 in neoplastic mast cells in systemic mastocytosis: subcellular distribution and role of the transforming oncoprotein KIT D816V (in preparation)

Kornfeld JW, Pospisilik A, Friedbichler K, Esterbauer H, Hasselblatt P, Kerenyi MA, Wagner KU, Engblom D, Haemmerle G, Kratky D, Kenner L, Terraciano L, Zechner R, Schütz G, Heim M and Moriggl R

Loss of transcription factors Stat5 and GR in hepatocytes leads to severe steatosis and peripheral lipodystrophy (in preparation)

Kornfeld JW, Grebien F, Kerenyi MA., Friedbichler K., Kovacic B, Zankl B, Hoelbl A, Nivarti H, Beug H, Sexl V, Muller M, Mullner EW, Kenner L, Gouilleux F and Moriggl R

The different functions of Stat5 and chromatin alteration through Stat5 proteins *Front Biosci* 1;13:6237-54 (2008)

Engblom D*, **Kornfeld JW*** Schwake L, Tronche F, Reimann A, Beug H, Hennighausen L, Moriggl R and Schutz G

Direct glucocorticoid receptor-Stat5 interaction in hepatocytes controls body size and maturation-related gene expression. *Genes Dev* 15;21(10):1157-62 (2007) (*=**equal contribution**)

Riethdorf S, Reimers N, Assmann V, **Kornfeld JW**, Terracciano L, Sauter G and Pantel K

High incidence of EMMPRIN expression in human tumors. *Int J Cancer* 15;119(8):1800-10 (2006)

References

Dr. Richard Moriggl, Director
Ludwig Boltzmann Institute
for Cancer Research (LBICR)
Vienna, Austria

Doctoral supervisor
Phone: + 43 - 1 - 4277 - 64111
Email: richard.moriggl@lbicr.lbg.ac.at

Dr. Robert Eferl, PI
Ludwig Boltzmann Institute
for Cancer Research (LBICR)
Vienna, Austria

Doctoral collaborator
Phone: + 43 - 1 - 4277 - 64111
Email: robert.eferl@lbicr.lbg.ac.at

Dr. Sabine Riethdorf, PI
Institute for Tumor Biology
Hamburg, Germany

Doctoral collaborator
Phone: + 49 - 40 - 42803 - 2628
Email: s.riethdorf@uke.uni-hamburg.de

Dr. Andrew Pospisilik
Institute of Molecular Biotechnology (IMBA)
Vienna, Austria

Doctoral collaborator
Phone: + 43 - 1 - 79044 - 4724
Email: andrew.pospisilik@imba.oeaw.ac.at